SEEDED GROWTH OF NOBLE METAL NANOCRYSTALS

A Dissertation
Presented to
The Academic Faculty

by

Yiqun Zheng

In Partial Fulfillment
of the Requirements for the Degree
of Doctor of Philosophy in the
School of Chemistry and Biochemistry

Georgia Institute of Technology
December, 2013

SEEDED GROWTH OF NOBLE METAL NANOCRYSTALS

Approved by:

Dr. Younan Xia, Advisor
Department of Biomedical Engineering
Georgia Institute of Technology

Dr. Angus Wilkinson
School of Chemistry and Biochemistry
Georgia Institute of Technology

Dr. Joseph Sadighi
School of Chemistry and Biochemistry
Georgia Institute of Technology

Dr. Z. John Zhang
School of Chemistry and Biochemistry
Georgia Institute of Technology

Dr. Christopher W. Jones
School of Chemical and Biomolecular Engineering
Georgia Institute of Technology

Date Approved: October 29, 2013

ACKNOWLEDGEMENTS

First of all, I would like to thank my advisor, Professor Younan Xia, for all his guidance and support. In particular, I would like to appreciate for his helpful discussions about research, for continually encouraging me to improve my work, and all the opportunities to share it with the scientific community. I would also like to express my appreciation to Professor Dong Qin for her advice and support.

I have also been fortunate to have excellent collaborators and am grateful to them for making this interdisciplinary work possible: Professor Zhi-Yuan Li, Dr. Xiaolan Zhong, and Chao Zhang at the Institute of Physics, Chinese Academy of Sciences for theoretical simulations of UV-vis extinction spectra, Dr. Jing Tao and Dr. Yimei Zhu at Brookhaven National Lab for HRTEM imaging, and Professor Jingyue Liu and Dr. Hongyang Liu at University of Missouri-St. Louis for CO oxidation catalytic tests.

Special thanks go to Dr. Yanyun Ma for initially teaching me how to make Au nanocrystals, Dr. Mingshang Jin for teaching me how to use HRTEM and electrochemical workstation, and many other former and current Xia group members who have provided me with suggestions, thought-provoking conversations, and friendship. In particular, Professor Jie Zeng has given me valuable mentorship and advice over the years – thank you.

I would also like to express my gratitude to all those who have inspired me along the path that led me to graduate school. In particular, I would like to thank Professor Qianwang Chen and Dr. Jing Ye at University of Science and Technology of China, who introduced me to the research of nanomaterials and encouraged me to keep on working in this field.

Finally, I would like to express my deep thanks to my friends and family, who have been continually encouraging and supporting me throughout all my academic endeavors.

TABLE OF CONTENTS

Page

ACKNOWLEDGEMENTS i

LIST OF TABLES vi

LIST OF FIGURES vii

LIST OF SYMBOLS AND ABBREVIATIONS x

SUMMARY xi

CHAPTER

1 Introduction 1

1.1 Importance of Size, Shape, and Composition 1

1.2 Advantages of Seeded Growth 2

1.3 Control of Size, Shape, Composition, and Crystallinity as Enabled by Seeded Growth 3

1.3.1 Size Control 3

1.3.2 Shape Control 4

1.3.3 Composition Control 6

1.4 Scope of This Work 7

1.5 Reference for Chapter 1 8

2 Synthesis of Au Nanospheres with Controlled Diameters in the range of 5-150 nm and Their Self-Assembly upon Dilution 11

2.1 Introduction 11

2.2 Synthesis of the Initial Au Seeds 15

2.3 Synthesis of Au Spheres with Controlled Sizes in the Range

of 5-150 nm 15

2.4 Self-Assembly of Au Spheres upon Dilution with Water 21

2.5 Conclusion 23

2.5 Experimental Section 24

2.6 Reference for Chapter 2 44

3 Seed-Mediated Synthesis of Au Tetrahedra in High Purity and with Well-Controlled Sizes 50

3.1 Introduction 50

3.2 Results and Discussion 51

3.3 Conclusion 55

3.4 Experimental Section 56

3.5 Reference for Chapter 3 65

4 Controlling the Size and Morphology of Au@Pd Core-Shell Nanocrystals 67

4.1 Introduction 67

4.2 Results and Discussion 70

4.3 Conclusion 75

4.4 Experimental Section 76

4.5 Reference for Chapter 4 85

5 Crystallinity Change in Seeded Growth of Au Nanocrystals 88

5.1 Introduction 88

5.2 Results and Discussion 89

5.3 Conclusion 92

5.4 Experimental Section 94

5.5 Reference for Chapter 5 104

VITA 107

LIST OF TABLES

Page

Table 2.1: The average diameter (d_{av}) and its standard deviation (σ), the average hydrodynamic diameter (d_{hydro}) and its standard deviation (σ_{hydro}), the type of seed, and the volume (V) of seed solution for the Au nanospheres displayed in Figures 2.4-2.6. 27

LIST OF FIGURES

Page

Figure 2.1: Representative TEM images of Au nanospheres with different sizes in literature. 28

Figure 2.2: Size distribution, UV-Vis spectrum, and positive-ion MALDI mass spectrum of the initial Au seeds. 29

Figure 2.3: Schematics illustrating the successive growth procedure used for the preparation of Au nanospheres with controlled diameters increasingly tuned from 5 nm to 150 nm. 30

Figure 2.4: TEM images of single-crystal Au nanospheres with controlled diameters in the range of 5-16 nm. 31

Figure 2.5: TEM images of single-crystal Au nanospheres with controlled diameters in the range of 15-80 nm. 32

Figure 2.6: TEM images of single-crystal Au nanospheres with controlled diameters in the range of 70-150 nm. 33

Figure 2.7: TEM images of Au nanocrystals obtained using the standard dropwise injection procedure, with the addition of 20 μL of the 46-nm seed solution. 34

Figure 2.8: TEM images of Au nanospheres prepared using the first-round growth procedure with different amounts of CTAB and AA. 35

Figure 2.9: The effect of injection rate of Au precursor on the morphology of final products. 36

Figure 2.10: The effect of the reductant on the morphology of final products. 37

Figure 2.11: The effect of halide ions on the morphology of final products. 38

Figure 2.12: Experimental and calculated UV-Vis extinction spectra of Au nanospheres with different diameters. 39
Figure 2.13: Hydrodynamic diameter distributions of Au nanospheres with different diameters as measured by dynamic light scattering. 40
Figure 2.14: TEM and HRTEM images of Au nanostructures in the form of dimers/trimmers and wavy wires. 41
Figure 2.15: TEM image of Au nanostructures in the form of large aggregates. 42
Figure 2.16: TEM images of Au nanostructures obtained by diluting an aqueous suspension of 5-nm and 17-nm Au nanospheres. 43
Figure 3.1: TEM images of Au nanocrystals evolved from spherical seeds to tetrahedral products. 58
Figure 3.2: TEM images of tetrahedral Au nanocrystals with different sizes. 59
Figure 3.3: Experimental and calculated UV-vis extinction spectra of tetrahedral Au nanocrystals with different sizes. 60
Figure 3.4: The effect of the amount of injection rate of Au precursor on the morphology of final products. 61
Figure 3.5: The effect of the amount of CTAB on the morphology of final products. 62
Figure 3.6: The effect of the amount of CTAC on the morphology of final products. 63
Figure 3.7: Schematic illustration of shape evolution from a sphere to tetrahedrons of different sizes. 64
Figure 4.1: TEM images of Au@Pd nanocrystals obtained at different stages of a standard synthesis in the presence of CTAB and CTAC as a capping agent, respectively. 79

Figure 4.2: TEM images of Au@Pd nanocubes and concave nanocubes with different sizes. 80

Figure 4.3: TEM images of Au@Pd core-shell nanocrystals prepared using different amounts of reductant. 81

Figure 4.4: TEM images of Au@Pd core-shell nanocrystals with different morphologies: rectangular bar, concave octahedron, and octahedron. 82

Figure 4.5: TEM images of Au-Pd multi-shelled nanocrystals. 83

Figure 4.6: Schematic illustration of morphology evolution associated with the Au@Pd core-shell nanocrystals as a function of reaction rate. 84

Figure 5.1: TEM images of Au spherical seeds before and after treatment of $Na_2S_2O_3$. 97

Figure 5.2: TEM images of two types of Au nanocrystals grow from the spherical seeds before and after treatment of $Na_2S_2O_3$, respectively. 98

Figure 5.3: XPS analysis of the Au spherical seeds before and after treatment of $Na_2S_2O_3$. 99

Figure 5.4: TEM images of Au nanocrystals obtained from the standard procedure, except for the use of seeds treated with other sulfuric species. 100

Figure 5.5: TEM images of Au rod-like seeds before and after the treatment of $Na_2S_2O_3$ and corresponding products obtained from same procedures. 101

Figure 5.6: High-resolution TEM images and the corresponding ED patterns of Au rod-like seeds before and after the treatment of $Na_2S_2O_3$. 102

Figure 5.7: Detailed structural characterization of single-crystal and twinned Au nanorods. 103

LIST OF SYMBOLS AND ABBREVIATIONS

ED	electron diffraction
fcc	face-centered cubic
FFT	fast-Fourier transform
HRTEM	high-resolution transmission electron microscopy
ICP-MS	inductively-coupled plasma mass spectroscopy
LSPR	localized surface plasmon resonance
NIR	near infrared
PVP	poly(vinyl pyrrolidone)
SEM	scanning electron microscopy
TEM	transmission electron microscopy
UV-vis	ultraviolet-visible

SUMMARY

This research emphasizes on the use of seeded growth in synthesis of noble metal nanocrystals with precise control over the size, shape, and composition.

In the first part of this work, I have produced Au nanocrystals with single-crystal structure and truly spherical profiles and investigated their optical properties and self-assembly as induced by dilution with water. These Au nanospheres were generated in high yield and purity, together with controllable sizes continually increased from 5 to 150 nm. I also found these Au nanospheres self-assembled into dimers, larger aggregates, and wavy nanowires, respectively, as diluted with water.

In the second part of this work, I demonstrate the kinetic control can be implemented to control the shape of mono- and bi-metallic nanocrystals in seeded growth. The as-prepared single-crystal nanospheres of Au were employed as seeds to synthesize of tetrahedral Au nanocrystals and Au@Pd core-shell nanocrystals with six distinct shapes. The success of the two demonstrations relies on manipulation of reaction kinetics to achieve different product shapes. The reaction kinetics was controlled by varying a set of reaction parameters, including the type and concentration of capping agent, the amount of reductant, and the injection rate of metal precursor solution.

In the final part of this work, I will discuss an unusual change in crystallinity observed in seeded growth of Au nanocrystals on Au seeds. In particular, single-crystal Au seeds treated with a chemical species could develop twin defects during the seed-mediated growth process to yield multiply twinned products.

CHAPTER 1

INTRODUCTION

1.1 Importance of Size, Shape, and Composition of Noble Metal Nanocrystals

Nanocrystals are crystals with at least one dimension between 1 and 100 nm. Interest in nanocrystals has been growing steadily due to their unique position as a bridge between atoms and bulk solids as well as their fascinating properties and potential applications. In principle, the electron confinement by a nanocrystal provides the most powerful means to manipulate the electronic, optical, and magnetic properties of a solid material. This notion explains why nanocrystals have been the primary source for discovering and studying quantum size effects, with examples of quantized excitation, Coulomb blockade, metal–insulator transition, and superparamagnetism.[1-4]

Noble-metal nanocrystals, especially those composed of Au, Ag, Pd, Pt and their combinations, have attracted significant attentions in the past decades, owing to their unique physicochemical properties and potential applications in optics, electronics and catalytics. For Ag and Au, the applications are mainly based on their optical properties while for Pd and Pt, the applications are largely in catalysis. The properties of a noble-metal nanocrystal are determined by a set of physical parameters that may include its size, shape, and composition. For example, localized surface plasmon (LSP) is charge density oscillation confined to the surface of metallic nanocrystals. Excitation of LSP by an incident light at a wavelength where resonance can occur can result in strong light scattering, in the appearance of intense localized surface plasmon resonance (LSPR) absorbance peak. Computational and experimental studies have shown that the shape of a Ag or Au nanocrystal plays the most important role in determining the number, position, and intensity of LSPR peaks.[5] Another typical example would be the catalytic

activity/selectivity of Pd and Pt, which has been found to be highly sensitive to the facets expressed on the surface and thus the shape. For instance, it has been shown that Pt nanocrystals can selectively catalyze different types of reactions depending on the facets, with {100} and {210} facets being most active for reactions involving H_2 and CO, respectively.[6-7] In addition to size and shape, the composition of noble-metal nanocrystals can also be an important parameter owing to the potential coupling of physicochemical properties between the constituent metals and thus enhancement of their performance in an array of applications. For example, the Pt_3Ni alloyed (111) surface is 10-fold more active for the oxygen reduction reaction (ORR) than the corresponding Pt(111) surface. Similar dependences have also been observed for many other different combinations of metals and reactions. These and many other examples clearly illustrate the importance of size, shape, and composition controls to the efficient utilization of metal nanocrystals. To this end, mastery over the size, shape, and composition of a noble-metal nanocrystal enables control of its properties and enhancement of its usefulness for a given application.

1.2 Advantages of Seeded Growth

Conventionally, the synthesis of noble-metal nanocrystals is conducted via a one-pot reaction, in which a salt precursor is reduced (or decomposed in some cases) to zero-valent atoms, followed by self-nucleation and growth into clusters, seeds, and then nanocrystals. Although it has been widely recognized as a general synthetic strategy, individual recipes typically offer only a small window for tuning the size, shape and composition. As a result, one has to rely on a number of different procedures if particles of multiple sizes and shapes are needed, leading to inconsistent surface properties, as well as particle morphology and size distributions. This difficulty can be attributed to a lack of control over the concentration and the structure of nuclei and the kinetics of the growth in

a one-pot synthesis, which impedes the rational design of the size and shape of a target nanocrystal.

Seeded growth, also often referred as "seed-mediated growth" in literature, is built on the notion that pre-formed nanocrystals with well-defined facets can be added to a synthesis and serve as primary sites for nucleation (in this case, heterogeneous) and growth of larger nanocrystals from the same or a different metal. This approach was initially demonstrated by Murphy for growing Au nanorods from Au seeds and by our group for growing pentagonal Ag nanowires from Pt seeds.[8-9] Later, this approach was successfully extended to many other noble metals and their combinations.[10-19] The advantage of this approach is that the nucleation and growth steps can be independently manipulated. In a typical seeded growth process, pre-formed metal nanoparticles were employed as the seeds, which were then introduced into a growth solution containing a metal precursor and a capping agent, to initiate the growth of a secondary metal on the seeds. With the use of appropriate seeds and a suitable combination of reducing agent and capping agent, it is also feasible to manipulate the shape or morphology of the resultant nanocrystals. Seeded growth process can also be expected in multiple rounds to achieve successive growth. In this case, the goal of a significant size increase or fabrication of multi-shelled nanocrystals can be easily reached.

1.3 Control of Size, Shape, and Composition Enabled by Seeded Growth

Thanks to research efforts from many groups, it is now possible to achieve a relatively successful control over the size, shape, and composition of noble metal nanocrystals via a myriad of strategies based on seeded growth. Here, several examples were provided along with discussions of their mechanisms.

1.3.1 Size Control

As a major advantage over the conventional methods based on homogeneous nucleation, seeded growth allows one to control the dimensions of resultant nanocrystals by simply varying the ratio of the seeds to the added precursor. This principle was proposed by Murphy and co-workers in their pioneering works for the synthesis of polycrystalline Au nanospheres with desired sizes in the range of 5-40 nm.[20] In the case of Ag, our group enabled the synthesis of Ag nanocubes with controllable edge lengths in the range of 30-200 nm via seeded growth.[21] In particular, the edge length of the resultant nanocubes was controlled by the ratio of Ag seeds to Ag precursor. Following these strategies, success in size control has also been achieved in a number of other systems, such as single-crystal Pd nanocubes and stacking-fault-involved Ag nanoplates.[22-23] All these successful examples demonstrated the feasibility of tuning the size of noble-metal nanocrystals via seeded growth.

1.3.2 Shape Control

Both thermodynamic and kinetic approaches can be employed to control the morphology of a nanocrystal. The thermodynamic control, including the use of a capping agent, is based on the requirement to minimize the total surface energy of a system. It is known that nanocrystals can take completely different shapes in the presence of different capping agents. This phenomenon can be ascribed to the anisotropy in binding energy between a capping agent and various crystallographic planes. The binding selectivity of a capping agent also has a profound impact on the shape taken by a nanocrystal because it could alter the order of free energies of different facets through selective chemisorption. For example, Br^- ions bind most strongly to Pd{100} facets, resulting in the formation of Pd cubes or bars enclosed by those thermodynamically less favored {100} facets.[24] To this end, this principle can be employed to produce nanocrystals with desired facets by choosing a specific capping agent in the growth step. For example, it has been

demonstrated that PVP binds more strongly to the {100} facets of Ag relative to {111}, while citrate shows an opposite trend. As a result, cuboctahedral Ag seeds can be directed to grow into cubes and octahedrons when PVP and sodium citrate are used as the capping agents, respectively.[25]

Shaping noble-metal nanocrystals can also be realized using strategies focused on kinetic control. Unlike thermodynamic control, the kinetic control is based on manipulation of growth rate at which atoms are generated and added to the surface of a growing seed. The product of kinetically controlled growth is not confined by thermodynamics; notable examples include nanocrystals exhibiting unsymmetrical shapes or enclosed by high-energy facets and/or with a concave structure on the surface.[26-28]

In general, the reaction rate can be manipulated using at least four different strategies: 1) variation of the reductant and/or precursor. In particular, the reducing power of a reductant and the ligand coordinating with the metal ion was found to be critical to the reduction rate of a precursor and thus changing the resultant growth pattern. For example, in the case of overgrowth of Au on cubic Pd seeds, localized and conformal overgrowth can be selectively promoted when citrate and ascorbic acid were used as reductants, respectively.[29] In addition, Pd octahedrons and tetrahedrons enclosed by eight and four {111} facets, were obtained from cuboctahedral Pd seeds by using Na_2PdCl_4 and $Pd(acac)_2$, respectively, as the precursors.[30] The difference in growth pattern was attributed to the reduction rates of these two precursors; 2) tuning of the reaction temperature. The increase in temperature can be a feasible method to increase the reaction rate constant and thus accelerate the reduction rate. For example, in the case of overgrowth of Pd over octahedral Au seeds, an elevated reaction temperature was identified to be a key factor in facilitating the formation of nanocrystals enclosed with {730} high-index facets while {111}-facet-encased products were obtained at a low temperature;[31] 3) control of precursor concentration. The use of a syringe pump can be

an effective means to manipulate the precursor concentration. For example, the overgrowth of Rh along the corners and edges rather than side faces of a cubic Rh seed can be enhanced at a relatively low injection rate of Rh precursor.[26] This principle has also found important use in the formation of bimetallic nanocrystals with a variety of different structures and even in breaking the cubic symmetry of face-centered cubic (fcc) lattice;[27-28, 32] and 4) introducing an oxidative etchant such as Cl^-/O_2, Fe^{II}/Fe^{III}, and Cu^I/Cu^{II} to retard the growth kinetics. In short, by adopting either thermodynamic or kinetic approaches, the shape of noble-metal nanocrystals can be facilely controlled.

1.3.3 Composition Control

Seeded growth offers a versatile route for controlling the composition of noble-metal nanocrystals. The basic concept behind this process consists of growing a new layer of material over an existing metal core seed. In principle, it is possible for this new layer to possess the composition identical to that of the core, or to consist of a different metal entirely. The advantages of seeded growth in controlling the composition of noble-metal nanocrystals can be summarized using the three following aspects: i) it is possible to incorporate different metals into a single product with ordered shell sequences. For example, our group introduced a synthesis of multi-shelled nanocrystals composed of alternating Pd and Pt shells.[33] The synthesis was conducted by sequentially adding $PdCl_4^{2-}$ or $PtCl_4^{2-}$ precursors into a system containing either Pd or Pt seeds; ii) The atomic ratios in resultant product can be readily tuned by simply varying the ratio of the seeds to the added precursor. For example, the thickness of Ag shell in Au@Ag core-shell nanocubes can be tuned by changing either the amount of Ag precursor or the volume of Au seed solution;[34] iii) It is possible to control the spatial distribution of metals in the final product by manipulating the reaction kinetics, and thus the growth pattern. Taken together, the use of seeded growth allows for convenient composition control of multi-

metallic noble metal nanocrystals that are otherwise difficult to produce through direct syntheses.

In short, seeded growth has been demonstrated as a facile and versatile route to preparation of noble-metal nanocrystals. Since the structure and concentration of the seeds, as well as their growth, can all be manipulated independently, it enables convenient and precise control over the size, shape, and composition of nanocrystals.

1.4 Scope of this Work

This work is organized into three main sections: synthesis of spherical Au seeds, the use of seeded growth to control the shape of Au nanocrystals and Au-based bimetallic nanocrystals, and an unusual change in crystallinity observed during observed growth of Au nanocrystals.

Chapter 2 discusses synthetic methods I developed to generate Au nanocrystals with i) a single-crystal structure and ii) a truly spherical shape, as well as investigation of their optical properties and self-assembly upon dilution with water. For the first time, Au nanospheres with a single-crystal structure could be generated in high yield and purity. Their size could be continuously tuned in the range of 5-150 nm by simply changing the type and/or amount of seeds while keeping their single crystallinity and a truly spherical shape. Interestingly, these Au nanospheres self-assembled into dimers, larger aggregates, and wavy nanowires, respectively, when diluted with water.

Chapters 3 and 4 discuss the use of these single-crystal, spherical Au nanocrystals as seeds to fabricate mono- and bi-metallic nanocrystals with more complex shapes. In Chapter 3, I present a facile method for successful synthesis of Au nanocrystals with a tetrahedral shape and well-controlled sizes in the range of 30-60 nm. The success of this synthesis relies on the scarce supply of Au atoms enabled by dropwise injection of Au precursor using a syringe pump, together with the use of a combination of

cetyltrimethylammonium bromide (CTAB) and cetyltrimethylammonium chloride (CTAC) as stabilizers to promote an unsymmetrical growth and thus formation of tetrahedral Au nanocrystals in high yields.

Chapter 4 discusses how kinetic control can be implemented in the seeded growth to obtain Au@Pd core-shell nanocrystals with six distinct shapes in the same reaction system. In particular, the reaction kinetics was controlled by changing only one or two of the reaction parameters, including the type and concentration of capping agent, the amount of reductant, and the injection rate of Pd precursor solution. As a result, along with the increase of reaction rate in the seed-mediated growth, the resultant core-shell nanocrystals evolved into octahedron, concave octahedron, rectangular bar, cube, concave cube, and dendrite, respectively.

Finally, Chapter 5 discusses an unusual change in crystallinity observed in seeded growth of Au nanocrystals from Au seeds. In particular, single-crystal Au seeds treated with a chemical species could develop twin defects during the seed-mediated growth process to yield multiply twinned products.

1.5 References for Chapter 1

[1] A. P. Alivisatos, *Science* **1996**, *271*, 933.

[2] V. Maheshwari, J. Kane, R. Saraf, *Adv. Mater.* **2008**, *20*, 284.

[3] G. Markovich, C. P. Collier, S. E. Henrichs, F. Remacle, R. D. Levine, J. R. Heath, *Acc. Chem. Res.* **1999**, *32*, 415.

[4] U. Jeong, X. Teng, Y. Wang, H.Yang, Y. Xia, *Adv. Mater.* **2007**, *19*, 33.

[5] M. A. El-Sayed, *Acc Chem Res.* **2001**, *34*, 257.

[6] L. M. Falicov, G. A. Somorjai, *Proc. Natl. Acad. Sci. USA* **1985**, *82*, 2207.

[7] A.-C. Shi, R. I. Masel, *J. Catal.* **1989**, *120*, 421.

[8] N. R. Jana, L. Gearheart, C. J. Murphy, *J. Phys. Chem. B* **2001**, *105*, 4065.

[9] Y. Sun, B. Gates, B. Mayers, and Y. Xia, *Nano Lett.* **2002**, *2*, 165.

[10] B. Rodriguez-Gonzalez, A. Burrows, M. Watanabe, C. J. Kiely, L. M. Liz-Marzan, *J. Mater. Chem.* **2005**, *15*, 1755.

[11] P. D. Cozzoli, T. Pellegrino, L. Manna, *Chem. Soc. Rev.* **2006**, *35*, 1195.

[12] S. G. Zhou, K. McIlwrath, G. Jackson, B. Eichhorn, *J. Am. Chem. Soc.* **2006**, *128*, 1780.

[13] S. E. Habas, H. Lee, V. Radmilovic, G. A. Somorjai, P. Yang, *Nature Mater.* **2007**, *6*, 692.

[14] F. Tao, M. E. Grass, Y. Zhang, D. R. Butcher, J. R. Renzas, Z. Liu, J. Y. Chung, B. S. Mun, M. Salmeron, G. A. Somorjai, *Science* **2008**, *322*, 932.

[15] H. Lee, S. E. Habas, G. A. Somorjai, P. Yang, *J. Am. Chem. Soc.* **2008**, *130*, 5406.

[16] D. Seo, C. Yoo, J. Jung, H. Song, *J. Am. Chem. Soc.* **2008**, *130*, 2940.

[17] B. Lim, M. Jiang, P. H. C. Camargo, E. C. Cho, J. Tao, X. Lu, Y. Zhu, Y. Xia, *Science* **2009**, *324*, 1302.

[18] R. Costi, A. E. Saunders, U. Banin, *Angew. Chem. Int. Ed.* **2010**, *49*, 4878.

[19] M. R. Langille, J. Zhang, C. A. Mirkin, *Angew. Chem. Int. Ed.* **2011**, *50*, 3543.

[20] N. R. Jana, L. Gearheart, C. J. Murphy, Langmuir **2001**, *17*, 6782.

[21] Q. Zhang, W. Li, C. Moran, J. Zeng, J. Chen, L.-P. Wen, Y. Xia, *J. Am. Chem. Soc.* **2010**, *132*, 11372.

[22] W. Niu, Z.-Y. Li, L. Shi, X. Liu, H. Li, S. Han, J. Chen, G. Xu, *Crys. Growth & Des.* **2008**, *8*, 4440.

[23] J. Zeng, X. Xia, M. Rycenga, P. Henneghan, Q. Li, Y. Xia, *Angew. Chem. Int. Ed.* **2011**, *50*, 244.

[24] Y. Xiong, H. Cai, B. J. Wiley, J. Wang, M. J. Kim, Y. Xia, *J. Am. Chem. Soc.* **2007** *129*, 3665.

[25] J. Zeng, Y. Zheng, M. Rycenga, J. Tao, Z.-Y. Li, Q. Zhang, Y. Zhu and Y. Xia, *J. Am. Chem. Soc.*, 2010, **132**, 8552.

[26] H. Zhang, W. Li, M. Jin, J. Zeng, T. Yu, D. Yang, Y. Xia, *Nano Lett.* **2010**, *11*, 898.

[27] J. Zeng, C. Zhu, J. Tao, M. Jin, H. Zhang, Z. Y. Li, Y. Zhu, Y. Xia, *Angew. Chem. Int. Ed.* **2012**, *51*, 2354.

[28] C. Zhu, J. Zeng, J. Tao, M. C. Johnson, I. Schmidt-Krey, L. Blubaugh, Y. Zhu, Z. Gu, Y. Xia *J. Am. Chem. Soc.* **2012**, *134*, 15822.

[29] B. Lim, H. Kobayashi, T. Yu, J. Wang, M. J. Kim, Z.-Y. Li, Y. Xia, *J. Am. Chem. Soc.*, **2010**, *132*, 2506.

[30] Y. Wang, S. Xie, J. Liu, J. Park, C. Z. Huang, Y. Xia, *Nano Lett.* **2013**, *13*, 2276.

[31] C.-L. Lu, K. S. Prasad, H.-L. Wu, J. A. Ho, M. H. Huang, *J. Am. Chem. Soc.*, **2010**, *132*, 14546.

[32] X. Xia, Y. Xia, *Nano Lett.* **2012**, *12*, 6038.

[33] H. Zhang, M. Jin, J. Wang, M. J. Kim, D. Yang, Y. Xia, *J. Am. Chem. Soc.*, **2011**, *133*, 10422.

[34] Y. Ma, W. Li, E. C. Cho, Z. Li, T. Yu, J. Zeng, Z. Xie, Y. Xia, *ACS Nano*, 2010, **4**, 6725-6734.

CHAPTER 2

SYNTHESIS OF AU NANOSPHERES WITH CONTROLLED DIAMETERS IN THE RANGE OF 5-150 NM AND THEIR SELF-ASSEMBLY UPON DILUTION

2.1 Introduction

Gold nanocrystals have been extensively studied for many decades due to their fascinating optical properties known as localized surface plasmon resonance (LSPR), and their widespread use in applications related to plasmonics, surface-enhanced Raman scattering (SERS), imaging, sensing, and drug delivery.[1-7] It is well-known that the LSPR properties of Au nanocrystals are dependent on the size, shape, and morphology.[8-11] For example, the LSPR peaks of Au spherical nanoparticles were found to red-shift as their diameters were increased.[12-16] Red-shift was also observed when the nanoparticles changed their shape from spherical to cubic while the size was largely retained. In this case, the sharp corners on the surface could result in a greater separation of charges and thus reduction of the restoring force for electron oscillation, causing the resonance peak to shift to longer wavelengths.[17-19] Therefore, it is of great importance to manipulate both the size and shape of Au nanocrystals in an effort to tailor and tune the LSPR properties. Thanks to the efforts from many research groups, it is now feasible to generate Au nanocrystals with tunable sizes and shapes in aqueous solutions using a number of different methods. The products typically took polyhedral shapes enclosed by a set of low-index facets, with notable examples including cubes, octahedrons, cuboctahedrons, tetrahedrons, rhombic dodecahedrons, prisms, decahedrons, and icosahedron.[20-34] In recent years, Au nanocrystals encased by high-index facets, including concave cubes, trisoctahedrons, tetrahexahedrons, and hexoctahedrons, have also been reported by a number of groups.[35-38] For some of these Au nanocrystals, such as cubes, octahedrons,

decahedrons, tetrahexahedrons, and concave cubes, their sizes could be varied over a broad range by controlling the experimental conditions.

In addition to the polyhedrons, preparation of Au nanocrystals with a spherical shape has also received great interest due to the simplicity to deal with such a highly symmetric shape in theoretical modeling. Depending on whether there are twin defects involved, the Au nanospheres can be classified into two major categories: polycrystalline (involving twin defects) and single-crystal (free of twin defects). Compared with the polycrystalline counterparts, it is much easier to work with single-crystal spheres as the presence of sharp corners and/or edges may have a great impact on the LSPR properties. It is also much easier to quantify and understand seed-mediated growth when single-crystal nanospheres are involved. Generally, the final shape of a single-crystal polyhedral nanocrystal is largely determined by the ratio of growth rates for {111} and {100} facets.[39] Since the proportions of {111} and {100} facets on the surface of a single-crystal Au nanosphere are roughly the same, the use of single-crystal nanospheres as seeds would provide a simple model system for conveniently monitoring the shape evolution and thus singling out the factors that determine the final shape displayed by a product.[40] For example, Au octahedrons, cubes, and trisoctahedrons have recently been obtained in the same reaction system by simply changing the concentration of ascorbic acid (the reductant) in the presence of 8.7 ± 0.3 nm single-crystal Au nanospheres as the seeds.[41] In addition to seeded growth of a monometallic system, the formation of Au@Ag and Au@Pd core-shell bimetallic nanocrystals with various morphologies has also been explored via the use of single-crystal Au nanospheres as the seeds.[42,43] These studies clearly demonstrate that the use of single-crystal Au nanospheres will greatly contribute to our understanding of seed-mediated growth.

For Au nanoparticles with a more or less spherical shape and suspended in hydrophilic media, they were typically synthesized using a one-pot reduction method. One of the most commonly used one-pot protocols involves the reduction of choloauric

acid by citrate ions, which was first reported by Turkevich and coworkers in 1951.[44] Since then, this protocol has been constantly refined to produce Au nanoparticles with sizes controllable in the range of 15-200 nm.[45-52] Other capping agents such as poly(vinyl pyrrolidone) (PVP) and poly(methacrylic acid) have also been used in recent reports.[53-59] Although the one-pot synthesis is very simple and convenient to conduct, it is rather difficult to control the nucleation and growth steps. The final products are typically polycrystalline and characterized by a relatively broad size distribution. In comparison, seeded growth offers a much better control over the uniformity, and the range of size can also be finely controlled simply by varying the ratio of seed to metal salt. To this end, Murphy and co-workers have demonstrated the use of seeded growth for generating spherical Au nanoparticles with uniform sizes in the range of 5-40 nm.[60] Liz-Marzan and co-workers extended this strategy to prepare quasi-spherical Au nanoparticles in a relatively large size range from 12 up to 180 nm.[61] Despite the successful control over size distribution, the products of these syntheses were often plagued by the presence of a noticeable amount of non-spherical particles (i.e., rods and plates). As shown in Figure 2.1, it is not difficult to identify many sharp features (and twin defects) on (and in) the nanoparticles. To date, the most successful protocol for the preparation of single-crystal Au nanospheres was based on overgrowth of single-crystal Au nanorods.[28] However, the use of Au nanorods more than 20 nm in length makes it impossible to generate nanospheres with diameters smaller than 20 nm. As a result, it remains a technical challenge to generate single-crystal Au nanospheres in high yield and purity, together with precisely controlled sizes.

In this section, I present a facile route to the synthesis of single-crystal Au nanospheres with narrow size distributions. The value of this work can be understood from three different aspects. First, single-crystal Au nanospheres could be generated in high yield and purity. As discussed above, single-crystal Au nanospheres are useful, but so far there is no systematic study. The key to the success of the current synthesis is to

modify the seed-mediated growth, originally developed by Murphy, El-Sayed, and others,[62,63] to emphasize a relatively fast reduction rate for the Au precursor in the first-round growth. Secondly, these single-crystal Au nanospheres could be obtained with precisely controlled sizes, especially in the sub-10 nm size range. In particular, the sizes of the Au nanospheres could be controlled by simply varying the amount of seeds used in the growth step. Through successive growth, the diameters of the Au nanospheres could be increased from 5 to 150 nm while keeping their single crystallinity and a truly spherical shape. In contrast, the size-control strategy included in previous reports mainly focused on the polycrystalline products. Since the nanospheres were single crystals with uniform, well-controlled diameters, their LSPR properties could be directly compared with the results obtained from theoretical modeling based on Mie theory. Thirdly, surface diffusion was identified as a critical parameter in determining the evolution of seeds into particles of increasing sizes without losing the spherical shape. In particular, a slow deposition rate for the atoms, enabled by dropwise addition of Au precursor and the presence of reductant at a low concentration, gives atoms added onto a seed enough time to diffuse across the surface, leading to the formation of a shape favored by thermodynamics. Finally, it is a new discovery that the CATC-stabilized Au nanoparticles are not stable upon dilution with pure deionized water. Typically, when excessive CTAC molecules were removed from the system, a simple dilution of Au nanospheres suspension would lead to significant aggregation. It was found that the Au nanospheres self-assembled into dimers, larger aggregates, and wavy nanowires, respectively, as more water was introduced.

2.2 Synthesis of Initial Au Seeds

The first step of our synthesis involved the preparation of Au clusters capped by CTAB that are referred to as "the initial seeds" in our discussion. In this case, aqueous solutions of $HAuCl_4$ and CTAB were mixed at room temperature, followed by rapid injection of an ice-cold aqueous $NaBH_4$ solution. The resultant suspension displayed a brown color, which could be directly used as seeds to generate Au nanospheres. To gain a better understanding of the initial seeds, I firstly measured their size distribution by dynamical light scattering (DLS). As shown in Figure 2.2a, their size distribution was relatively narrow, with an average value of 0.75 nm for the hydrodynamic radii. Within this range of size, it became very difficult to characterize them using electron microscopy. Figure 2.2b shows a UV-Vis extinction spectrum of the initial seeds. Instead of seeing a single peak at 520 nm characteristic of the LSPR of Au nanoparticles, I observed an interesting pattern of absorption bands with three distinct peaks positioned at 350, 470, and 600 nm. This pattern resembles the spectroscopic feature of small Au clusters.[64-66] To validate this assumption, I characterized the seeds using matrix-assisted laser desorption ionization (MALDI) mass spectrometry.[67] As shown in Figure 2.2c, the majority of the seeds in the sample had a size of six Au atoms. No peak was detected at larger sizes in the mass spectrum. Although I could not resolve the exact size and structure of the initial seeds, our data suggests that they were dominated by small clusters with a relatively uniform size around six Au atoms.

2.3 Synthesis of Au Spheres with Controlled Sizes in the Range of 5-150 nm

Figure 2.3 shows a schematic illustration of the procedure used for the preparation of Au nanospheres with diameters controlled in the range of 5-150 nm. In a typical process, $HAuCl_4$, CTAC, and AA served as Au precursor, stabilizing agent, and

reductant, respectively. More specifically, Au nanospheres with diameters in the range of 5–16 nm were obtained first by using CTAB-capped Au clusters as the seeds. In the following two steps, the 10- and 46-nm Au nanospheres were employed as the seeds to generate Au nanospheres with diameters in the range of 15-80 nm and 70-150 nm, respectively. It should be noted that the Au precursor solution had to be added into the reaction solution in one-shot injection with a pipette in the first step whereas the Au precursor had to be added dropwise using a syringe pump in the second and third rounds of growth. Figure 2.4 shows TEM images of Au nanospheres with diameters in the range of 5-16 nm that were prepared by seeding the growth with the initial, CTAB-capped Au clusters. The diameters of the Au nanospheres could be easily varied by controlling the volume of the cluster solution added into the reaction mixture. Specifically, when the volumes of the cluster solution were 1000, 500, 50, and 20 μL, respectively, the diameters of the resultant nanospheres were 5, 8, 10, and 16 nm, respectively.

In the second round of growth, the as-prepared 10-nm Au nanospheres served as the seeds to generate Au nanospheres with diameters increasingly tuned from 15 nm to 80 nm. As shown in Figure 2.5, when the volumes of the 10-nm seed solution were 300, 100, 10, and 5 μL, respectively, the diameters of the resultant nanospheres were tuned to 15, 23, 46, and 80 nm, respectively. The third round of growth used the same synthetic procedure as that for the second round except for the use of the as-prepared 46-nm Au nanospheres as the seeds. As shown in Figure 2.6, when the volumes of the 46-nm seed solution were 1500, 500, and 50 μL, respectively, the resultant nanospheres were 70, 100, and 150 nm, respectively, in diameter. Beyond this size, the products tended to evolve into nonspherical particles (Fig. 2.7). The average diameter (d_{av}), standard deviation (σ), and percentage of spherical particles (f), and detailed experimental conditions are summarized in Table 2.1. It should be noted that for each type of Au nanospheres, the standard deviation was less than 5% and the percentage of spherical particle was higher than 90%, indicating a high uniformity and purity for all the products.

To further validate the uniformity of our Au nanospheres, I also analyzed them using techniques other than electron microscopy, including UV-vis extinction spectroscopy and DLS, that work with an ensemble of particles. Figure 2.8 shows experimental and calculated UV-vis extinction spectra of Au nanospheres with different diameters. Both types of spectra displayed similar features in terms of extinction peak shape and position. Given the fact that the calculation was based on individual particles and the particle had a perfectly spherical shape, the matching of experimental and calculated spectra suggest that our Au nanospheres had a spherical shape as shown in the TEM images.

Figure 2.9 shows DLS data from these Au nanospheres. Only one peak was observed for the size distribution of each sample of Au nanospheres, indicating its monodispersity in size. The average hydrodynamic diameters and standard deviations obtained from the DLS data are listed in Table 2.1. I noticed that the average hydrodynamic diameters were larger than the average diameters derived from the TEM images. Such differences could be attributed to the surfactant/solvation layer on the particle surface, such as water and CTAC molecules. In addition, the standard deviations obtained from DLS measurements differed significantly from those determined by TEM imaging. This discrepancy can be ascribed to the procedure used for the transformation of the Fredholm first kind of equation in the DLS method, which is irrelevant to the characteristics of a colloidal suspension.[68] Similar widening of the size distribution in the DLS method has already been noted repeatedly in the literature.[69-71] Due to the presence of CTA micelles in the system, the DLS data of Au nanospheres of 5, 8, and 10 nm in diameter became unreliable so I decided not to include them. Taken together, I have characterized and confirmed the monodispersity of our Au nanospheres using TEM, UV-vis extinction spectra, and DLS.

As a reductant in the growth step, AA was oxidized to a stable form of dehydroascorbic acid by losing two electrons so that only 1.5 moles of AA would be

needed to reduce 1 mole of Au(III) precursor to Au(0). In the first-roung growth, however, the molar ratio between AA and $HAuCl_4$ was set to 150, and the large excess amount of AA would ensure a relatively fast reduction, which seemed to play a critical role in the formation of single-crystal nanoparticles. To evaluate the impact of reduction rate on the crystallintiy of resultant particles, I conducted two control experiments with relatively slower reduction rates for the Au(III) precursor. In one experiment, the molar ratio of AA to $HAuCl_4$ was reduced from 150 to 1.5. In the other experiment, the capping agent CTAC was replaced with CTAB at the same concentration. Due to a fast ligand change between $[AuCl_4]^-$ and Br^- ions from CTAB, the actual Au(III) precursor in the reaction system should be $[AuBr_4]^-$ rather than $[AuCl_4]^-$. Since the standard redox potential of $AuBr_4^-/Au$ (+0.85 V) is lower than that of $AuCl_4^-/Au$ pair (+0.93 V), it is more difficult to reduce $AuBr_4^-$ and thus the reduction will be slowed down.[72] As shown in Figure 2.10, a large number of twinned particles appeared in the final products of both syntheses. In these cases, it is not unreasonable to assume that the difference in crystallinity was caused by the difference in reduction rate for the Au precursor. Similar to what was reported for other metals, a fast reduction rate tended to favor the formation of single-crystal products.[73,74]

Unlike the one-shot injection of Au precursor in the first round, I had to add the Au precursor dropwise using a syringe pump in the second and third rounds. This modification was found to be critical to the formation of Au nanospheres with diameters larger than 30 nm due to the large length scale involved in the diffusion of surface atoms. To confirm the role played by the injection rate of Au precursor in determining the formation of Au nanospheres, I varied the injection rate of precursor solution in the second round. As shown in Figure 2.11, for the 23-nm Au nanospheres, if the precursor solution was injected in one-shot while all other parameters were kept the same; the products were dominated by cubic Au nanocrystals (Fig. 2.11a). A slightly slower injection rate would still lead to the formation of nanocrystals with nonspherical shapes.

Specifically, when the injection rates were set to 1 mL/h and 0.5 mL/h, cuboctahedrons and truncated octahedrons (Fig. 2.11, b and c) were obtained, respectively. These results indicate the critical role played by the injection rate of Au precursor in maintaining the spherical shape during seed-mediated growth.

As demonstrated in our recent study, the growth pattern of a seed is governed by the ratio between the rates for atom deposition and surface diffusion.[75] Considering that the rate for surface diffusion is mainly determined by the reaction temperature and each set of the experiments were conducted under the same conditions except for the injection rate of Au precursor, the diffusion rate was supposed to be fixed and thus the observed shape variations could be attributed to the change in deposition rate. When the Au precursor was rapidly injected into a reaction solution, the growth should be dominated by atom deposition only as surface diffusion over a large length scale could be neglected. A preferential deposition along <111> directions on a spherical seed led to the formation of nanocube mainly covered by {100} facets.[76] In contrast, when Au precursor solution was added slowly in a dropwise manner, the deposition rate would be significantly reduced. In this case, the newly deposited Au atoms could have sufficient time to migrate to adjacent {100} facets. As a result, the growth pathway, enabled by surface diffusion, became partially switched to <100> directions, leading to a gradually reduced proportion for {100} facets in the final product and truncated octahedrons would be formed. At a moderate injection rate for Au precursor, the growth rates along the <111> and <100> directions could become roughly the same, making it possible to maintain the shape spherical Au seeds during successive, seed-mediated growth.

I also investigated the role of reductant (AA) concentration in the formation of Au nanospheres. Figure 2.12 shows the products obtained using the same procedure except for the variation of AA amount. When the amount of AA was increased from 1.3 μmol to 1.5 μmol, the products were still dominated by nanocrystals with a spherical profile (Fig. 2.12a). At relatively larger amounts of AA (e.g., 2.0 μmol and 3.0 μmol), I observed a

noticeable loss of spherical shape for the resultant Au nanocrystals (Fig. 2.12, b and c). Although a limited supply of Au precursor was involved due to the dropwise addition of $HAuCl_4$, a relatively high concentration of AA could still accelerate the reduction and thus increase the deposition rate.[77] Taken together, an appropriate ratio between the rates for atom deposition and surface diffusion was critical to promoting the growth of seeds into larger particles without losing the spherical shape. In general, fast deposition rates or slow surface diffusion rates would force the spherical seeds to evolve into nonspherical ones.

Besides the injection rate for the Au precursor and the amount of reductant, I also tried to modulate the reaction by varying the type of halide ions present in the system. When Br^- anions were added into the reaction system, the products were dominated by nanocrystals with a cuboctahedral shape (Fig. 2.13a). A replacement of Br^- ions by I^- ions at the same concentration would lead to the formation of Au nanocrystals exhibiting a truncated octahedral profile (Fig. 2.13b). In both cases, the presence of Br^- or I^- ions, in addition to Cl^- anions, could no longer promote the formation of Au nanocrystals with a spherical profile. This shape variation may arise from the difference in affinity between halide ions toward the surface of Au nanocrystals. According to hard and soft Lewis acids and bases (HSAB) theory, a larger and less electronegative halide can have an increasing binding affinity with Au.[78] Therefore, a higher affinity to the surface of Au nanocrystals should be expected when either Br^- or I^- anions were present.[79-83] Their interactions may have changed the growth mode and thus be responsible for the observed shape variation. Unlike the common use of CTAB in the previous syntheses of Au nanocrystals, i.e., rods and octahedrons, I include sufficient amount of CTAC in the current synthesis. The use of CTAC not only protected nanocrystals from aggregations, but also completely excluded those halide anions with larger affinity with Au from the reaction system and thus contributed to the growth of spherical seeds without noticeable shape change.[84-85]

2.4 Self-Assembly of Au Spheres upon Dilution with Water

Besides their use as seeds, the as-prepared Au nanospheres were found to self-assemble into nanostructures with a number of interesting morphologies when their aqueous suspensions were diluted with deionized water. In a typical demonstration, 1 mL of the as-prepared suspension of 10-nm Au nanospheres was centrifuged and washed with deionized water once. Then, the collected precipitates were re-dispersed in 1 mL of deionized water, forming a new suspension. No dimerization or aggregation was found in this suspension, as indicated in Figure 2.4c. However, if this suspension was diluted two times in volume, some of the nanospheres self-assembled into dimers and trimers (Fig. 2.14a). When this suspension was further diluted by two folds in volume, the dimers and trimers further aggregated into larger structures (Fig. 2.15). Interestingly, further dilution by two times led to the formation of Au wavy nanowires (Fig. 2.14b).[86,87] The aggregation was likely triggered by the drop in surface coverage by surfactant during dilution with deionized water. When the suspension was diluted to 2, 4, and 8 times in volume, the zeta-potential also dropped from 39.4 to 29.5, 22.0, and 14.7 mV. The zeta potentials for all these samples were positive in sign due to the presence of CTA (which contains a positively charged end group) on the surface.[88] The zeta-potential decreased along with dilution because the CTA molecules were expected to desorb from the surface as a result of dilution. Figure 2.14c shows a high-resolution TEM image of the portion that connects the two Au nanospheres in a dimer, where the boundary can hardly be resolved due to atomic fusion of the two surfaces. Figure 2.14d shows a high-resolution TEM image taken from a representative segment of a Au wavy nanowire. Both single-crystal and boundary zones can be observed on this segment.

It should be pointed out that the 10-nm Au nanospheres were capped and stabilized by a double layer of CTAC molecules on the surface. The surface-bound CTAC molecules were in equilibrium with those dissolved in the solution phase. When

the Au nanospheres were collected by centrifugation and then re-dispersed in deionized water, the concentration of CTAC molecules in the solution was greatly reduced and thus the equilibrium had to be shifted. Some of the surface-bound CTAC molecules would start to desorb from the surface and enter into the solution phase. As such, some of the Au nanospheres would change their surfaces from hydrophilic (for a double layer) to hydrophobic (for a partial double layer).[89] The hydrophobic interaction between these Au nanospheres would drive them to assemble into dimers and trimers. Upon further dilution, the dimers and trimers preferentially assembled into larger aggregates and some of them assemble linearly to form necklaces.[90] Based on previous studies, the diffusion barrier for a single metal atom on a metal surface is quite low (typically less than 1 eV).[91] When the surface was not capped with enough CTAC molecules, it became much easier for Au atoms to diffuse on the surface of the necklace and reduce the total surface energy, leading to the formation of Au wavy nanowires. Similar assembly of nanostructures has also been observed in the case of semiconductor nanomaterials. For instance, CdTe nanoparticles were found to spontaneously reorganize into crystalline nanowires upon controlled removal of the protective shell of organic stabilizer.[92]

In addition, I also tested the stability of CTAC-capped Au nanospheres with sizes of 5 and 17 nm, respectively. As shown in Figure 2.16, a-c, the 5-nm Au nanospheres were found to self-assemble into dimers, larger aggregates, and wavy nanowires, when they were diluted to 2, 4, and 8 times of volume, respectively. This trend of morphological change was in good agreement with the case of the 10-nm Au nanospheres. For the 17-nm Au nanospheres, however, similar small structures were produced but no formation of wavy nanowires was observed (Fig. 2.16, d-f). As the particles increased in size, it might be difficult for Au atoms to diffuse and fully occupy the gap regions. In this case, only aggregations or necklace-like nanostructures could be obtained for relatively large Au nanospheres upon dilution. Taken together, it is not

unreasonable to conclude that the size also played a critical role in influencing the stability of CTAC-capped Au nanoparticles.

2.5 Conclusion

In summary, I have successfully synthesized single-crystal Au nanospheres with controlled diameters in the range of 5-150 nm via successive seed-mediated growth. In the first step, I obtained Au nanospheres with diameters tunable in the range of 5-16 nm by varying the amount of CTAB-capped Au clusters that served as the initial seeds. In the second round, the as-obtained 10-nm Au nanospheres served as the seeds to generate Au nanospheres with diameters continuously tunable from 15 nm to 80 nm. Following the same protocol for the second round, the next step involved the use of the 46-nm Au nanospheres as the seeds to synthesize Au nanospheres with even larger diameters in the range of 70-150 nm. I found that dropwise injection of Au precursor solution using a syringe pump, a relatively low amount of reductant, and the absence of halide anions with strong affinity toward Au in the second and third rounds were all critical to the formation of spherical Au nanocrystals in high yields. Interestingly, when the 10-nm Au nanospheres were collected by centrifugation, dispersed in deionized water, and diluted to different volumes, they spontaneously assembled into dimers, trimers, necklace, and finally wavy nanowires, depending on the degree of dilution. This work offers a simple and robust route to the synthesis of single-crystal Au nanospheres with uniform, controllable diameters over a broad range from 5 nm to 150 nm, which will find immediate use in the syntheses of bimetallic nanostructures, fabrication of metallic photonic crystals, and biomedical research.

2.6 Experimental Section

Chemicals and materials. Gold(III) chloride trihydrate ($HAuCl_4$ $3H_2O$, ≥99.9%), ascorbic acid (AA, ≥99.0%), sodium borohydride ($NaBH_4$, 98%), cetyltrimethylammonium bromide (CTAB, ≥99%), and cetyltrimethylammonium chloride (CTAC, 25 wt.% in water) were all obtained from Sigma-Aldrich and used as received. In all experiments, I used deionized water with a resistivity of 18.2 MΩcm, which was prepared using an ultrapure water system (Millipore, Billerica, MA). Aqueous $NaBH_4$ solution (10 mM) was prepared by dissolving 15.1 mg of $NaBH_4$ powder in 40 mL of water. The 10-mL syringe (part No. 309604) and syringe pump (part No. 14831200) were obtained from BD and Thermo Fisher Scientific, respectively.

Preparation of the initial, CTAB-capped Au clusters. A fresh aqueous $NaBH_4$ solution (10 mM, 0.6 mL) was rapidly added into a thoroughly mixed 10-mL aqueous solution containing $HAuCl_4$ (0.25 mM) and CTAB (100 mM) using a pipette. A brown solution immediately formed upon the introduction of $NaBH_4$. The mixture was placed on an orbital shaker at a speed of 300 rpm for 2 min, and then kept undisturbed at 27 ℃ for 3 h to ensure complete decomposition of $NaBH_4$ remaining in the reaction mixture.

Standard procedure for the preparation of Au nanospheres with diameters in the range of 5-16 nm. Aqueous solutions of CTAC (200 mM, 2 mL), AA (100 mM, 1.5 mL), and the initial, CTAB-capped Au clusters were mixed in a 20 mL glass vial, followed by one-shot injection of an aqueous $HAuCl_4$ solution (0.5 mM, 2 mL). See Table 2.1 for the volume of cluster solution and the corresponding diameter. The reaction was allowed to continue at 27 ^{o}C for 15 min. The product was collected by centrifugation at 14,500 rpm for 30 min, and then washed with water once for further use and characterization. The 10-nm Au nanospheres were dispersed in 1 mL of aqueous CTAC solution (20 mM) after washing, which was used as seeds in the second round of growth.

Standard procedure for the preparation of Au nanospheres with diameters in the range of 15-80 nm. Aqueous solutions of CTAC (100 mM, 2 mL), AA (10 mM, 130

μL), and the 10-nm seeds were mixed in a 20 mL glass vial, followed by dropwise addition of aqueous $HAuCl_4$ solution (0.5 mM, 2 mL) using a syringe pump at an injection rate of 2 mL/h. See Table 2.1 for the volume of the 10-nm seed solution and the corresponding diameter. The reaction was allowed to proceed at 27 ^oC for 10 min after the injection had been finished. The final product was collected by centrifugation at 14,500 rpm for 10 min and washed with water once for characterization. The aqueous suspension of 46-nm Au nanospheres was mixed with 0.86 mL of water and then used as seeds for the third round of growth.

Standard procedure for the preparation of Au nanospheres with diameters in the range of 70-150 nm. Aqueous solutions of CTAC (100 mM, 2 mL), AA (10 mM, 130 μL), and the 46-nm seed solution were mixed in a 20 mL glass vial, followed by dropwise addition of aqueous $HAuCl_4$ solution (0.5 mM, 2 mL) using a syringe pump. The injection rate was 2 mL/h. See Table 2.1 for the volume of the 46-nm seed solution and the corresponding diameter. The reaction was allowed to proceed at 27 ^oC for 10 min after the injection had been finished. The final product was collected by centrifugation at 14,500 rpm for 10 min, and then washed with water once prior to characterization.

Self-assembly of Au nanospheres upon dilution with deionized water. 1 mL of the as-prepared suspension of Au nanospheres was centrifuged (5-nm sample: 55,000 rpm for 30 min; 10-nm and 16-nm samples: 14,500 rpm for 30 min) and washed with deionized water once. The precipitate was collected and re-dispersed in 1 mL of deionized water. Finally, this suspension was diluted to different volumes with deionized water to obtain the nanostructures shown in Figure 2.14-2.16.

Experimental details for MALDI mass spectroscopy analysis. MALDI mass spectra were obtained using a time-of-flight mass spectrometer (Voyager System 4254, Applied Biosystems, Carlsbad, CA) equipped with a N_2 laser (337 nm). The matrix solution was prepared by dissolving 1 mg of DCTB powder in 50 μL of methanol. The suspension of initial CTAB-capped Au seeds was filtered through a syringe filter with a

pore size of 200 nm to remove crystals of CTAB. 10 μL of the filtered suspension was mixed with 10 μL of the as-prepared matrix solution in a centrifuge tube. The mixture was vortexed for 5 min to ensure complete mixing. Finally, the solution was cast on a stainless steel plate and dried under air for 1 h. The spectra were obtained in positive ionization and linear configuration at an acceleration voltage of 20 kV with delayed extraction mode. In general, 200 laser shots were used for the acquisition of each spectrum.

Instrumentation. Transmission electron microscopy (TEM) images were captured using a Tecnai G2 Spirit Twin microscope operated at 120 kV (FEI, Hillsboro, OR). High-resolution TEM images were obtained using a field-emission JEM-2100F microscope operated at 200 kV (JEOL, Tokyo, Japan). The samples were prepared by dropping aqueous suspensions of the nanoparticles onto carbon-coated Cu grids (Ted Pella, Redding, CA) and dried under ambient conditions in air. The concentration of Au nanoparticles was measured through a combination of TEM imaging and ICP-MS (Elan DRC II, PerkinElmer, Waltham, MA). UV-vis extinction spectra were recorded using a Lambda 750 UV-vis spectrometer (PerkinElmer, Waltham, MA). The size distributions and zeta potentials were measured using Zetasizer Nano ZS (Malvern, Westborough, MA).

Table 2.1. The average diameter (d_{av}) and its standard deviation (σ), the average hydrodynamic diameter (d_{hydro}) and its standard deviation (σ_{hydro}), the type of seed, and the volume (V) of seed solution for the Au nanospheres displayed in Figures 2.4-2.6. The average diameter (d_{av}) and its standard deviation were calculated from the TEM images by counting 50-100 particles. The average hydrodynamic diameter (d_{hydro}) and its standard deviation were obtained from DLS measurements.

d_{av} (nm)	σ (%)	d_{hydro} (nm)	σ_{hydro} (%)	type of seed	V (μL)
5.2	0.52	n/a	n/a	clusters	1000
8.0	0.54	n/a	n/a		500
10	0.81	n/a	n/a		50
16	1.6	26.81	35.6		20
15	1.1	26.25	42.2	10-nm spheres	300
23	1.1	36.46	34.8		100
46	1.9	58.55	20.2		10
80	1.3	103.0	26.8		5
70	1.5	103.5	14.1	46-nm spheres	1500
1.0×10^2	3.1	131.9	23.2		500
1.5×10^2	4.8	198.0	29.2		50

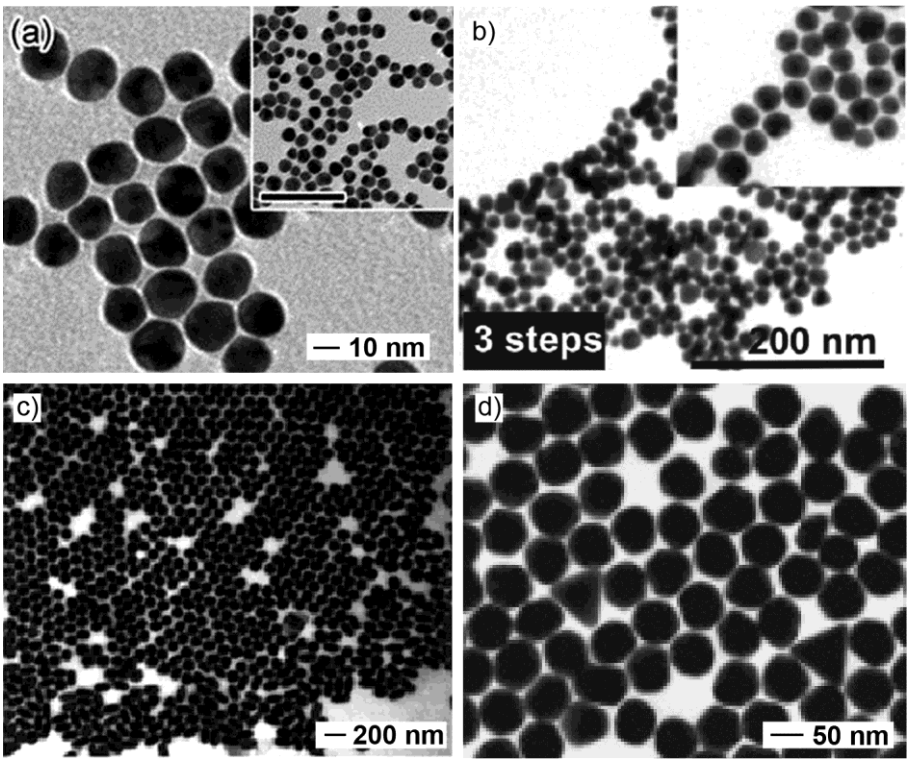

Figure 2.1. Representative TEM images of Au nanospheres with different sizes: a) 17.5 nm,[93] b) 19.2 ±2.6 nm,[94] c) 37 ±5 nm,[95] and d) 66 nm.[96] , which have been reported in literature.

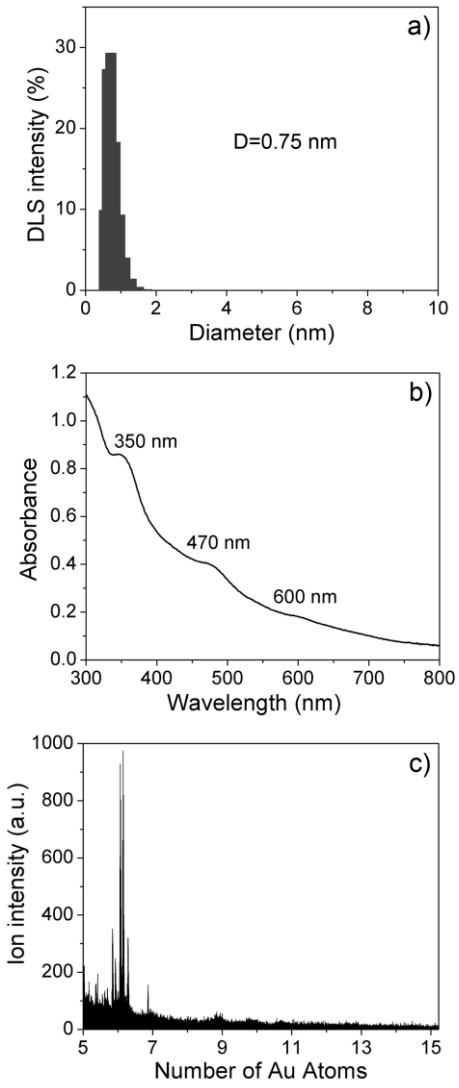

Figure 2.2. a) Size distribution of the initial Au seeds as measured by DLS. b) UV-vis spectrum of the initial Au seeds suspended in water. c) Positive-ion MALDI mass spectrum of the initial Au seeds.

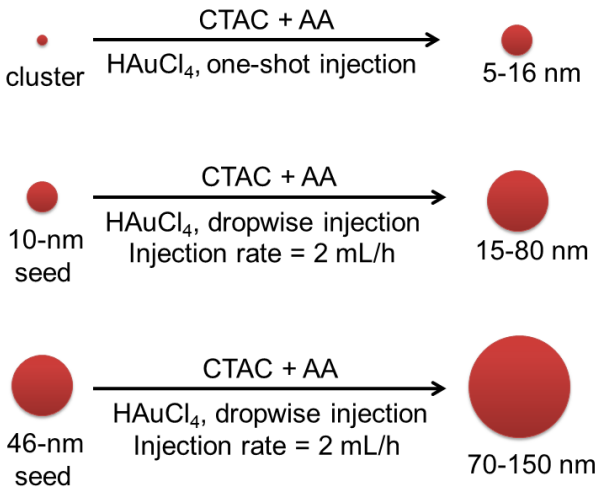

Figure 2.3. Schematics illustrating the successive growth procedure used for the preparation of Au nanospheres with controlled diameters increasingly tuned from 5 nm to 150 nm.

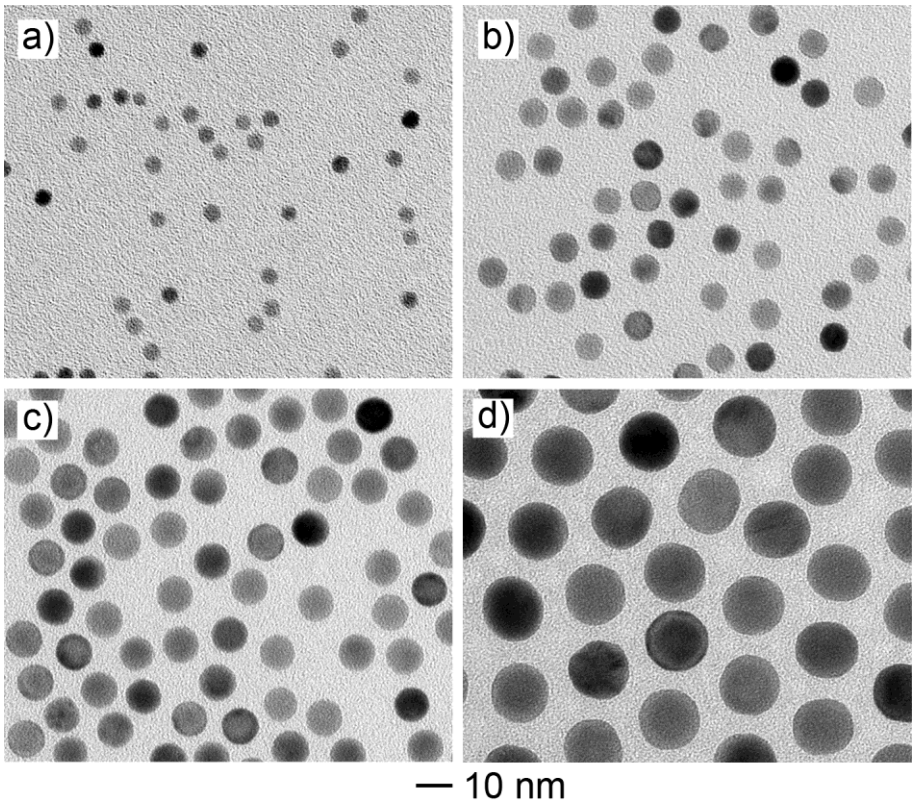

Figure 2.4. TEM images of single-crystal Au nanospheres with controlled diameters in the range of 5-16 nm: a) 5 nm; b) 8 nm; c) 10 nm; and d) 16 nm. They were obtained using the standard one-shot injection procedure, except that the volumes of the initial, CTAB-capped cluster solution were: a) 1000 μL; b) 500 μL; c) 50 μL; and d) 20 μL, respectively.

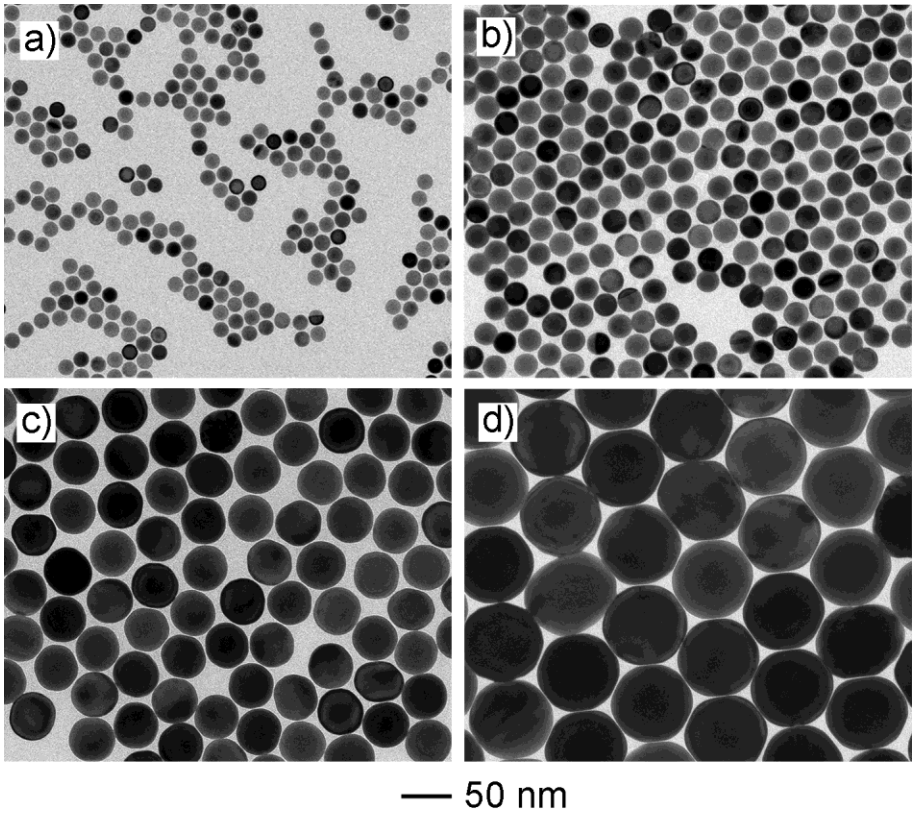

Figure 2.5. TEM images of single-crystal Au nanospheres with controlled diameters in the range of 15-80 nm: a) 15 nm; b) 23 nm; c) 46 nm; and d) 80 nm. They were obtained using the standard dropwise injection procedure, except that the volumes of the 10-nm seed solution were: a) 300 μL; b) 100 μL; c) 10 μL; and d) 5 μL, respectively.

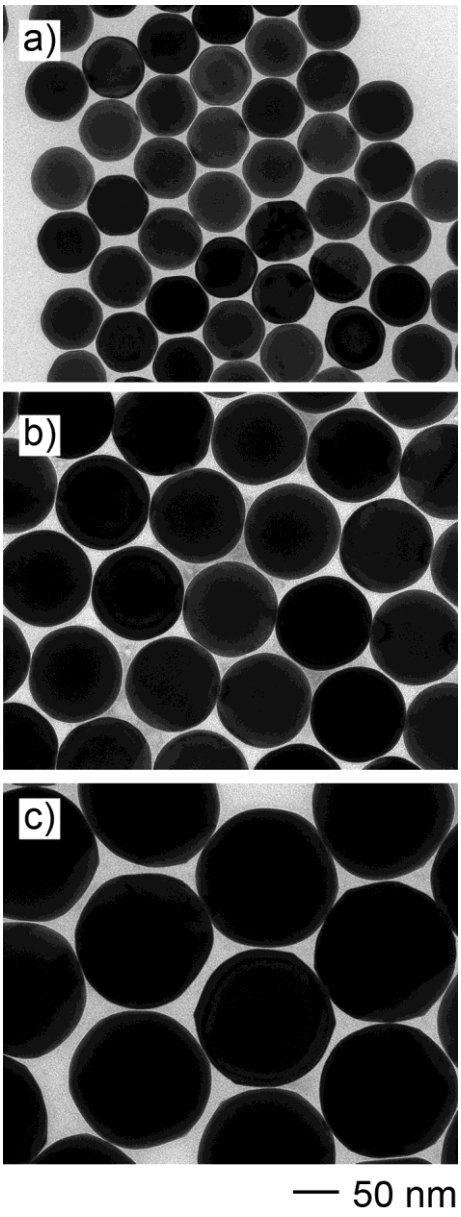

Figure 2.6. TEM images of single-crystal Au nanospheres with controlled diameters in the range of 70-150 nm: a) 70 nm; b) 100 nm; and c) 150 nm. They were obtained using the standard dropwise injection procedure, except that the volumes of the 46-nm seed solution were: a) 1500 μL; b) 500 μL; and c) 50 μL, respectively.

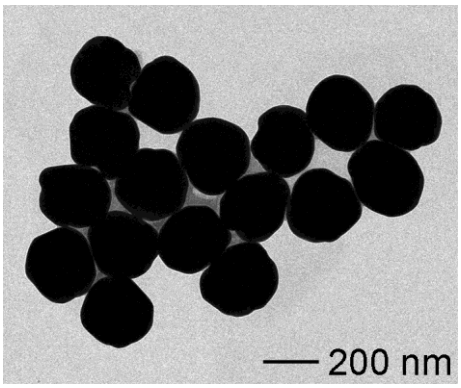

Figure 2.7. TEM images of Au nanocrystals obtained using the standard dropwise injection procedure, with the addition of 20 μL of the 46-nm seed solution.

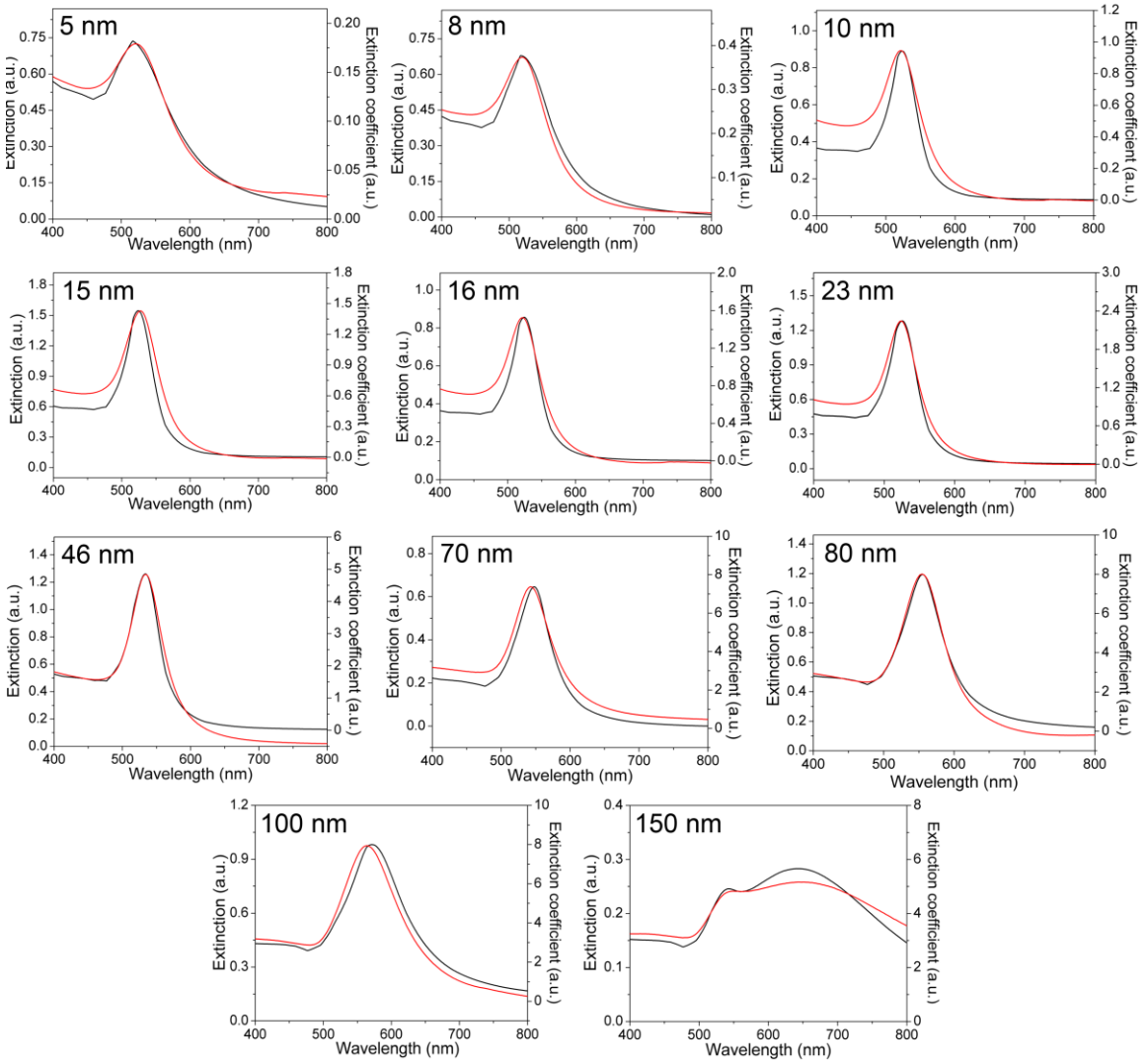

Figure 2.8. Experimental (red curve) and calculated (black curve) UV-vis extinction spectra of Au nanospheres with different diameters. The calculated spectra were obtained for individual particles using Mie theory by taking into consideration that the Au nanospheres were coated by a CTAC double layer on the surface (with a reflective index of 1.45 and 5 nm in thickness). Surface corrections were applied in the calculations for 5-nm and 8-nm Au nanospheres.[1]

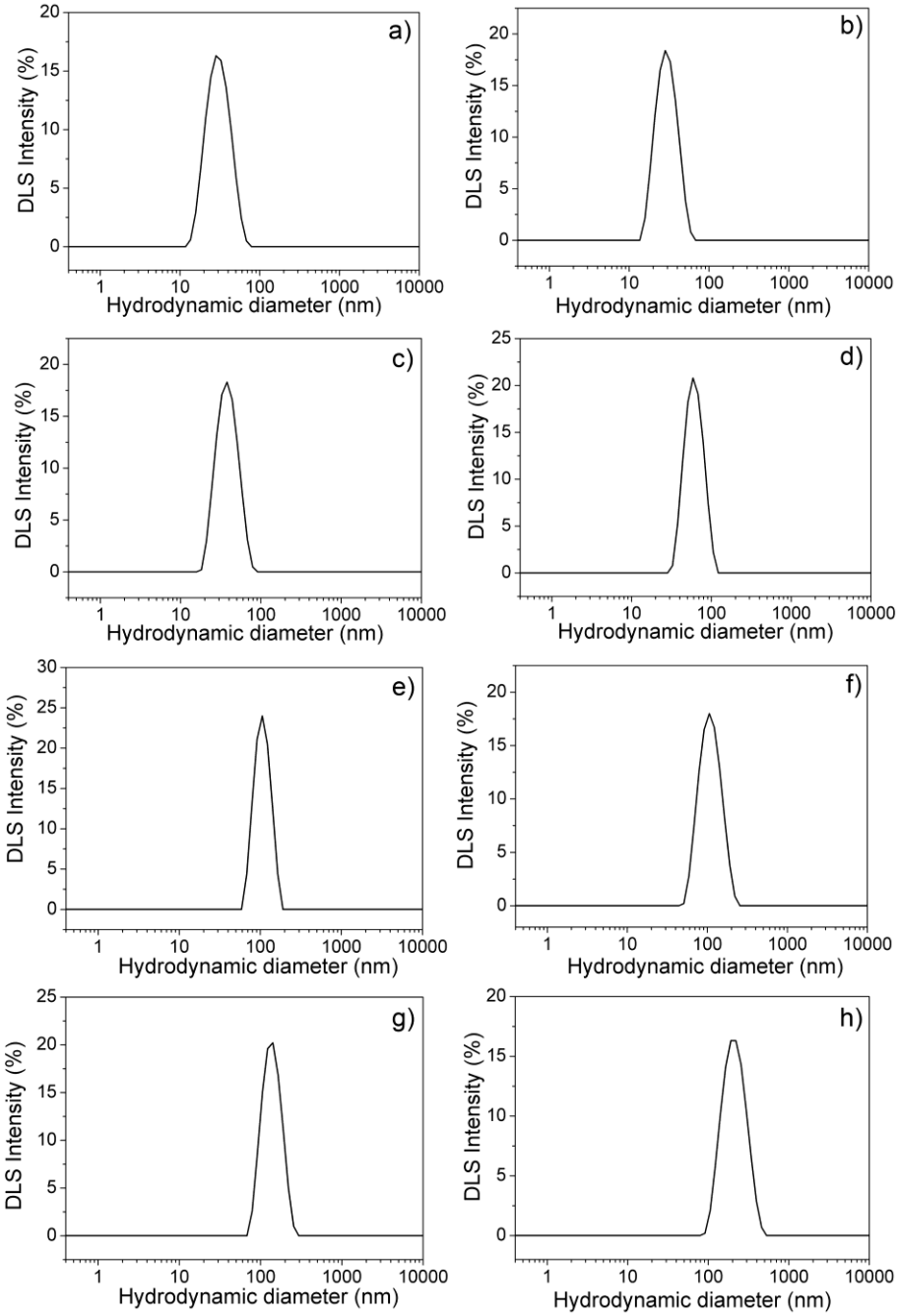

Figure 2.9. Hydrodynamic diameter distributions of Au nanospheres with different diameters as measured by DLS: a) 15 nm; b) 16 nm; c) 23 nm; d) 46 nm; e) 70 nm; f) 80 nm; g) 100 nm; and h) 150 nm.

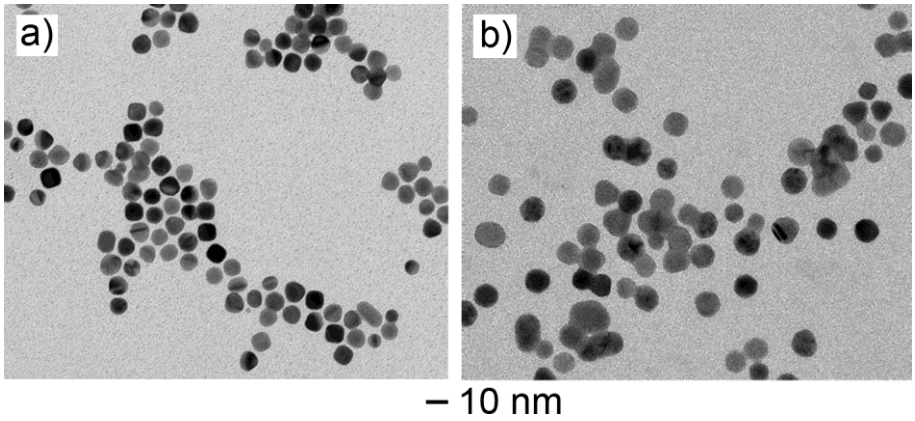

Figure 2.10. TEM images of Au nanospheres prepared using the standard procedure for 10-nm Au spheres except that a) the amount of ascorbic acid solution was reduced to 1.5 μmol and b) the capping agent was substituted by CTAB at the same concentration.

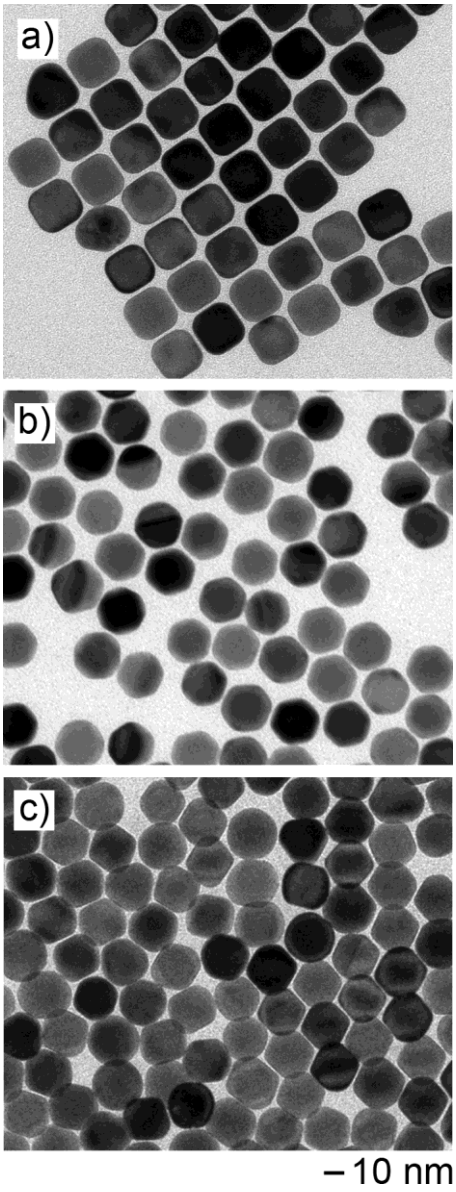

Figure 2.11. The effect of injection rate of Au precursor on the morphology of final products. TEM images of Au nanocrystals that were prepared using a procedure similar to what was used for the 23-nm Au nanospheres, except that 2 mL of Au precursor solution was added via a) one-shot injection and b, c) dropwise introduction at injection rates of b) 1 mL/h and c) 0.5 mL/h, respectively.

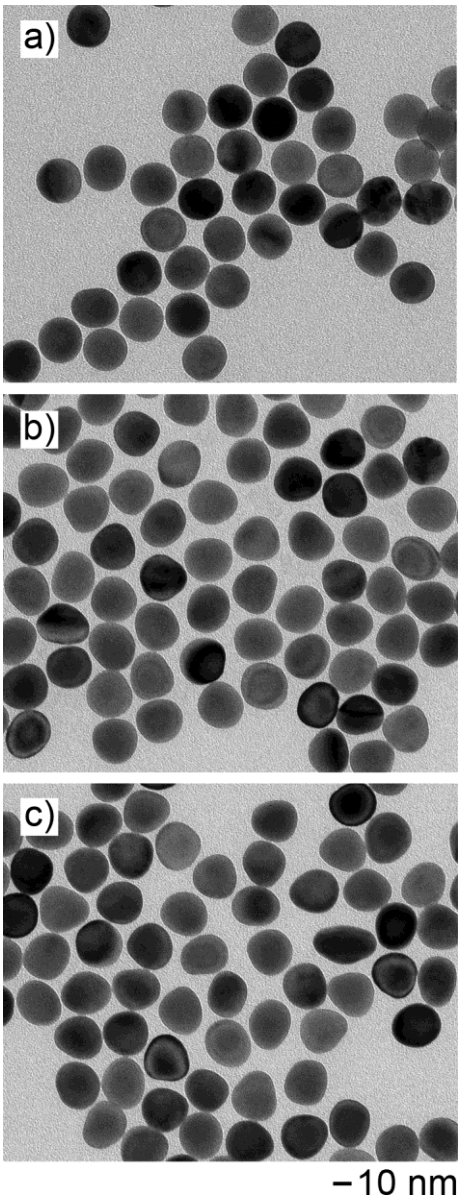

Figure 2.12. The effect of reductant (AA) amount on the morphology of final products. TEM images of Au nanocrystals that were prepared using a procedure similar to what was used for the 23-nm Au nanospheres, except that the amount of AA was increased from 1.3 μmol to a) 1.5 μmol; b) 2.0 μmol; and c) 3.0 μmol, respectively.

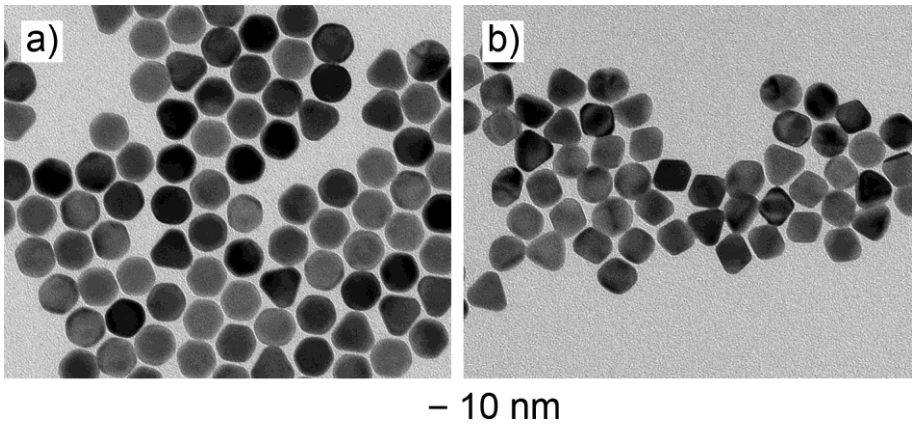

Figure 2.13. The effect of halide ions on the morphology of final products. TEM images of Au nanocrystals that were prepared using the a procedure similar to what was used for the 23-nm Au nanospheres, except for the additional 10 μmol of a) KBr and b) KI, respectively.

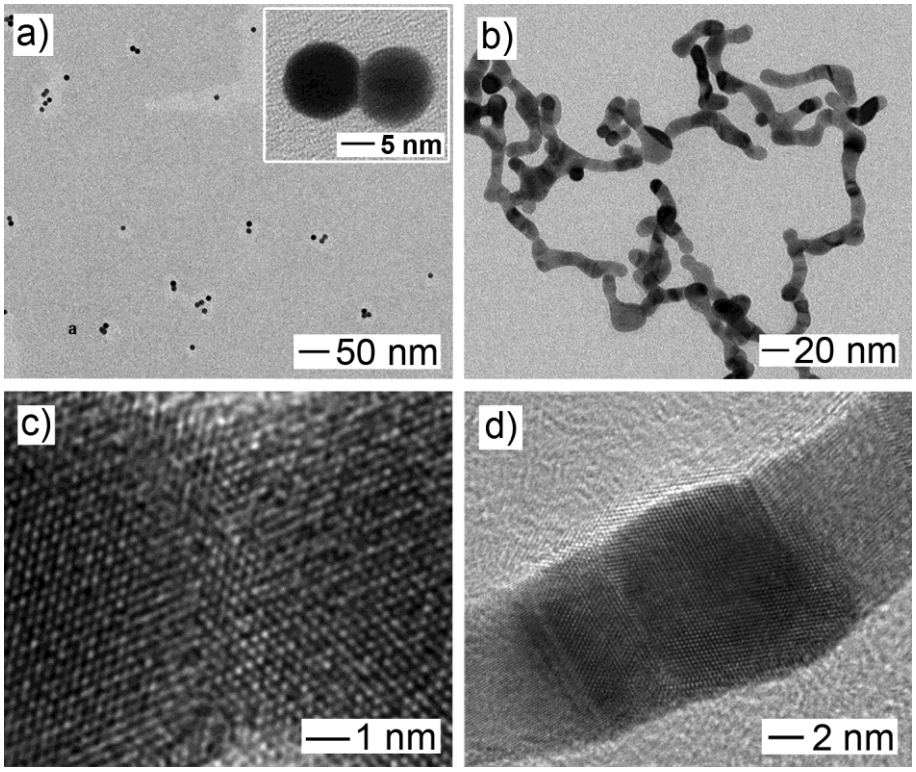

Figure 2.14. a-b) TEM of Au nanostructures in the form of a) dimers and trimmers and b) wavy wires. The nanostructures were formed by simply diluting an aqueous suspension of the 10-nm Au nanospheres (after washing) to different times of volume: a) 2 and b) 8 times. c, d) High-resolution TEM images of c) the connection region of a Au dimer and d) a representative section taken from a Au wavy wire.

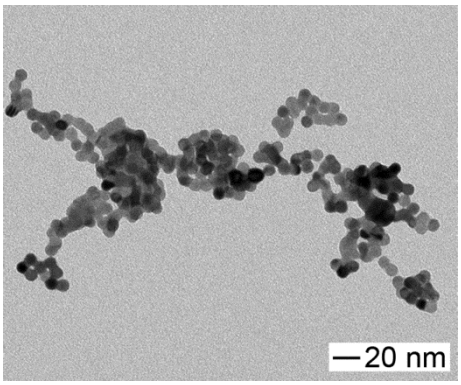

Figure 2.15. TEM image of Au nanostructures in the form of large aggregates.

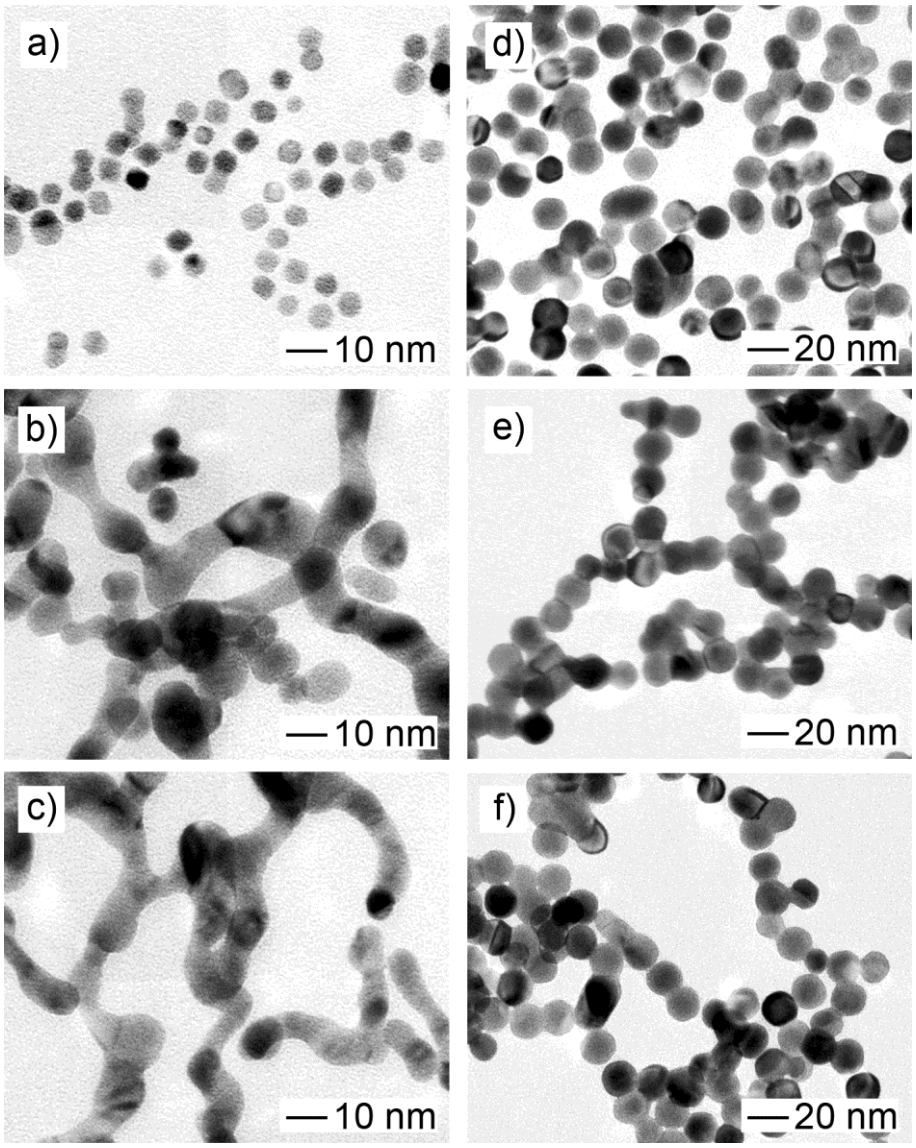

Figure 2.16. TEM images of Au nanostructures obtained by diluting an aqueous suspension of the a-c) 5-nm and d-f) 16-nm Au nanospheres (after washing) to a, d) 2; b, e) 4; and c, f) 8 times of volume.

2.7 References for Chapter 2

[1] C. J. Murphy, T. K. Sau, A. M. Gole, C. J. Orendorff, J. Gao, L. Gou, S. E. Hunyadi and T. Li, *J. Phys. Chem. B*, 2005, **109**, 13857-13870.

[2] E. C. Dreaden, A. M. Alkilany, X. Huang, C. J. Murphy and M. A. El-Sayed, *Chem. Soc. Rev.*, 2012, **21**, 2740-2779.

[3] C. J. Murphy, A. M. Gole, J. W. Stone, P. N. Sisco, A. M. Alkilany, E. C. Goldsmith and S. C. Baxter, *Acc. Chem. Res.*, 2008, **41**, 1721-1730.

[4] M.-C. Daniel and D. Astruc, *Chem. Rev.*, 2003, **104**, 293-346.

[5] M. Hu, J. Chen, Z.-Y. Li, L. Au, G. V. Hartland, X. Li, M. Marquez and Y. Xia, *Chem. Soc. Rev.*, 2006, **35**, 1084-1094.

[6] S. Eustis and M. A. El-Sayed, *Chem. Soc. Rev.*, 2006, **35**, 209-217.

[7] D. A. Giljohann, D. S. Seferos, W. L. Daniel, M. D. Massich, P. C. Patel and C. A. Mirkin, *Angew. Chem. Int. Ed.*, 2010, **49**, 3280-3294.

[8] H. Chen, X. Kou, Z. Yang, W. Ni and J. Wang, *Langmuir*, 2008, **24**, 5233-5237.

[9] P. K. Jain, K. S. Lee, I. H. El-Sayed and M. A. El-Sayed, *J. Phys. Chem. B*, 2006, **110**, 7238-7248.

[10] C. J. Orendorff, T. K. Sau and C. J. Murphy, *Small*, 2006, **2**, 636-639.

[11] S. E. J. Bell and M. R. McCourt, *Phys. Chem. Chem. Phys.*, 2009, **11**, 7455-7462.

[12] S. Link and M. A. El-Sayed, *J. Phys. Chem. B*, 1999, **103**, 4212-4217.

[13] P. N. Njoki, I. I. S. Lim, D. Mott, H.-Y. Park, B. Khan, S. Mishra, R. Sujakumar, J. Luo and C.-J. Zhong, *J. Phys. Chem. C*, 2007, **111**, 14664-14669.

[14] W. Haiss, N. T. K. Thanh, J. Aveyard and D. G. Fernig, *Anal. Chem.*, 2007, **79**, 4215-4221.

[15] V. Amendola and M. Meneghetti, *J. Phys. Chem. C*, 2009, **113**, 4277-4285.

[16] X. Liu, M. Atwater, J. Wang and Q. Huo, *Colloid Surface B*, 2007, **58**, 3-7.

[17] K. A. Willets and R. P. Van Duyne, *Annu. Rev. Phys. Chem.*, 2007, **58**, 267-297.

[18] B. J. Wiley, S. H. Im, Z.-Y. Li, J. McLellan, A. Siekkinen and Y. Xia, *J. Phys. Chem. B*, 2006, **110**, 15666-15675.

[19] K.-S. Lee and M. A. El-Sayed, *J. Phys. Chem. B*, 2006, **110**, 19220-19225.

[20] S. S. Shankar, A. Rai, B. Ankamwar, A. Singh, A. Ahmad and M. Sastry, *Nature Mater.*, 2004, **3**, 482-488.

[21] J. E. Millstone, G. S. Métraux and C. A. Mirkin, *Adv. Func. Mater.*, 2006, **16**, 1209-1214.

[22] T. K. Sau and C. J. Murphy, *J. Am. Chem. Soc.*, 2004, **126**, 8648-8649.

[23] X. Sun, S. Dong and E. Wang, *Langmuir*, 2005, **21**, 4710-4712.

[24] C. Li, K. L. Shuford, Q. H. Park, W. Cai, Y. Li, E. J. Lee and S. O. Cho, *Angew. Chem. Int. Ed.*, 2007, **46**, 3264-3268.

[25] D. Seo, J. C. Park and H. Song, *J. Am. Chem. Soc.*, 2006, **128**, 14863-14870.

[26] D. Seo, C. I. Yoo, I. S. Chung, S. M. Park, S. Ryu and H. Song, *J. Phys. Chem. C*, 2008, **112**, 2469-2475.

[27] F. Kim, S. Connor, H. Song, T. Kuykendall and P. Yang, *Angew. Chem. Int. Ed.*, 2004, **43**, 3673-3677.

[28] W. Niu, S. Zheng, D. Wang, X. Liu, H. Li, S. Han, J. Chen, Z. Tang and G. Xu, *J. Am. Chem. Soc.*, 2008, **131**, 697-703.

[29] K. Kwon, K. Y. Lee, Y. W. Lee, M. Kim, J. Heo, S. J. Ahn and S. W. Han, *J. Phys. Chem. C*, 2006, **111**, 1161-1165.

[30] J. Xu, S. Li, J. Weng, X. Wang, Z. Zhou, K. Yang, M. Liu, X. Chen, Q. Cui, M. Cao and Q. Zhang, *Adv. Func. Mater.*, 2008, **18**, 277-284.

[31] H.-L. Wu, C.-H. Kuo and M. H. Huang, *Langmuir*, 2010, **26**, 12307-12313.

[32] P.-J. Chung, L.-M. Lyu and M. H. Huang, *Chem. Eur. J.*, 2011, **17**, 9746-9752.

[33] T. K. Sau and C. J. Murphy, *Langmuir*, 2004, **20**, 6414-6420.

[34] B. Nikoobakht and M. A. El-Sayed, *Chem. Mater.*, 2003, **15**, 1957-1962.

[35] Y. Ma, Q. Kuang, Z. Jiang, Z. Xie, R. Huang and L. Zheng, *Angew. Chem. Int. Ed.*, 2008, **47**, 8901-8904.

[36] J. Zhang, M. R. Langille, M. L. Personick, K. Zhang, S. Li and C. A. Mirkin, *J. Am. Chem. Soc.*, 2010, **132**, 14012-14014.

[37] T. Ming, W. Feng, Q. Tang, F. Wang, L. Sun, J. Wang and C. Yan, *J. Am. Chem. Soc.*, 2009, **131**, 16350-16351.

[38] J. W. Hong, S.-U. Lee, Y. W. Lee and S. W. Han, *J. Am. Chem. Soc.*, 2012, **134**, 4565-4568.

[39] Z. L. Wang, *J. Phys. Chem. B*, 2000, **104**, 1153-1175.

[40] J. Zeng, Y. Zheng, M. Rycenga, J. Tao, Z.-Y. Li, Q. Zhang, Y. Zhu and Y. Xia, *J. Am. Chem. Soc.*, 2010, **132**, 8552-8553.

[41] M. Eguchi, D. Mitsui, H.-L. Wu, R. Sato and T. Teranishi, *Langmuir*, 2012, **28**, 9021–9026.

[42] Y. Ma, W. Li, E. C. Cho, Z. Li, T. Yu, J. Zeng, Z. Xie and Y. Xia, *ACS Nano*, 2010, **4**, 6725-6734.

[43] J. Li, Y. Zheng, J. Zeng, and Y. Xia, *Chem. Eur. J.*, 2012, **18**, 8150-8156.

[44] J. Turkevich, P. C. Stevenson and J. Hillier, *Disscuss. Faraday Soc.*, 1951, **11**, 55-75.

[45] K. R. Brown, D. G. Walter and M. J. Natan, *Chem. Mater.*, 1999, **12**, 306-313.

[46] G. Frens, *Nature: Phys. Sci.*, 1973, **241**, 20-22.

[47] B.-K. Pong, H. I. Elim, J.-X. Chong, W. Ji, B. L. Trout and J.-Y. Lee, *J. Phys. Chem. C*, 2007, **111**, 6281-6287.

[48] J. Kimling, M. Maier, B. Okenve, V. Kotaidis, H. Ballot and A. Plech, *J. Phys. Chem. B*, 2006, **110**, 15700-15707.

[49] M. K. Chow and C. F. Zukoski, *J. Colloid Interface Sci.*, 1994, **165**, 97-109.

[50] X. Ji, X. Song, J. Li, Y. Bai, W. Yang and X. Peng, *J. Am. Chem. Soc.*, 2007, **129**, 13939-13948.

[51] J. R. Polte, T. T. Ahner, F. Delissen, S. Sokolov, F. Emmerling, A. F. Thünemann and R. Kraehnert, *J. Am. Chem. Soc.*, 2010, **132**, 1296-1301.

[52] C. Ziegler and A. Eychmüller, *J. Phys. Chem. C*, 2011, **115**, 4502-4506.

[53] I. Hussain, S. Graham, Z. Wang, B. Tan, D. C. Sherrington, S. P. Rannard, A. I. Cooper and M. Brust, *J. Am. Chem. Soc.*, 2005, **127**, 16398-16399.

[54] Z. Wang, B. Tan, I. Hussain, N. Schaeffer, M. F. Wyatt, M. Brust and A. I. Cooper, *Langmuir*, 2006, **23**, 885-895.

[55] J. Niu, T. Zhu and Z. Liu, *Nanotechnology*, 2007, **18**, 325607.

[56] S. D. Perrault and W. C. W. Chan, *J. Am. Chem. Soc.*, 2009, **131**, 17042-17043.

[57] J. Song, D. Kim and D. Lee, *Langmuir*, 2011, **27**, 13854-13860.

[58] Y. Huang and D.-H. Kim, *Langmuir*, 2011, **27**, 13861-13867.

[59] C. Gao, J. Vuong, Q. Zhang, Y. Liu and Y. Yin, *Nanoscale*, 2012, **4**, 2875-2878.

[60] N. R. Jana, L. Gearheart and C. J. Murphy, *Langmuir*, 2001, **17**, 6782-6786.

[61] J. Rodríguez-Fernández, J. Pérez-Juste, F. J. García de Abajo and L. M. Liz-Marzán, *Langmuir*, 2006, **22**, 7007-7010.

[62] N. R. Jana, L. Gearheart and C. J. Murphy, *J. Phys. Chem. B*, 2001, **105**, 4065-4067.

[63] B. Nikoobakht and M. A. El-Sayed, *Langmuir*, 2001, **17**, 6368-6374.

[64] Y. Zhu, H. Qian, M. Zhu and R. Jin, *Adv. Mater.*, 2010, **22**, 1915-1920.

[65] J. M. Pettibone and J. W. Hudgens, *ACS Nano*, 2011, **5**, 2989-3002.

[66] N. Shao, Y. Pei, Y. Gao and X. C. Zeng, *J. Phys. Chem. A*, 2009, **113**, 629-632.

[67] H. Tsunoyama and T. Tsukuda, *J. Am. Chem. Soc.*, 2009, **131**, 18216-18217.

[68] R. Pecora, *Dynamic Light Scattering: Applications of Photon Correlation Spectroscopy*, Plenum, New York, NJ, USA **1985**.

[69] B. N. Khlebtsov, N. G. Khlebtsov, *Colloid J.*, **2011**, 73, 118.

[70] V. V. Klyubin, L. A. Kruglova, H. A. Sakharova, Y. A. Tallier, *Kolloidn. Zh.*, **1990**, 52, 470.

[71] V. V. Klyubin, V. N. Bungov, *Kolloidn. Zh.*, **1998**, 60, 344.

[72] J. A. Dean, *Lange's Chemistry Handbook*, McGraw-Hill Professional, New York, 1998.

[73] Q. Zhang, J. Xie, Y. Yu, J. Yang and J. Y. Lee, *Small*, 2010, **6**, 523-527.

[74] Y. Tang and M. Ouyang, *Nature Mater.*, 2007, **6**, 754-759.

[75] X. Xia, S. Xie, M. Liu, H. -C. Peng, N. Lu, J. Wang, M. J. Kim, Y. Xia, *Proc. Natl. Acad. Sci. USA* **2013**, 110, 6669.

[76] Z. L. Wang, *J. Phys. Chem. B* **2000**, 104, 1153.

[77] M. R. Langille, M. L. Personick, J. Zhang, C. A. Mirkin, *J. Am. Chem. Soc.* **2012**, 134, 14542.

[78] R. G. Pearson, *J. Am. Chem. Soc.* **1963**, 85, 3533.

[79] P.-J. Chung, L.-M. Lyu, M. H. Huang, *Chem. Eur. J.* **2011**, 17, 9746.

[80] J. E. Millstone, W. Wei, M. R. Jones, H. Yoo, C. A. Mirkin, *Nano Lett.* **2008**, 8, 2526.

[81] D. K. Smith, N. R. Miller, B. A. Korgel, *Langmuir* **2009**, 25, 9518.

[82] R. G. Rayavarapu, C. Ungureanu, P. Krystek, T. G. van Leeuwen, S. Manohar, *Langmuir* **2010**, 26, 5050.

[83] C. J. Murphy, L. B. Thompson, D. J. Chernak, J. A. Yang, S. T. Sivapalan, S. P. Boulos, J. Huang, A. M. Alkilany, P. N. Sisco, *Curr. Opin. Colloid Interface Sci.* **2011**, 16, 128.

[84] M. Tréguer-Delapierre, J. Majimel, S. Mornet, E. Duguet, S. Ravaine, *Gold Bull* **2008**, 41, 195.

[85] C. J. Murphy, T. K. Sau, A. M. Gole, C. J. Orendorff, J. Gao, L. Gou, S. E. Hunyadi, T. Li, *J. Phys. Chem. B* **2005**, 109, 13857.

[86] M. Chirea, A. Freitas, B. S. Vasile, C. Ghitulica, C. M. Pereira and F. Silva, *Langmuir*, 2011, **27**, 3906-3913.

[87] L. Pei, K. Mori and M. Adachi, *Langmuir*, 2004, **20**, 7837-7843.

[88] T. K. Sau and C. J. Murphy, *Langmuir*, 2005, **21**, 2923-2929.

[89] C. Zhu, H.-C. Peng, J. Zeng, J. Liu, Z. Gu and Y. Xia, *J. Am. Chem. Soc.*, 2012, **134**, 20234–20237.

[90] J. Liao, Y. Zhang, W. Yu, L. Xu, C. Ge, J. Liu and N. Gu, *Colloid Surface A*, 2003, **223**, 177-183.

[91] D. E. Sanders and A. E. DePristo, *Surf. Sci.*, 1992, **260**, 116-128.

[92] Z. Tang, N. A. Kotov and M. Giersig, *Science*, 2002, **297**, 237-240.

[93] C. Gao, J. Vuong, Q. Zhang, Y. Liu and Y. Yin, *Nanoscale*, 2012, **4**, 2875-2878.

[94] N. G. Bastús, J. Comenge and V. Puntes, *Langmuir*, 2011, **27**, 11098–11105.

[95] N. R. Jana, L. Gearheart and C. J. Murphy, *Langmuir*, 2001, **17**, 6782-6786.

[96] J. Rodríguez-Fernández, J. Pérez-Juste, F. J. García de Abajo and L. M. Liz-Marzán, *Langmuir*, 2006, **22**, 7007-7010.

CHAPTER 3

SEED-MEDIATED SYNTHESIS OF GOLD TETRAHEDRA IN HIGH PURITY AND WITH WELL-CONTROLLED SIZES

3.1 Introduction

Single-crystal Au nanocrystals are obtained by controlling the growth of cuboctahedral seeds and the products are typically encased by a combination of three common low-index facets: {100}, {111}, and {110}.[1-3] Notable examples include cubes, spheres, cuboctahedra, octahedra, tetrahedra, rhombic dodecahedra, and their derivate with different truncations at the corners and/or edges, as well as concave structures on the surface.[4-9] Although most of these Au nanocrystals could be produced with reasonable yields and controllable sizes, there has been limited progress in the prepration of Au nanocrystals with a tetrahedral shape. The technical challenge could be attributed to the reduction in symmetry.[10] As constrained by the inherent, face-centered cubic (*fcc*) lattice, most single-crystal nanocrystals has a high level of symmetry, while the symmetry of tetrahedron is relatively low (*i.e.*, O_h for cube/cuboctahedron/octahedron *versus* T_h for tetrahedron). Such a reduction in symmetry during crystal growth is usally unfavored by thermodyanmics and often requires a precise and fine control over the reaction kinetics.[11] Although there have been serveal sucessful attempts to manipulate the reaction kinetics in seed-mediated growth of Au nanocrystals, most of the products were still doominated by the symmetry consistent with a cube or octahedron.[4, 12-19]

To date, there are only two reports on the synthesis of Au tetrahedra.[8, 17] Both of them are based on the polyol synthesis. For example, Yang and coworkers prepared Au tetrahedra with a size of 210±20 nm by reacting Au precursor ($HAuCl_4$) with ethylene glycol in the presence of poly(vinylpyrrolidone) (PVP) at 280 ^oC under argon protection.[8] Lee and coworkers obtained Au truncated tetrahedra with a size of 290±40

nm by the reduction of $HAuCl_4$ with tetra(ethylene glycol) at 200 ^oC.[17] These Au tetrahedra were relatively low in percateg yield (typically, <70%) and the smallest size was limited to >200 nm. Additionally, there was no successful approach to tuning the size of these Au tetrahedra, neither was there any discussion of formation mechanism. As a result, it is still a grand challenge to generate tetrahedral Au nanocrysatals with tunable and well-controlled sizes, together with a good understanding of the mechanism responsible for the symmetry reduction.

Herein, I describe a facile route to the preparation of Au tetrahedra in high purity. The success of this synthesis relies on the use of single-crystal, spherical Au nanocrystals (10 nm in size) as the seeds and manipulation of the reaction kinetics of Au precursor to achieve an unsymmetrical growth pattern. The value of this work can be understood from the following aspects. First, thanks to the advantage of seeded growth, I was able to monitor the shape evolution process from spherical seeds to final products step by step, which reveals the formation mechanism for shape evolution from a sphere to a tetrahedron. Secondly, their sizes could be increased from 30 to 60 nm without losing the tetrahedral shape by simply varying the amount of Au precursor added into the reaction solution. To our knowledge, this is the first time that Au nanocrystals with a tetrahedral shape could be obtained with an edge length as small as 30 nm. Finally, the dropwise injection of Au precursor using a syringe pump, together with the use of a combination of cetyltrimethylammonium bromide (CTAB) and cetyltrimethylammonium chloride (CTAC) as stabilizers was found to be critical to promoting an unsymmetrical growth pattern and thus symmetry reduction for the Au nanocrystals. This strategy based on kinetic control could also be further extended to other noble metals.

3.2 Results and Discussion

I employed seed-mediated growth to prepare the Au tetrahedra. The single-crystal, spherical seeds of Au were obtained using an approach described in our previous report.[5] As shown in Figure 3.1a, all the spherical seeds exhibited high uniformity in terms of both size and shape, with an average diameter of 10 nm. The following synthesis involved the use of $HAuCl_4$, AA, and a combination of CTAC and CTAB, as the reductant, Au precursor, and stabilizer, respectively. In a standard process, the spherical seeds were mixed with aqueous solutions of AA, CTAB, and CTAC, followed by dropwise addition of aqueous $HAuCl_4$ solution using a syringe pump. As shown in Figure 3.1b, when 0.05 μmol of $HAuCl_4$ was added, the seeds still maintained a quasi-spherical shape. As more $HAuCl_4$ was introduced, these spherical seeds evolved into larger particles with a truncated tetrahedral profile (Fig. 3.1, c and d). Figure 3.1e shows models of truncated tetrahedra with four typical projections. The products began to display a well-defined tetrahedral shape with an average edge length of 30 nm as the amount of Au precursor reached 0.38 μmol (Fig. 3.2a).

As a major advantage of seed-mediated synthesis, the size of the resultant Au tetrahedra could be readily tuned from 30 to 60 nm by simply increasing the amount of $HAuCl_4$ added into the reaction solution. Figure 3.2, b-d, show TEM images of the Au tetrahedra obtained by injecting different amounts of $HAuCl_4$ into aqueous suspensions containing the same amount of Au seeds. It can be seen that the edge length of the resultant Au tetrahedra increased from 30 to 38, 45, and 60 nm, respectively, when the amount of $HAuCl_4$ was increased from 0.38 to 0.5, 1.0, and 1.5 μmol. Despite the difference in size, it should be pointed out that all these products maintained the tetrahedral shape without any noticeable deviation.

Different from the characteristic red color of spherical Au nanocrystals, aqueous suspensions of the as-prepared Au tetrahedra exhibited a blue or green color, demonstrating the impact of shape on their optical properties (Fig. 3.3a). Figure 3.3, b

and c, shows UV-vis extinction spectra taken from aqueous suspensions of Au tetrahedra with edge lengths of 30 nm and 60 nm and the corresponding theoretical calculations. When the edge length was increased from 30 nm to 60 nm, the major extinction peak shifted from 595 nm to 629 nm. In addition, there was a shoulder peak located roughly at 537 nm in the extinction spectra of 60-nm Au tetrahedra. Compared to Au nanospheres with similar sizes, the extinction peaks of Au tetrahedra showed significant red-shifts. This can be ascribed to the presence of sharp corners and edges on the surface of Au tetrahedra, which could trap the surface charges at these sites, leading to an increase in the degree of charge separation. As a result, the restoring force for electron oscillation would be reduced and the resonance peak would be shifted to longer wavelengths.[18, 19] I also compared the experimental results with the data obtained using the Finite Difference Time Domain (FDTD) method. The simulated spectra are in good agreement with the experimental results in terms of the peak position. The minor discrepancy in peak shape could be attributed to the idealized structural models used in the simulation in contrast to the variation in shape for a real sample, where there was always heterogeneity with regards to size and corner/edge truncation.

Unlike the one-shot injection of Au precursor employed in the synthetic protocols developed by Murphy, El-Sayed, and others, I had to add the Au precursor dropwise using a syringe pump in the current synthesis. This modification was found to be critical to the formation of Au tetrahedra in high purity. For example, when $HAuCl_4$ was added at an accelerated injection rate, most particles in the products would no longer exhibit a tetrahedral shape. Instead, they would display either a quasi-spherical (Fig. 3.4, a and b) or truncated tetrahedral shape (Fig. 3.4c). In contrast, a relatively slower injection rate had little influence on the shape of the final products (Fig. 3.4d). These results clearly suggested that a relatively slow injection rate of Au precursor should be beneficial to the formation of tetrahedral products in high purity. At a slow injection rate, the concentration of Au atoms derived from $HAuCl_4$ could be maintained at a relatively low

level around the spherical seed. In this case, only some of the facets of a Au seed were involved in the heterogeneous nucleation and growth, leading to symmetry reduction.[20] This observation is in good agreement with our previous study on the synthesis of Pd tetrahedra, in which the preferential growth on four of the eight {111} facets of an octahedron led to the formation of a tetrahedron.[21] In contrast, when the injection rate was fast, the Au atoms around a Au seed were maintained at a level sufficiently high so that more facets of a Au seed would be involved in the heterogeneous nucleation and growth. In this case, the products took a shape of truncated tetrahedron or quasi-sphere.

I also evaluated the effect of stabilizer in the current synthesis. As shown in Figure 3.5a, if no CTAB was present in the reaction solution, the final products were dominated by quasi-trisoctahedral Au nanocrystals.[22] In addition, the presence of CTAB at a low (Fig. 3.5, b and c) or high concentration (Fig. 3.5d) would no longer favor the formation of Au nanocrystals with a well-defined tetrahedral shape. These results indicated that the reaction kinetics was very sensitive to the concentration of CTAB. This is because a fast ligand exchange reaction between $[AuCl_4]^-$ and CTAB could occur and most of the Au(III) complex in the system would become $AuBr_4^-$. Since the $[AuBr_4]^-$ /Au(0) pair has a lower redox potential, $[AuBr_4]^-$/Au(0) $\approx$0.85 eV versus $[AuCl_4]^-$/Au(0) $\approx$ 0.93 eV, it is more difficult to reduce $[AuBr_4]^-$ to Au(0) than $[AuCl_4]^-$.[23] Therefore, the concentration of CTAB in the system could significantly influence the reduction rate of Au precursor.[3, 24] Either more or less CTAB would be expected to change the concentration of Au atoms around the seed and thus the growth pattern.

Similar to CTAB, the concentration of CTAC was also found to influence the shape of final product. As shown in Figure 3.6, when the amount of CTAC was reduced to 0 or 100 μmol, the resultant Au nanocrystals still maintained a tetrahedral shape but with concave structure on the surface (Fig. 3.6, a and b). In contrast, a relatively larger amount of CTAC would lead to the formation of Au nanocrystals with a truncated tetrahedral profile (Fig. 3.6c). For CTA molecules, they not only participated in the

construction of a double layer on the Au nanocrystals, but also served as an effective coordination ligand for Au ions. The variation in the amount of CTA molecules would lead to an change to the coordination strength so that different reduction rates of Au precursor and growth patterns were expected. Additionally, the variation in the amount of halide in the system, such as Br^- and Cl^-, may influence the Au-halide interaction strength on the nanocrystals surface, which could also change the growth pattern.[25] In short, the presence of both CTAB and CTAC at appropriate concentrations was necessary to promote the formation of Au nanocrystals with a tetrahedral shape in high purity.

Figure 3.7 shows a schematic illustration of the morphology evolution along with the increase in Au precursor amount. In particular, spherical seeds were directed to grow into truncated tetrahedra and then tetrahedra when the amount of $HAuCl_4$ was increased. Further addition of $HAuCl_4$ enabled the size increase from 30 nm to 60 nm without any noticeable loss of shape. This unsymmetrical growth mode could be attributed to a relatively slow growth kinetics maintained during the growth. On the one hand, the Au atoms were scarcely provided by adding the Au precursor solution at a slow injection rate. On the other hand, the presence of CTAB and CTAC at appropriate concentrations ensures the reduction rate of Au precursor was rationally controlled via the coordination effect and ligand exchange. Both aspects contributed to the precise manipulation of reaction kinetics, promoting the symmetry reduction of Au nanocrystals and thus the formation of tetrahedra in high yield.

3.3 Conclusion

In summary, I have successfully demonstrated a facile approach to the preparation of Au tetrahedra. Their sizes could be increased from 30 to 60 nm by simply varying the amount of Au precursor added into the growth solution. UV-vis extinction spectra of these Au tetrahedra were recorded and compared with the results from theoretical

calculations. The slow addition of Au precursor, accompanied by the use of CTAB and CTAC at appropriate concentrations, played a critical role in promoting an unsymmetrical growth pattern on the spherical seeds and thus the formation of tetrahedral products in high yields. This strategy based on manipulation of reaction kinetics could find immediate use in rationally controlling the shape of noble-metal nanocrystals.

3.4 Experimental Details

Chemicals and materials. Gold(III) chloride trihydrate ($HAuCl_4$ $3H_2O$, ≥99.9%), ascorbic acid (AA, ≥99.0%), sodium borohydride ($NaBH_4$, 98%), cetyltrimethylammonium bromide (CTAB, ≥99%), and cetyltrimethylammonium chloride (CTAC, 25 wt.% in water) were all obtained from Sigma-Aldrich and used as received. In all experiments, I used deionized water with a resistivity of 18.2 MΩcm, which was prepared using an ultrapure water system (Millipore, Billerica, MA). Aqueous $NaBH_4$ solution (10 mM) was prepared by dissolving 15.1 mg of $NaBH_4$ powder in 40 mL of water.

Preparation of the initial, CTAB-capped Au clusters. A fresh aqueous $NaBH_4$ solution (10 mM, 0.6 mL) was rapidly added into a thoroughly mixed 10 mL aqueous solution containing $HAuCl_4$ (0.25 mM) and CTAB (100 mM) using a pipette. A brown solution immediately formed upon the introduction of $NaBH_4$. The mixture was placed on an orbital shaker at a speed of 300 rpm for 2 min, and then kept undisturbed at 27 ^oC for 3 h to ensure complete decomposition of $NaBH_4$ remaining in the reaction mixture.

Preparation of Au spherical seeds with a diameter of 10 nm. Aqueous solutions of $HAuCl_4$ (0.5 mM, 2 mL), CTAC (200 mM, 2 mL), and AA (100 mM, 1.5 mL) were mixed in a 20 mL glass vial, followed by rapid injection of 100 μL of the initial, CTAB-capped Au clusters. The reaction was allowed to continue at 27 ^oC for 10 min. The product was collected by centrifugation at 14,500 rpm for 30 min, washed with water once, and then dispersed in 1 mL of aqueous CTAC solution (20 mM) for further use.

Standard procedure for the synthesis of Au tetrahedra. Aqueous solutions of CTAC (200 mM, 0.75 mL), CTAB (100 mM, 0.5 mL), AA (100 mM, 1.0 mL), and the 10-nm seed solution (20 μL) were mixed with 0.75 mL of water in a 20 mL glass vial, followed by dropwise addition of aqueous $HAuCl_4$ solution (0.5 mM) using a syringe pump at an injection rate of 0.5 mL/h. See main text for the amount of $HAuCl_4$ and the corresponding size of Au tetrahedra. The reaction was allowed to proceed at 27 ^{o}C for 10 min after the injection had been completed. The final product was collected by centrifugation at 13,200 rpm for 10 min and washed with water once prior to characterization.

Instrumentation. Transmission electron microscopy (TEM) images were captured using a HT 7700 microscope operated at 120 kV (Hitachi, Tokyo, Japan). The samples were prepared by dropping aqueous suspensions of the nanoparticles onto carbon-coated copper grids (part No. FCF200-Cu, Electron Microscopy Science, Hatfield, PA) and dried under ambient conditions in air. All extinction spectra were recorded using a Lambda 750 UV-vis-NIR spectrometer (PerkinElmer, Waltham, MA).

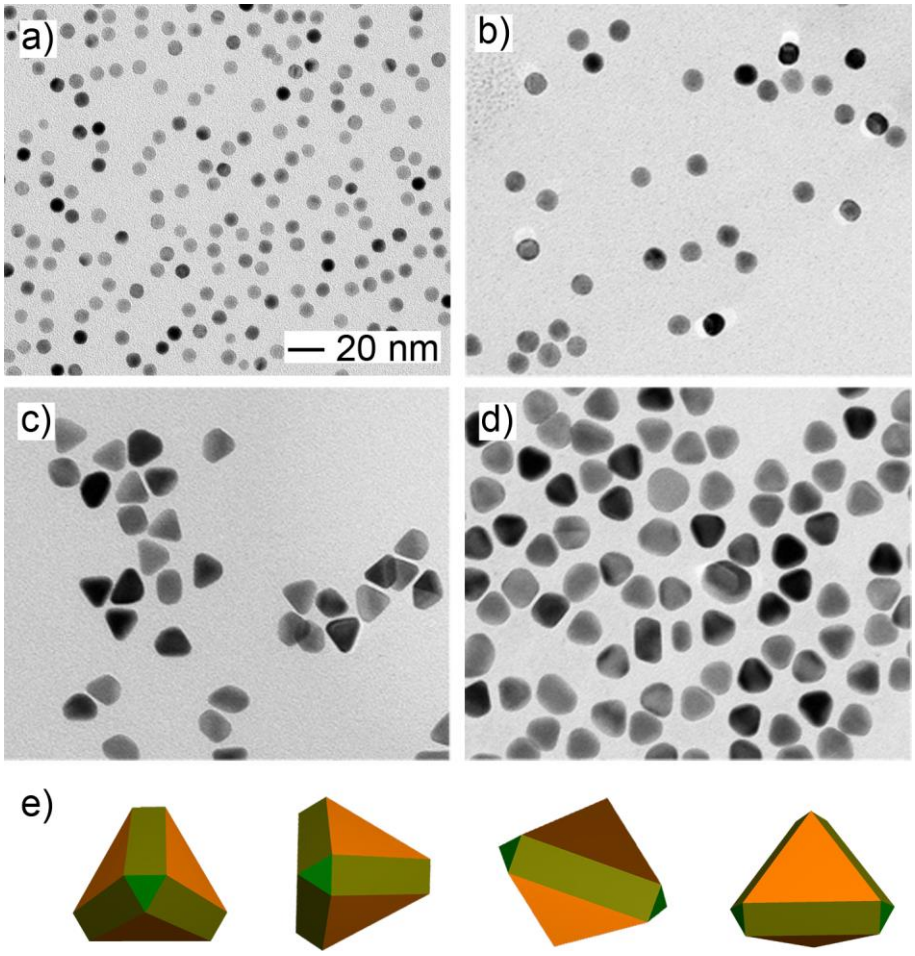

Figure 3.1. TEM images of a) 10-nm Au spherical seeds and b-d) Au nanocrystals obtained using the standard procedure except that the amounts of Au precursor added into the solutions were: b) 0.05; c) 0.13; and d) 0.25 μmol, respectively. The scale bar in (a) applies to (b-d). e) Models of truncated tetrahedra at four typical orientations.

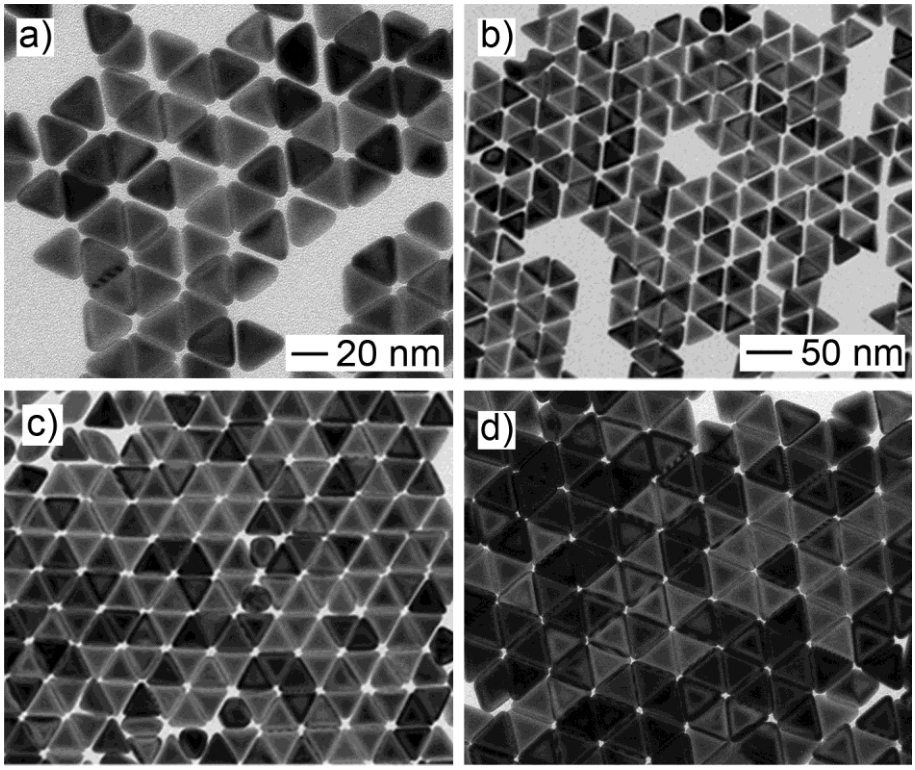

Figure 3.2. TEM images of Au tetrahedra with edge lengths of: a) 30; b) 38; c) 45; and d) 60 nm, respectively. They were obtained using the standard procedure except that the amounts of Au precursor were different: a) 0.38; b) 0.50; c) 1.0; and d) 1.5 μmol, respectively. The scale bar in (b) applies to (c-d).

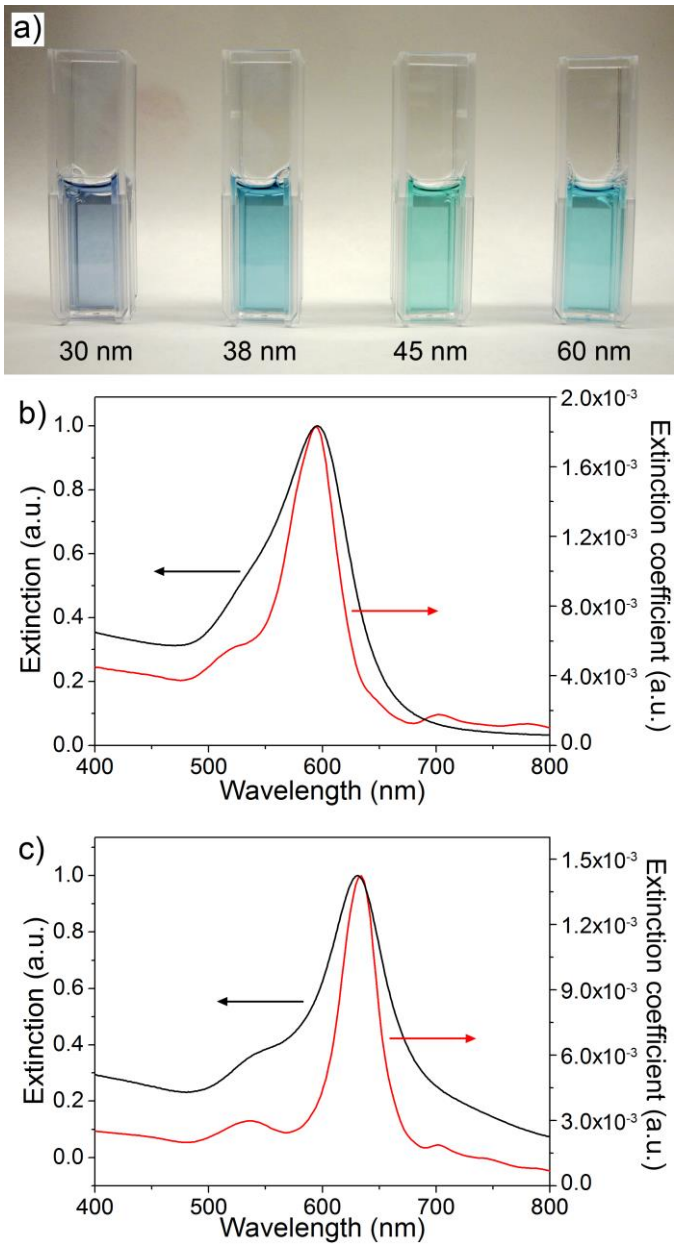

Figure 3.3. a) Photograph of aqueous suspensions of Au tetrahedra with different edge lengths. b, c) Experimental (black curve) and calculated (red curve) UV-vis extinction spectra of Au tetrahedra with edge lengths of b) 30 nm and c) 60 nm, respectively.

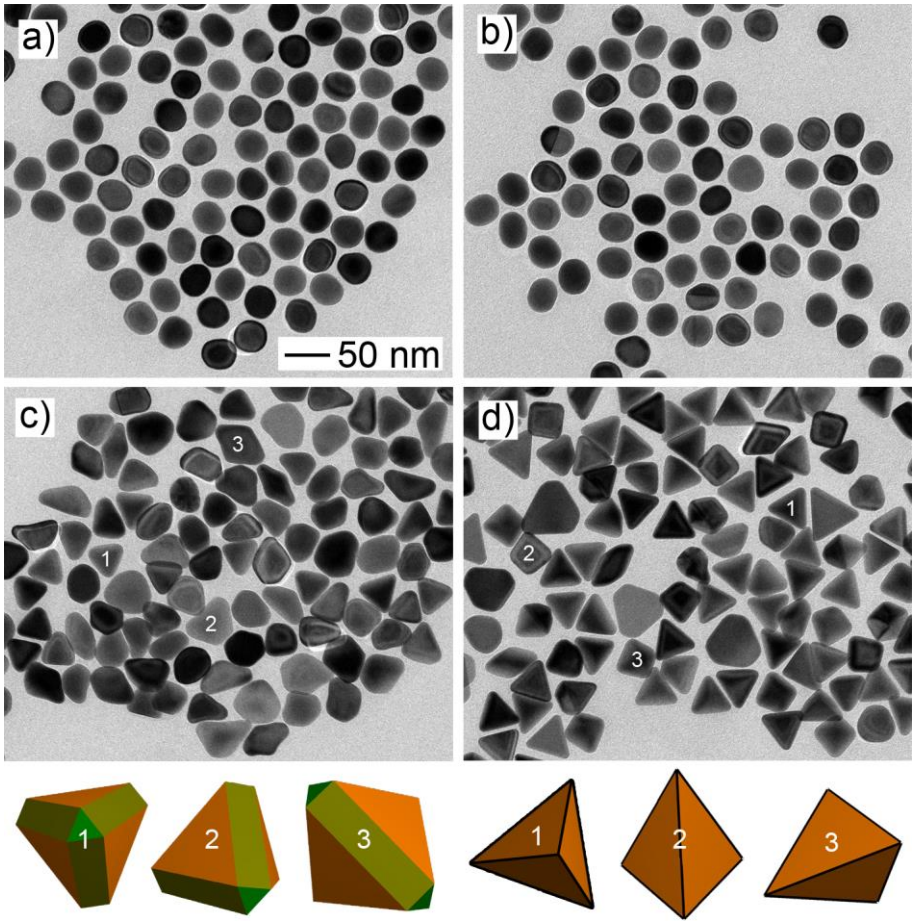

Figure 3.4. TEM images of Au nanocrystals that were prepared using a procedure similar to what was used for the 45-nm Au tetrahedra, except that the injection rate of Au precursor solution was varied from 0.5 mL/h to a) one-shot injection; b) 4.0; c) 1.0; and d) 0.25 mL/h, respectively. The scale bar in (a) applies to (b-d). The models at the bottom correspond to those particles in the TEM images labeled with the same number.

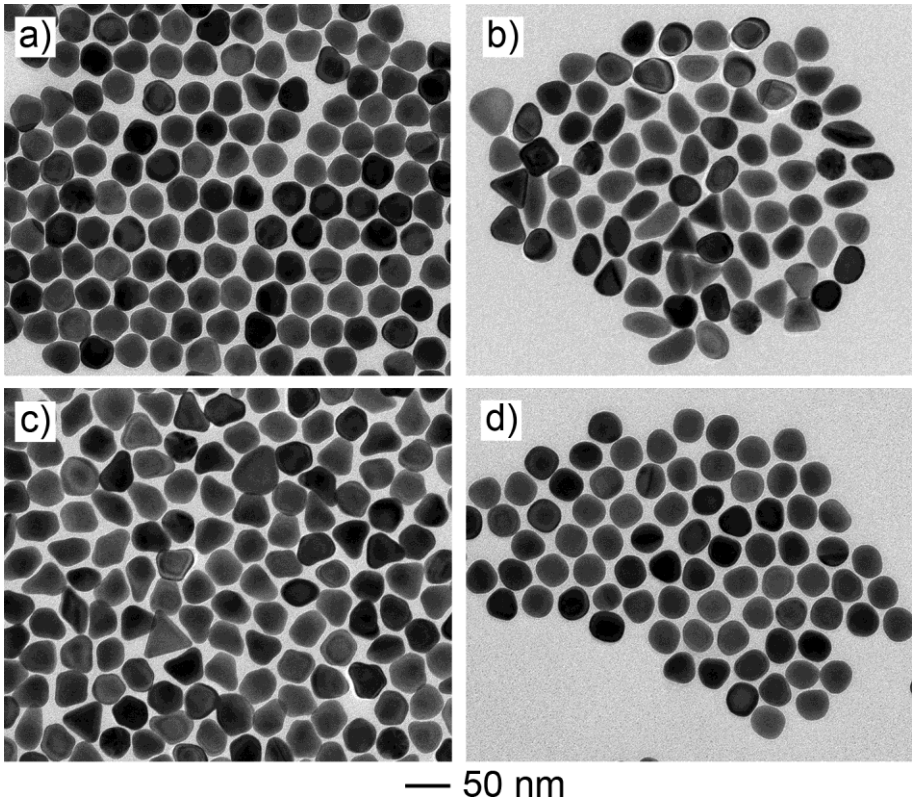

Figure 3.5. TEM images of Au nanocrystals that were prepared using a procedure similar to what was used for the 45-nm Au tetrahedra, except that the amount of CTAB was changed from 50 μmol to a) 0; b) 25; c) 75; and d) 100 μmol, respectively.

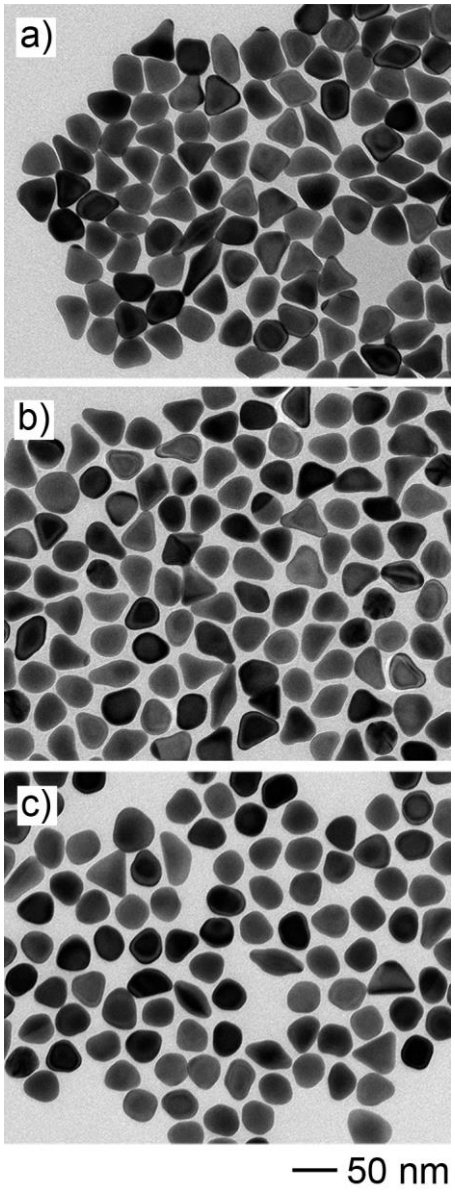

Figure 3.6. TEM images of Au nanocrystals that were prepared using a procedure similar to what was used for the 45-nm Au tetrahedra, except that the amount of CTAC was varied from 150 μmol to a) 0; b) 100; and c) 200 μmol, respectively.

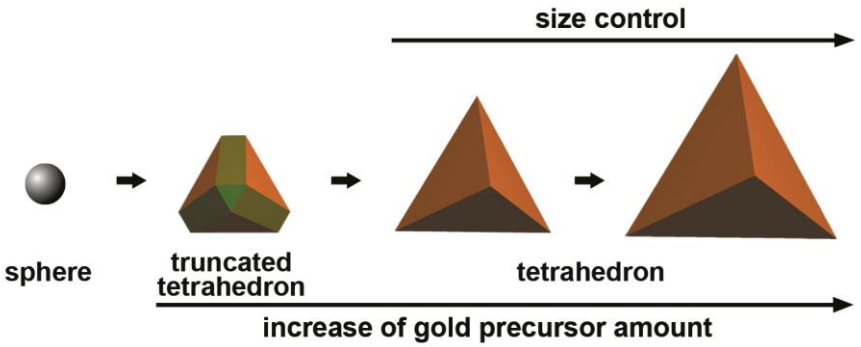

Figure 3.7. Schematic illustration of shape evolution from a sphere to tetrahedra of different sizes.

3.5 References for Chapter 3

[1] Y. Xia, Y. Xiong, B. Lim, S. E. Skrabalak, *Angew. Chem. Int. Ed.* **2009**, *48*, 60-103.

[2] L. D. Marks, *Rep. Prog. Phys.* **1994**, *57*, 603.

[3] M. R. Langille, M. L. Personick, J. Zhang, C. A. Mirkin, *J. Am. Chem. Soc.* **2012**, *134*, 14542-14554.

[4] W. Niu, S. Zheng, D. Wang, X. Liu, H. Li, S. Han, J. Chen, Z. Tang, G. Xu, *J. Am. Chem. Soc.* **2008**, *131*, 697-703.

[5] Y. Zheng, Y. Ma, J. Zeng, X. Zhong, M. Jin, Z.-Y. Li, Y. Xia, *Chem. Asia J.* **2013**, *8*, 792-799.

[6] Y. Zheng, X. Zhong, Z. Li, Y. Xia, *Part. Part. Syst. Charact.* **2013**, DOI: 10.1002/ppsc.201300256.

[7] D. Seo, J. C. Park, H. Song, *J. Am. Chem. Soc.* **2006**, *128*, 14863-14870.

[8] F. Kim, S. Connor, H. Song, T. Kuykendall, P. Yang, *Angew. Chem. Int. Ed.* **2004**, *43*, 3673-3677.

[9] T. K. Sau, C. J. Murphy, *J. Am. Chem. Soc.* **2004**, *126*, 8648-8649.

[10] X. Xia, Y. Xia, *Nano Lett.* **2012**, *12*, 6038-6042.

[11] H. Zhang, W. Li, M. Jin, J. Zeng, T. Yu, D. Yang, Y. Xia, *Nano Lett.* **2010**, *11*, 898-903.

[12] H.-L. Wu, C.-H. Kuo, M. H. Huang, *Langmuir* **2010**, *26*, 12307-12313.

[13] P.-J. Chung, L.-M. Lyu, M. H. Huang, *Chem. Eur. J.* **2011**, *17*, 9746-9752.

[14] M. Eguchi, D. Mitsui, H.-L. Wu, R. Sato, T. Teranishi, *Langmuir* **2012**, *28*, 9021-9026.

[15] C. Li, F. Fan, B. Yin, L. Chen, T. Ganguly, Z. Tian, *Nano Res.* **2013**, *6*, 29-37.

[16] H.-X. Lin, Z.-C. Lei, Z.-Y. Jiang, C.-P. Hou, D.-Y. Liu, M.-M. Xu, Z.-Q. Tian, Z.-X. Xie, *J. Am. Chem. Soc.* **2013**, *135*, 9311-9314.

[17] D. Seo, C. I. Yoo, I. S. Chung, S. M. Park, S. Ryu, H. Song, *J. Phys. Chem. C* **2008**, *112*, 2469-2475.

[18] C. J. Orendorff, T. K. Sau, C. J. Murphy, *Small* **2006**, *2*, 636-639.

[19] B. J. Wiley, S. H. Im, Z.-Y. Li, J. McLellan, A. Siekkinen, Y. Xia, *J. Phys. Chem. B* **2006**, *110*, 15666-15675.

[20] J. Zeng, C. Zhu, J. Tao, M. Jin, H. Zhang, Z. Y. Li, Y. Zhu, Y. Xia, *Angew. Chem. Int. Ed.* **2012**, *51*, 2354-2358.

[21] Y. Wang, S. Xie, J. Liu, J. Park, C. Z. Huang, Y. Xia, *Nano Lett.* **2013**, *13*, 2276-2281.

[22] Y. Ma, Q. Kuang, Z. Jiang, Z. Xie, R. Huang, L. Zheng, *Angew. Chem. Int. Ed.* **2008**, *47*, 8901-8904.

[23] J. A. Dean, *Lange's Chemistry Handbook*, 15th ed., McGraw-Hill Professional, New York, **1998**.

[24] D. K. Smith, B. A. Korgel, *Langmuir* **2008**, *24*, 644-649.

[25] T. H. Ha, H.-J. Koo, B. H. Chung, *J. Phys. Chem. C* **2006**, *111*, 1123-1130.

CHAPTER 4

CONTROLLING THE SIZE AND MORPHOLOGY OF AU@PD CORE-SHELL NANOCRYSTALS

4.1 Introduction

Core-shell bimetallic nanocrystals have recently attracted considerable interests because they allow for potential coupling of physicochemical properties between the constituent metals and thus enhancement of their performance in an array of applications.[1-10] With Au in the core and Pd in the shell, the resultant core-shell nanocrystals have been demonstrated with enhanced catalytic properties relative to the monometallic counterparts.[11-16] It has also been found that the properties of Au@Pd core-shell nanocrystals are highly dependent on their sizes and shapes (or morphologies). For example, Huang and coworkers reported that Au@Pd nanocrystals with tetrahexahedral shape exhibited a significantly higher electrocatalytic activity for ethanol oxidation than the octahedral counterpart.[17] Amatore and coworkers reported that Pd shells of 2-5 layers in thickness supported on Au seeds of 16 nm in size exhibited the highest catalytic activity for Suzuki–Miyaura reactions.[18] Therefore, it has become an important mission to control both the size and shape/morphology of Au@Pd core-shell nanocrystals in order to fully explore their properties and applications. Thanks to the efforts from many groups, it is now possible to generate Au@Pd core-shell nanocrystals with a myriad of polyhedral shapes, including cube, octahedron, rod, and rhombic dodecahedra, among others.[17, 19-26] Recently, Au@Pd core-shell nanocrystals enclosed by high-index facets other than {100} and {111} have also been reported, including hexoctahedron, tetrahexahedron, trisoctahedron, and concave octahedron.[27-31] Most of these syntheses started with polyhedral Au nanocrystals as seeds to generate Pd shells via epitaxial overgrowth. To this end, both octahedral and cubic Au seeds have been

employed to prepare Au@Pd core-shell nanocrystals.[17, 21, 26, 32] Despite the success, it should be pointed out that not all the morphologies were obtained in the same reaction system and the reaction conditions typically varied over a broad range from case to case. Therefore, it is difficult to elucidate the mechanisms responsible for the formation of different morphologies since no specific reaction parameter could be singled out for comparison and systematic investigation. As such, it still remains a grand challenge to generate Au@Pd nanocrystals with different morphologies in the same system by just tuning one or two reaction parameters.

In general, both thermodynamic and kinetic approaches can be employed to control the morphology of a nanocrystal. However, thermodynamic approach is ultimately limited by the obligation to minimize the total surface energy of a system. In contrast, kinetic control based on manipulation of growth rate at which atoms are generated and added to the surface of a growing seed seems to be more versatile in generating different shapes or morphologies.[33] It can also potentially generate novel nanocrystals with unusual shapes or morphologies. In fact, kinetic control has been demonstrated as a simple and effective means to manipulate the growth process and obtain nanocrystals with various morphologies in both monometallic and bimetallic systems. Typically, kinetic control can be achieved by substantially slowing down the reduction of a salt precursor through the use of a weaker reducing agent or a more stable precursor. Under these conditions, the atoms tend to form nuclei and seeds through random hexagonal close packing, together with the inclusion of stacking faults. This strategy has been used for the synthesis of Pd and Ag thin nanoplates.[34, 35] Most recently, our group demonstrated a simpler approach based on the use of a syringe pump for effectively manipulating the precursor concentration and thus the reduction rate to promote the overgrowth of Rh along the corners and edges rather than side faces of a cubic seed.[36] This method has also found use in the overgrowth of Ag over Pd cubic seeds, where a low injection rate of Ag precursor favored the formation of hybrid dimers

while a high injection rate promoted the formation of core-shell structures.[37]

Herein, we demonstrated that by implementing kinetic control in the overgrowth process, Au@Pd core-shell nanocrystals with six distinct shapes could be facilely obtained in the same reaction system. The key to the success of this synthesis was to manipulate the reaction kinetics by changing only one or two of the reaction parameters, including the type and concentration of capping agent, the amount of reductant, and the injection rate of Pd precursor solution. Along with the increase of reaction rate in the seed-mediated growth, the resultant core-shell nanocrystals evolved into octahedron, concave octahedron, rectangular bar, cube, concave cube, and dendrite, respectively. Different from previous reports on the synthesis of Au@Pd core-shell nanocrystals, the use of 11-nm Au nanospheres as the seeds offers a number of advantages. For example, the spherical shape helps to minimize the influence brought in by the sharp corners and edges of a seed on the evolution of morphology.[38-41] In addition, the sizes of the final products can be significantly reduced due to the use of spherical seeds with much smaller sizes. For the first time, Au@Pd core-shell nanocrystals with concave shapes could be obtained with sizes below 30 nm, in addition to the high purity and quality. Furthermore, Au@Pd@Au and Au@Pd@Au@Pd multi-shelled nanocrystals can be successfully prepared through alternative coatings of different metal layers on the as-prepared Au@Pd nanocubes.

4.2 Results and Discussion

A typical seed-mediated synthesis of Au@Pd core-shell nanocrystal can be divided into two steps. In the first step, Au nanospheres of 11 nm in diameter (see inset of Fig. 4.1a) were generated using a synthetic protocol described in Chapter 2.[42] These nanospheres were washed and then used as seeds for the next step, in which an aqueous solution containing H_2PdCl_4 and CTAB were mixed with a certain amount of the as-prepared Au spherical seeds, followed by quick injection of an aqueous solution containing the reductant AA. The color of the solution gradually turned from light yellow to brown and became stable after 60 min, indicating the formation of Au@Pd nanocrystals. See the experimental section for a detailed description of the parameters used for the standard procedure, from which all other syntheses discussed in this paper were slightly modified. To track the growth pattern, we monitored the reaction by taking out aliquots of the reaction solution at different stages of one batch of synthesis, followed by characterization using TEM. As shown in Figure 4.1a, the products obtained at t=10 min exhibited a cubic profile with slight truncations at corners, together with an edge length of about 15 nm. As the reaction was continued, these nanocrystals gradually grew into larger nanocubes with sharper edges and corners (Fig. 4.1, b and c). Finally, at t=60 min, uniformed Au@Pd nanocrystals with a perfect cubic profile were obtained with a purity approaching 100% (Fig. 4.1d). The edge length of these nanocubes was 24 nm. Interestingly, a crescent-like pattern was observed at the center of each Au@Pd nanocube. This pattern should be attributed to the existence of stress at the bimetallic interface.[43]

When the capping agent CTAB was replaced by CTAC while keeping all other reaction parameters the same, the color of the solution turned brown immediately after the injection of AA. This observation suggests a much faster reduction of H_2PdCl_4 by AA in the presence of CTAC. As shown in Figure 4.1e for a product sampled at t=10 min, the dominant shape was concave nanocube instead of perfect cube and the edge length also

increased from 15 to 23 nm. When the reaction was allowed to continue for another 10 min, we did not observe any obvious changes to the size and morphology of the products (Fig. 4.1f). Compared to the case of CTAB, the growth of Pd shells in the presence of CTAC was significantly accelerated.

Given the large difference in growth rate observed for systems involving CTAC and CTAB, it is not unreasonable to assume that the difference in morphology was caused by the different reduction rates for the Pd precursors. In fact, when CTAB was employed as a capping agent, H_2PdCl_4 should not be considered as the actual precursor. This is because a fast ligand change reaction between $[PdCl_4]^{2-}$ and Br^- could occur and the major Pd(II) complex in the system would become $[PdBr_4]^{2-}$. Based on the hard and soft acids and bases (HSAB) theory, Pd(II) cation is a soft acid that reacts faster and form a stronger bond with a soft base. Compared to Cl^-, Br^- is a softer base due to its larger ionic radius and lower electronegativity. Therefore, the ligand change process is thermodynamically favored. Since the $[PdBr_4]^{2-}$/Pd(0) pair has a lower redox potential, $[PdBr_4]^{2-}$/Pd(0) ≈ 0.49 eV versus $[PdCl_4]^{2-}$/Pd(0) ≈ 0.62 eV, it is more difficult to reduce $[PdBr_4]^{2-}$ to Pd(0) than $[PdCl_4]^{2-}$.[44] In other words, the presence of Br^- ions led to a slower reduction rate for the Pd precursor. This change could explain why a slower growth rate was observed for the Pd shells in the presence of CTAB. Moreover, the different morphologies could also be attributed to the difference in reaction kinetics. As indicated by the time-dependent studies with both capping agents, Au@Pd nanocrystals with a cubic shape were formed in the initial stage of overgrowth. Owing to a fast reduction rate for $[PdCl_4]^{2-}$ relative to $[PdBr_4]^{2-}$, Pd atoms in the vicinity to the corner sites of a growing seed could always be retained at a high level of supersaturation in the CTAC system. The growth at corner sites was accelerated and only a small number of Pd atoms could have enough time to migrate to the edges and side faces since the reaction rate dropped very rapidly due to the quick consumption of Pd precursor. Therefore, the morphology of the final products exhibited a concave structure on the surface. In the

presence of CTAB, however, it would take a relatively long time to achieve a high level of supersaturation around the corners of the growing seed. During this period of time, most of the Pd atoms at corner sites could have enough time to migrate to edges and side faces through surface diffusion. As a result, the as-formed cubic nanocrystals would grow at the entire surface of a seed and the final product would take a conventional cubic shape.

The size of the Au@Pd nanocubes and concave nanocubes could be readily varied in the range of 12-38 nm by simply controlling the amounts of Pd precursor and AA while the molar ratio between H_2PdCl_4 and AA and the amount of Au seeds were kept the same. Figure 4.2 shows TEM images of Au@Pd nanocubes and concave nanocubes with three typical sizes, respectively. The insets give their corresponding magnified TEM images of individual Au@Pd nanocrystals. The smallest sizes we have achieved for Au@Pd nanocubes and concave nanocubes were 12 and 13 nm, respectively. To our knowledge, it is the first time that sub-15 nm Au@Pd nanocubes and concave nanocubes were obtained in high purity and quality.

Besides the capping agent, other parameters were also examined in an effort to manipulate the reaction kinetics, including, for example, the amount of reductant and the injection rate for the Pd precursor. Figure 4.3, a and b, shows TEM images of products obtained by modifying the amount of AA used in the standard procedure. In the presence of CTAB, when the amount of AA was reduced to one half of the original value, most products still kept a conventional cubic shape (Fig. 4.3a). On the contrary, if the amount of AA was increased to 40 times of what was used in the standard procedure, a fast reduction compensated for the loss of reaction rate due to the presence of Br^-, leading to the formation of concave nanocubes (Fig. 4.3b). This result is similar to the case shown in Figure 4.1f, where the substitution of CTAB by CTAC led to the increase of reaction rate and thus formation of concave cubes. Figure 4.3, c and d, shows TEM images of products obtained by modifying the standard procedure with the use of CTAC and

different amounts of AA. When the amount of AA was decreased by one half, most products still kept the shape of concave nanocube. However, when the amount of AA was increased to 40 times of what was used in the standard procedure, the Au@Pd nanocrystal grew into a dendrite instead of a polyhedron. Owing to the overdosed amount of AA, the degree of supersaturation for Pd atoms would drastically increase. It facilitated the formation of several Pd clusters on the surface of a Au seed simultaneously. Each cluster tend to act as a nucleation site for the growth Pd dendritic nanostructure.[45]

To elucidate the influence of a lower reaction rate on the morphology, we further increased the concentration of CTAB while reducing the injection rate of Pd precursor through the use of a syringe pump. At a higher concentration of Br^- ions, more $[PdBr_4]^{2-}$ complex was formed and the reaction rate was significantly slowed down. Due to the limited solubility of CTAB at room temperature, the reaction was conducted in a 60 ^oC oil bath to ensure that no excess CTAB would crystallize out. Figure 4.4 shows TEM images of the Au@Pd nanocrystals that were synthesized by injecting Pd precursor solution into a growth solution in the presence of a high concentration of CTAB. When the injection rate of the precursor was set to 0.030 mL/min, the resultant nanocrystals became rectangular nanobars (Fig. 4.4a). In the projected TEM images of some nanobars, the crescent-like patterns were located near the side faces, edges, and corners instead of in the center as observed in the nanocubes, suggesting the involvement of localized, unidirectional growth on the Au seeds. Compared to the case of nanocube, the slow injection rate ensured that the concentration of Pd atoms was maintained at a relatively low level around the as-formed cubic Au@Pd nanoparticles. When the concentration was too low, the Pd atoms could not generate multiple nucleation sites. Instead, only one of the six faces of the as-formed cubic Au@Pd nanoparticle was involved in the heterogeneous nucleation process. A preferred growth would occur along one side face of the nanocube, leading to shape evolution from a nanocube into a nanobar. This result is consistent with our recent observation in the growth of Ag on cubic Pd seeds.[37]

Interestingly, when the injection rate was reduced to 0.014 mL/min, the obtained nanocrystals became concave octahedrons. As shown in Figure 4.4b, the curved edges and round corners indicates that the products were concave octahedrons. A lower injection rate (0.010 mL/min) led to the formation of octahedrons (Fig. 4.4c). Compared with cubic nanostructures enclosed by {100} facets, the octahedrons enclosed by {111} facets were even lower in surface energy and thus the formation of octahedral morphology was much more favored under a very low reaction rate.

The as-prepared Au@Pd core-shell nanocubes could be further used as seeds to generate core-shell nanostructures with multiple shells via successive overgrowth.[32, 46] Figure 4.5a shows TEM image of Au@Pd@Au double-shelled nanocrystals obtained by depositing Au on the as-prepared Au@Pd nanocubes with flat side faces. With another layer of Pd coating, the nanocrystals transformed into Au@Pd@Au@Pd nanocrystals with a triple-shelled structure (Fig. 4.5b). The Au and Pd layers could be clearly resolved under TEM imaging due to the high contrast between the two elements. The double-shelled Au@Pd@Au nanocrystals had a polyhedral shape while the triple-shelled Au@Pd@Au@Pd nanocrystals took a cubic shape.

Taken together, we conclude that the morphology of Au@Pd nanocrystals could be readily controlled by manipulating the reaction kinetics. Figure 4.6 shows a schematic illustration of the morphology evolution along with the increase in reaction rate. When the reaction rate was very low, the growth was located in the thermodynamic-controlled regime. In this case, Pd atoms could migrate on the nanocrystal surface to minimize the total surface energy, and accordingly octahedral and concave octahedral profiles mostly enclosed by {111} facets would be obtained. A higher reaction rate would favor the formation of polyhedrons enclosed by {100} facets, i.e., cubes and rectangular bars, which have higher surface energies. As the reaction rate increased beyond the thermodynamic-controlled regime, anisotropic overgrowth would occur owing to a faster rate of atomic addition than that of adatom diffusion on the surface. In this case, concave

cubes or branched morphologies might appear in the final products.

4.3 Conclusion

In summary, we have demonstrated that the size and shape (or morphology) of Au@Pd core-shell nanocrystals could be readily controlled via seed-mediated growth. By manipulating the reaction kinetics through a set of experimental parameters, including the type and concentration of capping agent, the amount of reductant, and the injection rate for the precursor solution, a variety of morphologies were obtained. Specifically, the shape or morphology changed from octahedrons to concave octahedrons, rectangular bars, cubes, concave cubes, and dendrites, respectively, as the reaction rate was increased. Thanks to the use of Au seeds of only 10 nm in diameter, it was possible to generate Au@Pd nanocrystals with such diversified morphologies while their sizes could still be controlled below 30 nm. The sizes of the Au@Pd nanocubes and concave cubes could be even confined to a scale as small as 12 and 13 nm, respectively, by reducing the amount of Pd precursor added into the reaction solution. In addition, the as-prepared Au@Pd nanocubes could serve as seeds to generate Au@Pd@Au and Au@Pd@Au@Pd multi-shelled nanocrystals. This strategy based on manipulation of reaction kinetics could become a facile and effective means for rationally controlling the size and morphology of core-shell nanocrystals with a variety of different bimetallic compositions.

4.4 Experimental Section

Chemicals and materials. Gold(III) chloride trihydrate ($HAuCl_4 \cdot 3H_2O$, ≥99.0%), palladium(II) chloride ($PdCl_2$), sodium borohydride ($NaBH_4$, 99%), L-ascorbic acid (AA, >99%), hydrochloric acid (HCl, 37% by wt. in water), hexadecyltrimethylammonium bromide (CTAB, ≥99%), and hexadecyltrimethylammonium chloride (CTAC, ≥98%) were all obtained from Sigma-Aldrich and used as received. All aqueous solutions were prepared using deionized water with a resistivity of 18.2 MΩ cm. The H_2PdCl_4 (10 mM) aqueous solution was prepared by completely dissolving 17.7 mg $PdCl_2$ in 10 mL of HCl (0.2 M) heated to 60 ^oC in an oil bath and cooled down to room temperature.

Synthesis of 10-nm Au spherical seeds. The spherical Au seeds were prepared using a protocol described in our previous work.[42] To start with, an aqueous suspension of CTAB-capped Au clusters was prepared by quickly injecting 0.6 mL of ice-cold $NaBH_4$ aqueous solution (10 mM) into 10 mL of an aqueous solution containing $HAuCl_4$ (0.25 mM) and CTAB (100 mM). The as-obtained brownish solution was kept undisturbed in an oil bath held at 27 ^oC for 3 h to completely decompose the residual $NaBH_4$. In the following step, 1.5 mL of AA (100 mM) aqueous solution was added into 4 mL of an aqueous solution containing $HAuCl_4$ (0.25 mM) and CTAC (100 mM), followed by quick addition of 0.1 mL of the as-prepared CTAB-capped Au clusters suspension. The color of the solution changed from colorless to pink quickly, indicating the formation of Au nanoparticles. The product was collected by centrifugation at 14,500 rpm for 30 min and then washed with water once. The Au nanospheres were then re-dispersed in 1 mL of water to obtain the seed solution. The concentration of elemental gold in the seed solution was determined to be 7.205 mg/L.

Synthesis of Au@Pd nanocubes, concave nanocubes, and dendrites. For a standard synthesis of Au@Pd nanocubes, 1.8 mL of CTAB (20 mM) aqueous solution, 2.8 mL of deionized water, 140 μL of the 11-nm Au seeds suspension, and 133 μL of H_2PdCl_4 (10 mM) aqueous solution were mixed in a 20 mL glass vial, followed by quick

injection of 200 μL of AA (12.5 mM) aqueous solution. The solution changed color from yellow to brown gradually and then became stable after 60 min. The product was collected by centrifugation at 8,000 rpm for 5 min and then washed with water once for further use or characterization. For Au@Pd concave cubes, a similar procedure was used except that CTAC (20 mM) was used as the capping agent instead of CTAB. For Au@Pd dendrites, the procedure was similar to the synthesis of Au@Pd concave nanocubes except that the amount of AA was changed to 100 μmol.

Synthesis of Au@Pd rectangular bars, concave octahedrons, and octahedrons. For Au@Pd rectangular bars, the standard synthesis involved 3 mL of CTAB (200 mM) aqueous solution, 1 mL of deionized water, 200 μL of AA (12.5 mM) aqueous solution, and 70 μL of the 11-nm Au seeds suspension. These solutions were mixed in a 20-mL glass vial and heated in an oil bath to 60 ^{o}C for 5 min. Then, 1.5 mL of H_2PdCl_4 (0.88 mM) aqueous solution was injected into the reaction mixture at a rate of 0.030 mL/min using a syringe pump. The reaction was allowed to continue for 3 h after the injection. The product was collected by centrifugation at 6,000 rpm for 5 min and washed with water once for further use or characterization. For Au@Pd concave octahedrons, the procedure was similar to the synthesis of Au@Pd rectangular bars except that the injection rate was reduced to 0.014 mL/min. For Au@Pd octahedrons, the procedure was similar to the synthesis of Au@Pd rectangular bars except that the injection rate of H_2PdCl_4 solution was further reduced to 0.010 mL/min.

Synthesis of Au@Pd@Au double-shelled nanocrystals. 30 μL of $HAuCl_4$ (10 mM) aqueous solution was added into an aqueous solution contained 1.8 mL of CTAB (20 mM), 1 mL of the Au@Pd nanocubes suspension (before centrifugation) obtained using the standard procedure at t=60 min, 68.5 μL of AA (12.5 mM), and 1.5 mL of deionized water, generating a reddish solution in a 20 mL glass vial. The reaction was allowed to continue at room temperature for 3 h. The product was collected by centrifugation at 8,000 rpm for 5 min and washed with water once for further

characterization.

Synthesis of Au@Pd@Au@Pd triple-shelled nanocubes. 60 μL of H_2PdCl_4 (10 mM) aqueous solution was added into a solution containing 1.2 mL of CTAB (20 mM) aqueous solution, 1 mL of the as-obtained Au@Pd@Au double-shelled nanocubes suspension (before centrifugation), 120 μL of AA (12.5 mM) aqueous solution, and 3 mL of deionized water, generating a brownish solution in a 20 mL glass vial. The reaction was allowed to continue at room temperature for 3 h. The product was collected by centrifugation at 6,000 rpm for 5 min and washed with water once for further characterization.

Instrumentations. TEM images were captured on a FEI Tecnai G^2 Spirit microscope operated at 120 kV. The samples for TEM studies were prepared by drying a drop of the aqueous suspension of particles on a piece of carbon-coated copper grid (Ted Pella, Redding, CA) under ambient conditions. The sample was dried and stored under vacuum prior to TEM characterization. The concentration of elemental gold in a suspension was determined by inductively-coupled plasma mass spectrometry (Elan DRC II, PerkinElmer).

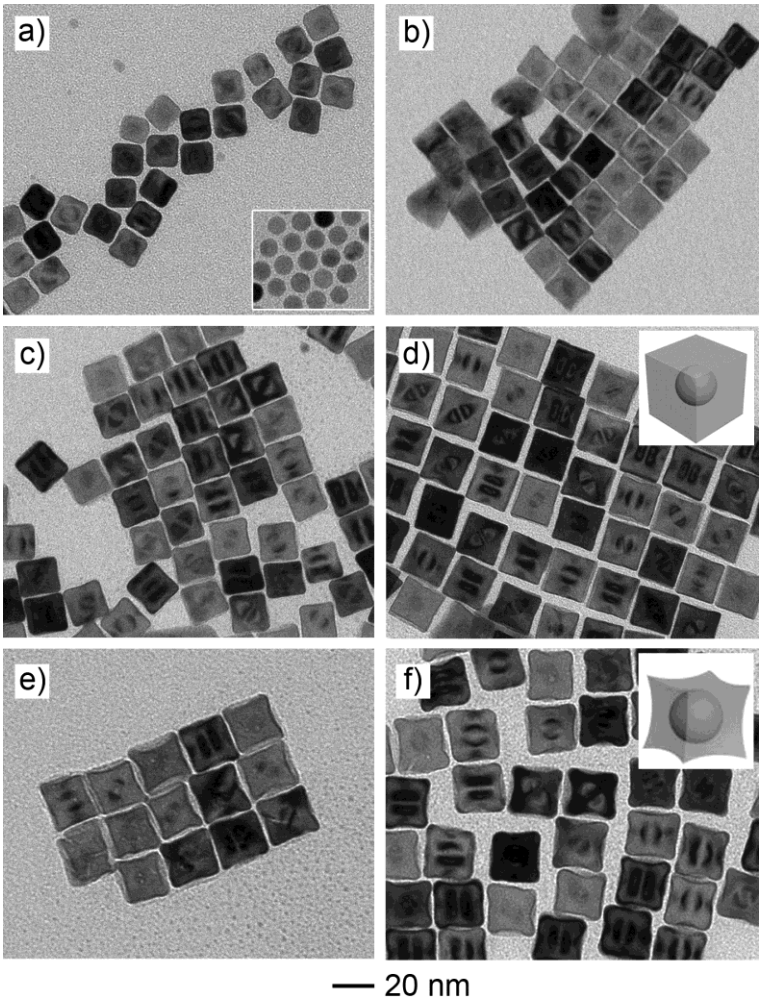

Figure 4.1. a-d) TEM images of Au@Pd nanocrystals obtained at different stages of a standard synthesis in the presence of CTAB as a capping agent: a) 10 min, b) 20 min, c) 40 min, and d) 60 min. The inset in (a) shows TEM image of the 11-nm Au spherical seeds. e, f) TEM images of Au@Pd nanocrystals obtained at different stages of a standard synthesis in the presence of CTAC as capping agent: e) 10 min and f) 20 min. The edge lengths of the cubic nanocrystals were a) 15 nm, b) 18 nm, c) 20 nm, d) 22 nm, e) 23 nm, and f) 24 nm, respectively. Note that the nanocrystals obtained in the presence of CTAC were more concaved on the surface than those obtained in the presence of CTAB.

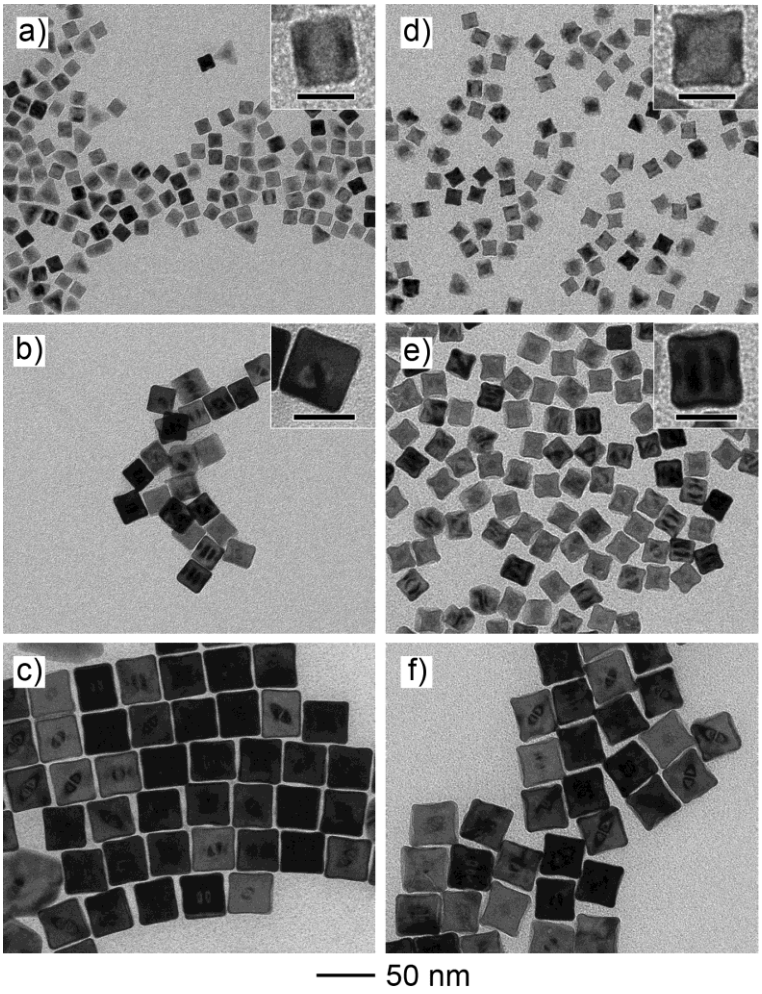

Figure 4.2. TEM images of a-c) Au@Pd nanocubes and d-f) Au@Pd concave nanocubes with different sizes. The particles sizes were measured to be a) 12 nm, b) 22 nm, c) 37 nm, d) 13 nm, e) 23 nm, and f) 38 nm. All the syntheses were conducted using the standard procedure, except for the use of different amount of H_2PdCl_4 and AA. The molar ratio between H_2PdCl_4 and AA was kept the same as that in the standard procedure. The totally added amounts of H_2PdCl_4 were (a, d) 0.20 μmol, (b, e) 0.80 μmol, and (c, f) 2.00 μmol. The scale bars in the insets are 10 nm in (a, d) and 20 nm in (b, e).

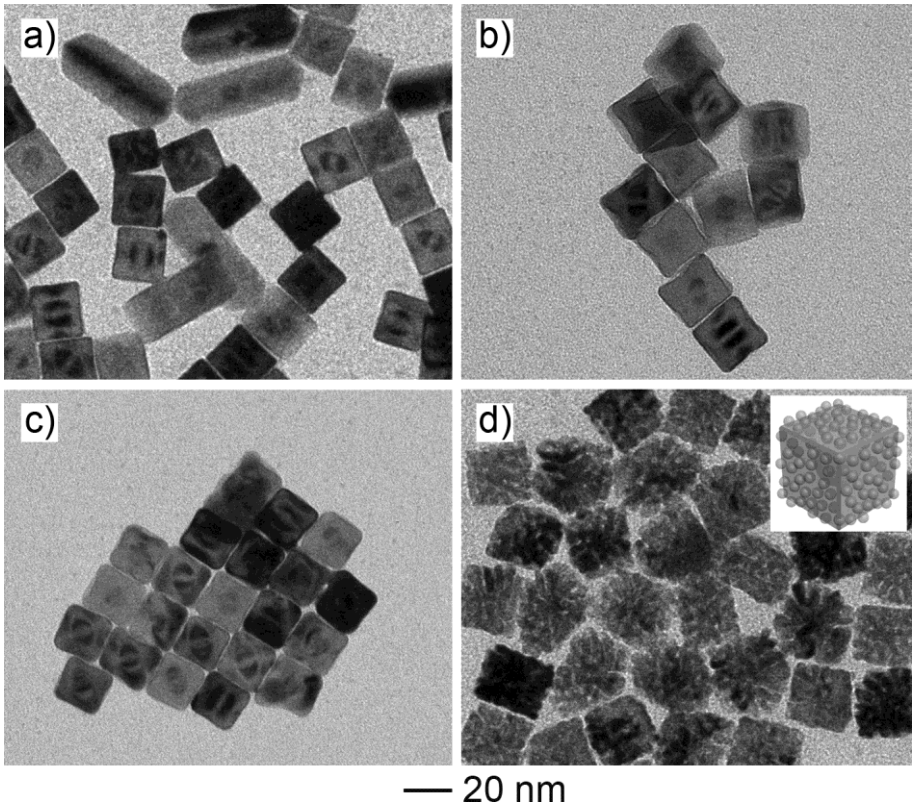

Figure 4.3. TEM images of Au@Pd core-shell nanocrystals prepared in the presence of a, b) CTAB and c, d) CTAC using the standard procedure, except for the use of different amounts of AA: (a, c) 1.25 μmol and (b, d) 100 μmol, respectively.

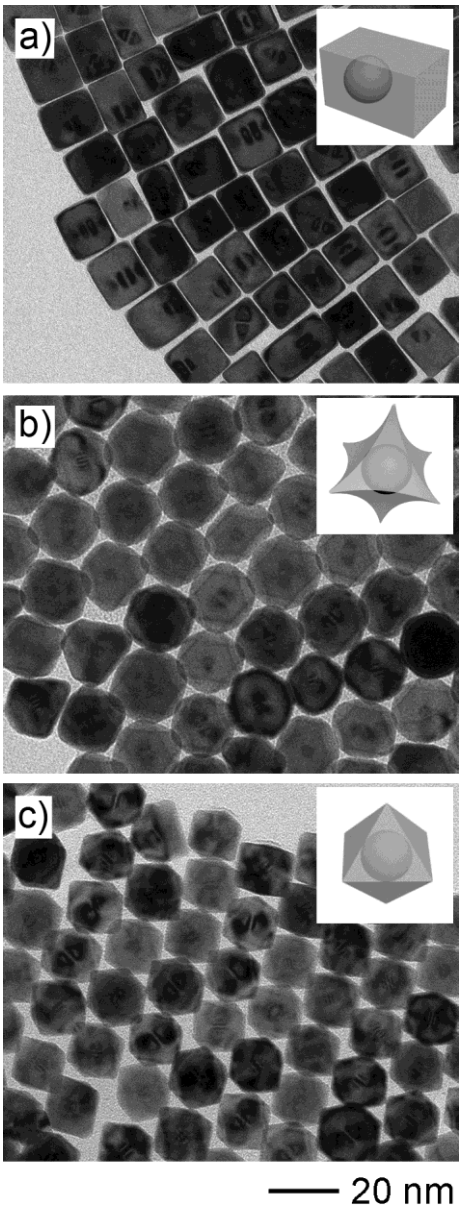

Figure 4.4. TEM images of Au@Pd core-shell nanocrystals with different morphologies: a) rectangular bar, b) concave octahedron, and c) octahedron. The nanocrystals were obtained by varying the injection rate for the H_2PdCl_4 solution: a) 0.030 mL/min, b) 0.014 mL/min, and c) 0.010 mL/min, respectively.

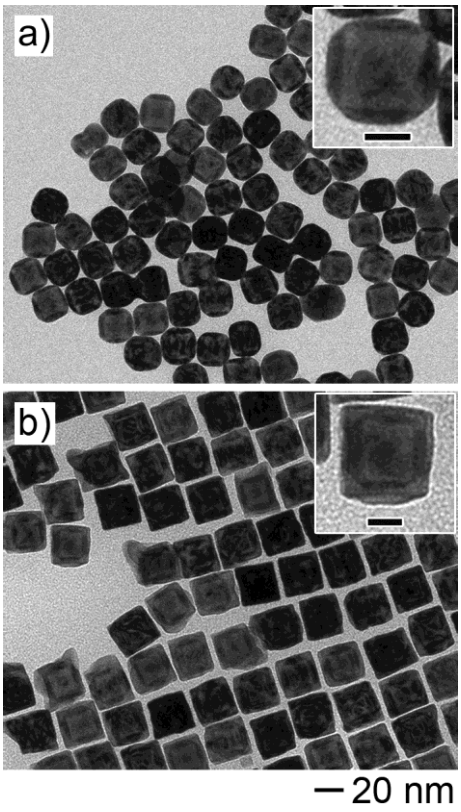

Figure 4.5. TEM images of multi-shelled nanocrystals derived from the Au@Pd nanocubes shown in Figure 4.1d: a) Au@Pd@Au double-shelled and b) Au@Pd@Au@Pd triple-shelled, respectively. The scale bars in both insets are 10 nm.

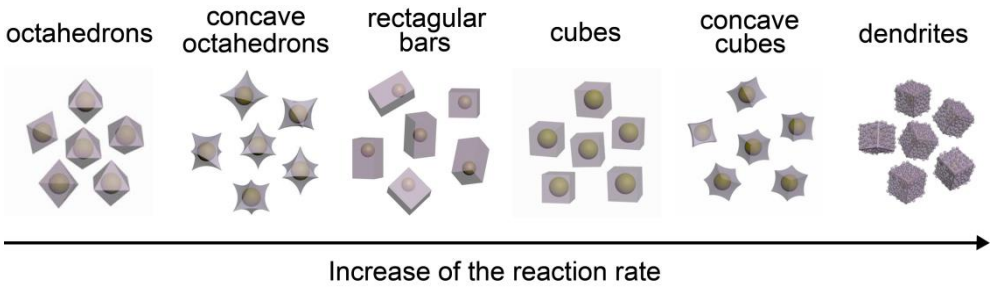

Figure 4.6. Schematic illustration of the evolution of morphology associated with the Au@Pd core-shell nanocrystals as a function of reaction rate.

4.5 References for Chapter 4

[1] B. Rodriguez-Gonzalez, A. Burrows, M. Watanabe, C. J. Kiely, L. M. Liz-Marzan, *J. Mater. Chem.* **2005**, *15*, 1755.

[2] P. D. Cozzoli, T. Pellegrino, L. Manna, *Chem. Soc. Rev.* **2006**, *35*, 1195.

[3] S. G. Zhou, K. McIlwrath, G. Jackson, B. Eichhorn, *J. Am. Chem. Soc.* **2006**, *128*, 1780.

[4] S. E. Habas, H. Lee, V. Radmilovic, G. A. Somorjai, P. Yang, *Nature Mater.* **2007**, *6*, 692.

[5] F. Tao, M. E. Grass, Y. Zhang, D. R. Butcher, J. R. Renzas, Z. Liu, J. Y. Chung, B. S. Mun, M. Salmeron, G. A. Somorjai, *Science* **2008**, *322*, 932.

[6] H. Lee, S. E. Habas, G. A. Somorjai, P. Yang, *J. Am. Chem. Soc.* **2008**, *130*, 5406.

[7] D. Seo, C. Yoo, J. Jung, H. Song, *J. Am. Chem. Soc.* **2008**, *130*, 2940.

[8] B. Lim, M. Jiang, P. H. C. Camargo, E. C. Cho, J. Tao, X. Lu, Y. Zhu, Y. Xia, *Science* **2009**, *324*, 1302.

[9] R. Costi, A. E. Saunders, U. Banin, *Angew. Chem. Int. Ed.* **2010**, *49*, 4878.

[10] M. R. Langille, J. Zhang, C. A. Mirkin, *Angew. Chem. Int. Ed.* **2011**, *50*, 3543.

[11] Z. Yang, Y. Li, Z. Li, D. Wu, J. Kang, H. Xu, M. Sun, *J. Chem. Phys.* **2009**, *130*, 234705.

[12] Y. W. Lee, M. Kim, Y. Kim, S. W. Kang, J.-H. Lee, S. W. Han, *J. Phys. Chem. C* **2010**, *114*, 7689.

[13] J. Xu, A. R. Wilson, A. R. Rathmell, J. Howe, M. Chi, B. J. Wiley, *ACS Nano* **2011**, *5*, 6119.

[14] F. Wang, C. Li, L.-D. Sun, H. Wu, T. Ming, J. Wang, J. C. Yu, C.-H. Yan, *J. Am. Chem. Soc.* **2010**, *133*, 1106.

[15] J. W. Hong, D. Kim, Y. W. Lee, M. Kim, S. W. Kang, S. W. Han, *Angew. Chem. Int. Ed.* **2011**, *50*, 8876.

[16] J. W. Hong, Y. W. Lee, M. Kim, S. W. Kang, S. W. Han, *Chem. Commun.* **2011**, *47*, 2553.

[17] C.-L. Lu, K. S. Prasad, H.-L. Wu, J.-a. A. Ho, M. H. Huang, *J. Am. Chem. Soc.* **2010**, *132*, 14546.

[18] P.-P. Fang, A. Jutand, Z.-Q. Tian, C. Amatore, *Angew. Chem. Int. Ed.* **2011**, *50*, 12184.

[19] J.-W. Hu, Y. Zhang, J.-F. Li, Z. Liu, B. Ren, S.-G. Sun, Z.-Q. Tian, T. Lian, *Chem. Phys. Lett.* **2005**, *408*, 354.

[20] Y. Xiang, X. Wu, D. Liu, X. Jiang, W. Chu, Z. Li, Y. Ma, W. Zhou, S. Xie, *Nano Lett.* **2006**, *6*, 2290.

[21] F.-R. Fan, D.-Y. Liu, Y.-F. Wu, S. Duan, Z.-X. Xie, Z.-Y. Jiang, Z.-Q. Tian, *J. Am. Chem. Soc.* **2008**, *130*, 6949.

[22] Y. W. Lee, M. Kim, Z. H. Kim, S. W. Han, *J. Am. Chem. Soc.* **2009**, *131*, 17036.

[23] Y. Ding, F. Fan, Z. Tian, Z. L. Wang, *J. Am. Chem. Soc.* **2010**, *132*, 12480.

[24] A. Wang, Q. Peng, Y. Li, *Chem. Mater.* **2011**, *23*, 3217.

[25] Y. W. Lee, M. Kim, S. W. Kang, S. W. Han, *Angew. Chem. Int. Ed.* **2011**, *50*, 3466.

[26] C.-W. Yang, K. Chanda, P.-H. Lin, Y.-N. Wang, C.-W. Liao, M. H. Huang, *J. Am. Chem. Soc.* **2011**, *133*, 19993.

[27] Y. Yu, Q. Zhang, B. Liu, J. Y. Lee, *J. Am. Chem. Soc.* **2010**, *132*, 18258.

[28] C. J. DeSantis, A. A. Peverly, D. G. Peters, S. E. Skrabalak, *Nano Lett.* **2011**, *11*, 2164.

[29] L. Zhang, J. Zhang, Q. Kuang, S. Xie, Z. Jiang, Z. Xie, L. Zheng, *J. Am. Chem. Soc.* **2011**, *133*, 17114.

[30] C. J. DeSantis, A. C. Sue, M. M. Bower, S. E. Skrabalak, *ACS Nano* **2012**, 6, 2617.

[31] D. Kim, Y. W. Lee, S. B. Lee, S. W. Han, *Angew. Chem. Int. Ed.* **2012**, *51*, 159.

[32] F. Wang, L.-D. Sun, W. Feng, H. Chen, M. H. Yeung, J. Wang, C.-H. Yan, *Small* **2010**, *6*, 2566.

[33] Y. Xia, Y. Xiong, B. Lim, S. E. Skrabalak, *Angew. Chem. Int. Ed.* **2009**, *48*, 60.

[34] Y. Xiong, J. M. McLellan, J. Chen, Y. Yin, Z.-Y. Li, Y. Xia, *J. Am. Chem. Soc.* **2005**, *127*, 17118.

[35] J. Zeng, J. Tao, W. Li, J. Grant, P. Wang, Y. Zhu, Y. Xia, *Chem. Asian. J.* **2011**, *6*, 376.

[36] H. Zhang, W. Li, M. Jin, J. Zeng, T. Yu, D. Yang, Y. Xia, *Nano Lett.* **2010**, *11*, 898.

[37] J. Zeng, C. Zhu, J. Tao, M. Jin, H. Zhang, Z.-Y. Li, Y. Zhu, Y. Xia, *Angew. Chem. Int. Ed.* **2012**, *51*, 2354.

[38] C. J. Murphy, N. R. Jana, *Adv. Mater.* **2002**, *14*, 80.

[39] C. J. Murphy, T. K. Sau, A. M. Gole, C. J. Orendorff, J. Gao, L. Gou, S. E. Hunyadi, T. Li, *J. Phys. Chem. B* **2005**, *109*, 13857.

[40] J. Park, J. Joo, S. G. Kwon, Y. Jang, T. Hyeon, *Angew. Chem. Int. Ed.* **2007**, *46*, 4630.

[41] D. Seo, C. I. Yoo, J. C. Park, S. M. Park, S. Ryu, H. Song, *Angew. Chem. Int. Ed.* **2008**, *47*, 763.

[42] Y. Ma, W. Li, E. C. Cho, Z. Li, T. Yu, J. Zeng, Z. Xie, Y. Xia, *ACS Nano* **2010**, *4*, 6725.

[43] D. B. Williams, C. B. Cater, *Transmission electron microscopy : a textbook for materials science*, Plenum Press, New York, **1996**.

[44] J. A. Dean, *Lange's Chemistry Handbook*, 15th ed., McGraw-Hill Professional, New York, **1998**.

[45] B. Lim, Y. Xia, *Angew. Chem. Int. Ed.* **2011**, *50*, 76.

[46] D. Ferrer, A. Torres-Castro, X. Gao, S. Sepúlveda-Guzmán, U. Ortiz-Méndez, M. José-Yacamán, *Nano Lett.* **2007**, *7*, 1701.

CHAPTER 5

CRYSTALLINITY CHANGE IN SEEDED GROWTH OF AU NANOCRYSTALS

5.1 Introduction

Crystallinity is an important attribute of nanocrystals as it may affect the catalytic, optical, and electrical properties.[1] Generally, crystallinity is referred to as the degree of structural order in a solid. For a single crystal, all the atoms are arranged in a perfect lattice with translational, long-range periodicity along all directions. The periodic structure can be disrupted locally when defects are introduced.[2] In this case, the arrangement of atoms in certain regions can lose the periodicity along at least one direction, which reduces the degree of structural perfection and thus leads to the change in crystallinity. Among various types of defects, twin is a typical planar defect. It is like a mirror plane, where arrangement of atoms on one side is a perfect reflection of what is on the other side.[3] Depending on the number and locations of twin defects in the product, the crystallinity of noble-metal nanocrystals can be classified into three major categories: single crystal, singly twinned, and multiply twinned.[4] Products with different degrees of crystallinity may exhibit a myriad of shapes and surface structures in addition to the difference in internal structure.[5,6] All these variations, as induced by the change in crystallinity, can exert significant impacts on their physicochemical properties and potential applications in fields such as optics, mechanics, electronics, and catalysis.[7-14] To this end, it is highly desirable to have an ability to manipulate the crystallinity of noble-metal nanocrystals.[15-18]

Although noble-metal nanocrystals with different degrees of crystallinity may co-exist in the final product of a typical synthesis, it is worth pointing out that the involvement of twin defects during the growth of single-crystal seeds may not be favored

by thermodynamics. This is because the presence of defects could break the intrinsic cubic symmetry of the lattice and thus increase the total free energy of the system.[19] In addition, the defect sites often bring in extra strain energy and thus can be more susceptible to corrosive environments involving species for oxidative etching.[20] Therefore, when single-crystal seeds are used to grow larger nanocrystals, the resultant product may exhibit differences in terms of size and shape but they generally will preserve the single crystallinity of the seeds.[21-25] This principle has been widely accepted and routinely used to direct the growth of noble-metal nanocrystals with a myriad of different shapes and thus facets on the surface.[26]

However, recent work indicated that change in crystallinity between the seed and the final product might take place in the seed-mediated growth of binary noble-metal nanocrystals. This can be attributed to the difference in intrinsic properties between the two different metals, such as lattice constant and bond dissociation energy, among others. For example, Pt-Au penta-twinned nanorods and Au-Ag multi-twinned icosahedrons have been obtained from seeds made of Pt or Au polyhedral particles with a single-crystal structure.[27,28] However, when the same metal is used for seed-mediated growth, change in crystallinity from single-crystal seeds to multiply twinned products has not been reported.

In this chapter, I report an unusual change to crystallinity observed in the seed-mediated growth of Au on single-crystal Au seeds. In particular, when the single-crystal Au seeds were treated with a chemical species containing sulfur, twin defects would develop during the seed-mediated growth process to yield multiply twinned nanocrystals.

5.2 Results and Discussion

The Au seeds with a single-crystal structure were prepared using a protocol described in previous publications.[29] As shown in Figure 5.1a, these seeds exhibited a truly spherical shape and their corresponding HRTEM image and electron diffraction

data confirmed their single-crystal structure (Fig. 5.1, b and c). The seeds were treated by mixing with an aqueous solution of sodium thiosulfate, followed by centrifugation and washing with water to remove the chemical species loosely bound to the surface of seeds. As shown in Figure 5.1d, the seeds exhibited no noticeable change in terms of both size and shape after the treatment. HRTEM imaging and electron diffraction confirmed that the seeds still showed a single-crystal structure after the treatment (Fig. 5.1, e and f). The seed-mediated growth involved the use of $HAuCl_4$, CTAC, and AA as the Au precursor, stabilizing agent, and reductant, respectively. When the spherical seeds without treating by $Na_2S_2O_3$ were used for growth, the final products were dominated by single-crystal Au nanocrystals with a cubic shape (Fig. 5.2a). In contrast, the use of seeds with treatment by $Na_2S_2O_3$ led to the formation of products exhibiting a significant difference in crystallinity (Fig. 5.2b). In particular, it is not difficult to identify twin defects in most of the nanoparticles (Fig. 5.2c). Their corresponding electron diffraction patterns also supported the notion that most of the nanoparticles had a twinned structure (Fig. 5.2d).[30] Given that all the other experimental conditions were kept the same, it is not unreasonable to assume that the treatment of seeds by $Na_2S_2O_3$ was a critical factor responsible for the resultant difference in crystallinity for the final products.

To verify our hypothesis, we analyzed the spherical Au seeds without and with the treatment by X-ray photoelectron spectroscopy (XPS). As shown by the survey spectra in Figure 5.3, a and b, there were peaks for Au 4f, Au 4d, C 1s, and N 1s, indicating the existence of CTA molecules on the surfaces of both types of Au seeds. However, we noticed that the survey spectrum of the seed with the treatment also contained the S 2p peaks while no such peak was observed in the spectrum of seeds without the treatment. Figure 5.3c shows high-resolution XPS spectra of the S 2p peaks for seeds with the treatment. The two peaks, roughly located at 168.4 eV and 161.7 eV, could be indexed to the central (oxidized sulfur) and peripheral (reduced sulfur) compartment of $S_2O_3^{2-}$ anion, respectively. Compared to the results of previous XPS

studies of bulk $Na_2S_2O_3$ (with binding energies of 168.4 eV and 161.1 eV for the central sulfur and peripheral sulfur, respectively), we noticed a blue-shift for the peripheral sulfur peak.[31] Such a shift implies a electron transfer from $S_2O_3^{2-}$ anions to the Au surface due to the strong Au-S interaction between them. In short, the XPS result implied that the thiosulfate ions had adsorbed onto the surface of the seeds during the treatment.

For the $S_2O_3^{2-}$ anion, it contains sulfur with two different oxidation numbers: +6 and -2. In addition, it can disproportionate into zero-valent sulfur and sulfur dioxide in an acidic medium.[32] To determine which form of sulfur played the most important role, we performed three control experiments by treating the seeds with other sulfur species. We chose three sulfur-containing compounds, sodium sulfate (Na_2SO_4), sodium polysulfide (Na_2S_x), and sodium sulfide (Na_2S), because they contained sulfur with oxidation numbers of +6, 0, and -2, respectively. The reason we chose Na_2S_x instead of sulfur powder as the source of zero-valent sulfur is due to the poor solubility of sulfur powder in water. As shown in Figure 5.4, the spherical Au seeds treated with Na_2SO_4 still favored the formation of Au nanocubes while the seeds treated either Na_2S_x or Na_2S resulted in the formation of products with multiply twinned structures. Based on these results, we believe the sulfur species with oxidation numbers of -2 and 0 were responsible for the change in crystallinity during the seed-mediated growth.

After the seed was treated with $S_2O_3^{2-}$ anions, a strong interaction between the Au surface and sulfur should be expected for the seed surface. Such interaction may not be strong to block the growth of the seed but it could locally interrupt the otherwise epitaxial growth involved in the deposition of Au on Au. In this case, twin defects tended to evolve in the newly deposited layers if the added atoms could not be promptly placed in the single-crystal lattice. In addition, the sulfur atoms on the seed surface, as released by the $S_2O_3^{2-}$ anions in an acidic medium, may change the seed surface topography and help create steps or kinks. Considering the difference in atomic radius between Au and S,

these steps and kinks can also induce the formation of defects if cubic close packing of atoms was no longer possible.

To further confirm our claim, we tried another type of single-crystal Au seeds – the nanorods originally developed by Murphy, El-Sayed, and other groups.[33,34] As shown by TEM images in Figure 5.5, a and b, these nanorods showed no noticeable change in both size and shape after the treatment with aqueous $Na_2S_2O_3$ solution. Figure 5.6 shows HRTEM images and electron diffraction patterns of the seeds with and without the treatment. Similar to the case of spherical seeds, no change in crystallinity for these rod-like seeds was observed after the treatment. When they were used as seeds for growth using a standard procedure, as shown by Figure 5.5, c and d, single-crystal products could be obtained when the rod seeds without treatment were employed while the use of seeds with treatment resulted in the formation of products with twin defects. As shown in Figure 5.7, in particular, we notice a set of twin planes at the end of the nanorods. The presence of more than one sets of diffraction spots in the corresponding ED pattern also demonstrated its twinned structure.

5.3 Conclusion

In summary, I have demonstrated a simple approach that could change the crystallinity of Au nanocrystals during seed-mediated growth. Single-crystal Au seeds in the form of either sphere or rod could develop multiple twin defects during a seed-mediated growth process if the seeds were treated with $S_2O_3^{2-}$ ions. Treatment with other sulfur-containing species, such as S^{2-} and S_x^{2-}, were also tested and similar changes in crystallinity were observed. The strong Au-S interaction on the surface of a seed made it difficult for the newly formed Au atoms to form a single-crystal structure. In this case, twin defects tended to evolve in the newly formed layers in order to reduce the surface free energy. The twinned structures were confirmed by both HRTEM imaging and

electron diffraction analysis. This method based on surface manipulation for crystallinity engineering is potentially extendable to other types of noble-metal nanocrystals.

5.4 Experimental Section

Chemicals and materials. cetyltrimethylammonium bromide (CTAB, ≥99%), cetyltrimethylammonium chloride (CTAC, ≥98.0%), gold(III) chloride trihydrate ($HAuCl_4 \bullet 3H_2O$, ≥99.9%), ascorbic acid (AA, ≥99.0%), sodium borohydride ($NaBH_4$, 98%), sodium thiosulfate ($Na_2S_2O_3$, 99%), and sodium sulfate (Na_2SO_4, ≥99.0%) were all obtained from Sigma-Aldrich and used as received. Sodium sulfide nonahydrate ($Na_2S \bullet 9H_2O$, 98.0%) was obtained from Spectrum Chemical Manufacturing Corporation. Sulfur powder (precipitated, 99.5%) was obtained from Alfa Aesar. In all experiments, we used deionized water with a resistivity of 18.2 MΩcm, which was prepared using an ultrapure water system (Millipore, Billerica, MA).

Preparation of the initial, CTAB-capped Au seeds. The initial, CTAB-capped Au seeds were prepared by adding 0.6 mL of an aqueous $NaBH_4$ solution (10 mM) into 10 mL of an aqueous solution containing $HAuCl_4$ (0.25 mM) and CTAB (100 mM). A brown solution immediately formed upon the introduction of $NaBH_4$. The mixture was then kept undisturbed at 27 ^oC for 3 h to ensure complete decomposition of $NaBH_4$ remaining in the reaction mixture.

Preparation of the Au spherical seeds. 2 mL of aqueous $HAuCl_4$ solution (0.5 mM), 2 mL of aqueous CTAC solution (200 mM), and 1.5 mL of aqueous AA solution (100 mM) were mixed in a 20-mL glass vial, followed by the introduction of 50 μL of the initial, CTAB-capped Au seeds. The reaction was allowed to continue at 27 ^oC for 10 min. The product was collected by centrifugation at 14,500 rpm for 30 min, washed with water once, and then re-dispersed in 1 mL of aqueous CTAC solution (20 mM) for further use.

Preparation of Au rod-like seeds. 2 mL of aqueous $HAuCl_4$ solution (0.5 mM), 2 mL of aqueous CTAB solution (100 mM), 100 μL mL of aqueous $AgNO_3$ solution (2 mM), and 110 μL of aqueous AA solution (10 mM) were mixed in a 20-mL glass vial, followed by the introduction of 2.4 μL of the initial, CTAB-capped Au seeds. The

reaction was allowed to continue at 27 ^{o}C for 30 min. The product was collected by centrifugation at 14,500 rpm for 10 min, washed with water once, and then re-dispersed in 1 mL of aqueous CTAC solution (200 mM) for further use.

Treatment of Au seeds with aqueous $Na_2S_2O_3$ solution. 1 mL of the seed solution (spheres or rods) was mixed with 120 μL of $Na_2S_2O_3$ aqueous solution (100 mM) and the mixture was aged at room temperature for 1 h. The mixture was centrifuged at 14,500 rpm for 30 min to remove excessive $Na_2S_2O_3$ and then re-dispersed in 1 mL of aqueous CTAC solution (20 mM) for further use.

Standard procedure for seed-mediated growth of Au nanocrystals. 2 mL of aqueous $HAuCl_4$ solution (0.5 mM), 2 mL of aqueous CTAC solution (100 mM), and 130 μL of aqueous AA solution (10 mM) were mixed in a 20-mL glass vial, followed by rapid injection of a certain volume of the seed suspension (100 μL for the spherical seeds and 500 μL for the rod-like seeds). The reaction was allowed to continue at room temperature for 30 min. The product was collected by centrifugation at 14,500 rpm for 30 min and then washed with water once for further characterizations.

Preparation of Na_2S_x aqueous solution. The Na_2S_x solution was prepared by reacting aqueous Na_2S with sulfur powders. In a typical process, 32 mg of sulfur powders were mixed with 11.7 mL of 50 mM Na_2S aqueous solution in a 20 mL vial. The suspension was agitated by vortexing and sonication for about 10 min. The vial was then capped and put in an oven held at 80 ^{o}C for 12 h. The color of the solution turned to bright yellow once all the sulfur powders had completely dissolved.

Instrumentation. Transmission electron microscopy (TEM) images were captured using a JEM-1400 microscope operated at 120 kV (JEOL, Tokyo, Japan). High-resolution TEM images and electron diffraction patterns were obtained using a field-emission JEM-2010F microscope operated at 200 kV (JEOL, Tokyo, Japan). The samples were prepared by dropping aqueous suspensions of the nanoparticles onto carbon-coated

Cu grids (Electron Microscopy Sciences, Hatfield, PA) and dried under ambient conditions in air.

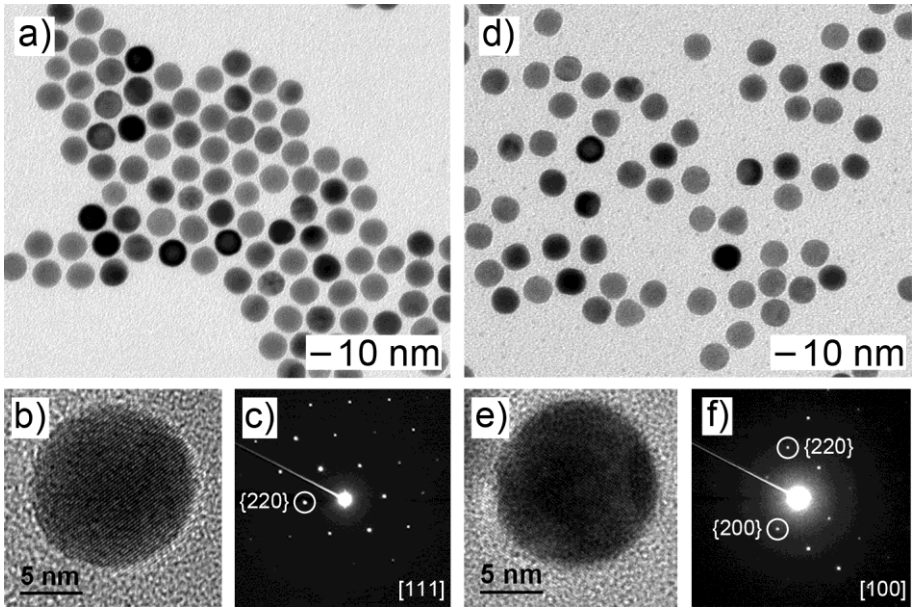

Figure 5.1. (a, d) TEM images of Au spherical seeds (a) before and (d) after treatment with aqueous $Na_2S_2O_3$ solution. (b, e) High-resolution TEM images and (c, f) the corresponding electron diffraction patterns of seed (b, c) before and (e, f) after the treatment, respectively.

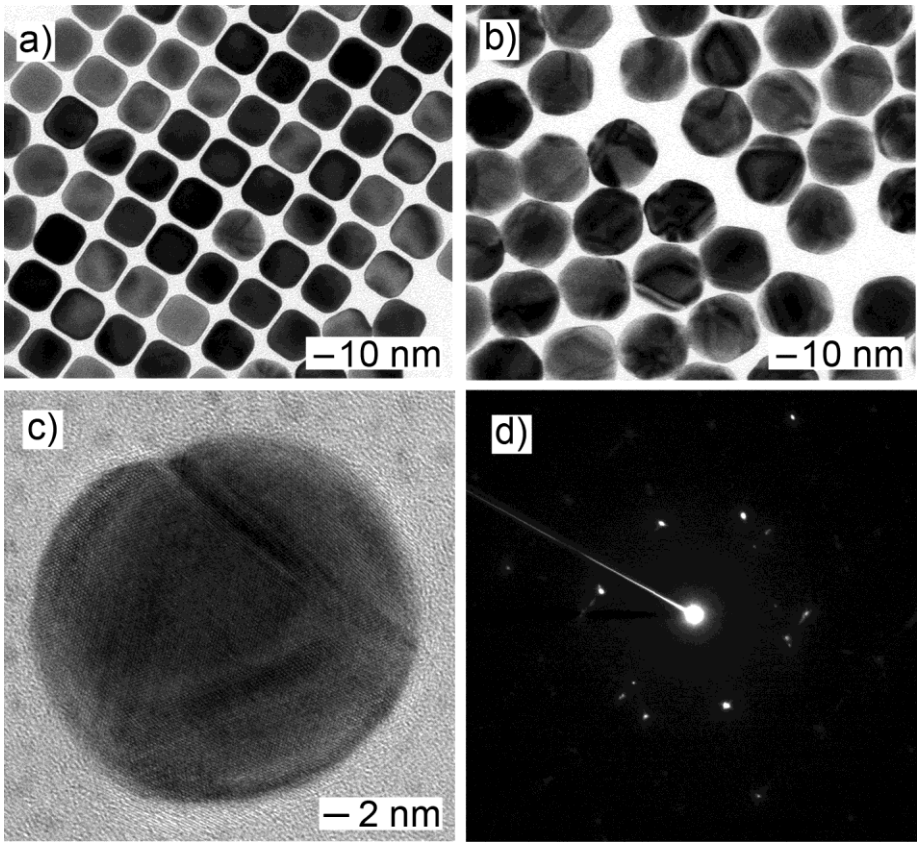

Figure 5.2. (a, b) TEM images of Au nanocrystals obtained using the same seed-mediated growth procedure, except that the Au seeds used for (b) had been treated with aqueous $Na_2S_2O_3$ solution. **(**c) High-resolution TEM image and (d) the corresponding electron diffraction pattern of the particles shown in (b).

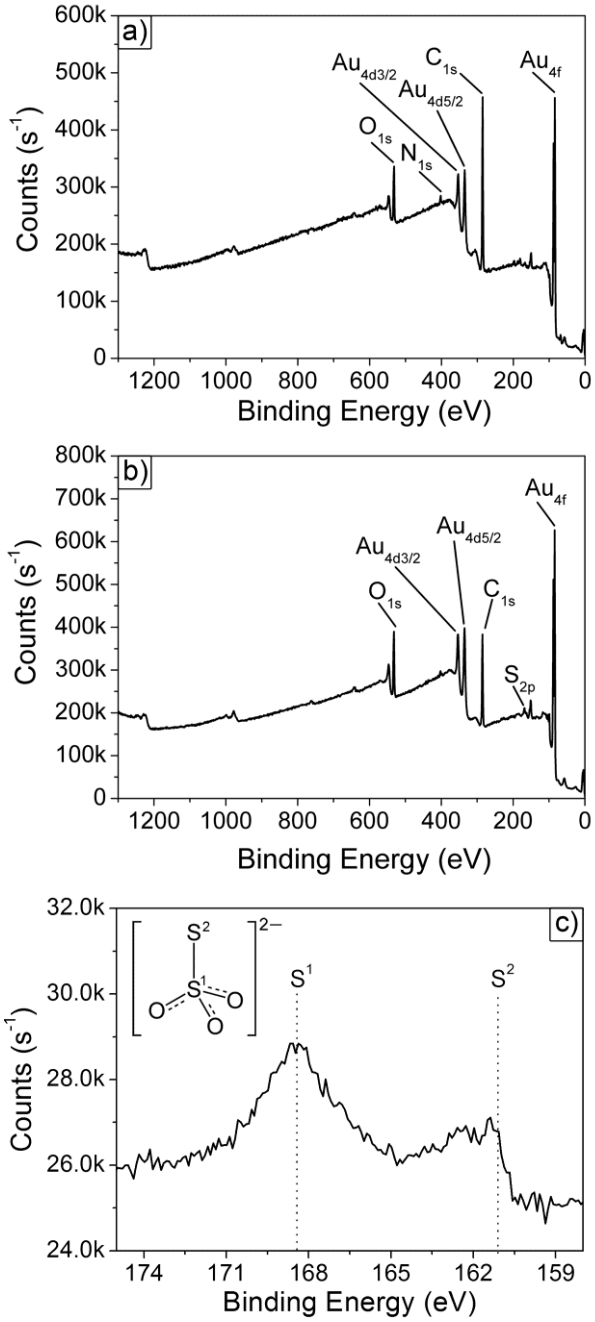

Figure 5.3. XPS analysis of the Au spherical seeds (a) before and (b, c) after the treatment with aqueous $Na_2S_2O_3$ solution: (a, b) survey scans; (c) S 2p scan of the seeds after the treatment. The dotted lines indicated the positions for the S 2p peaks of bulk $Na_2S_2O_3$, as reported in literature.

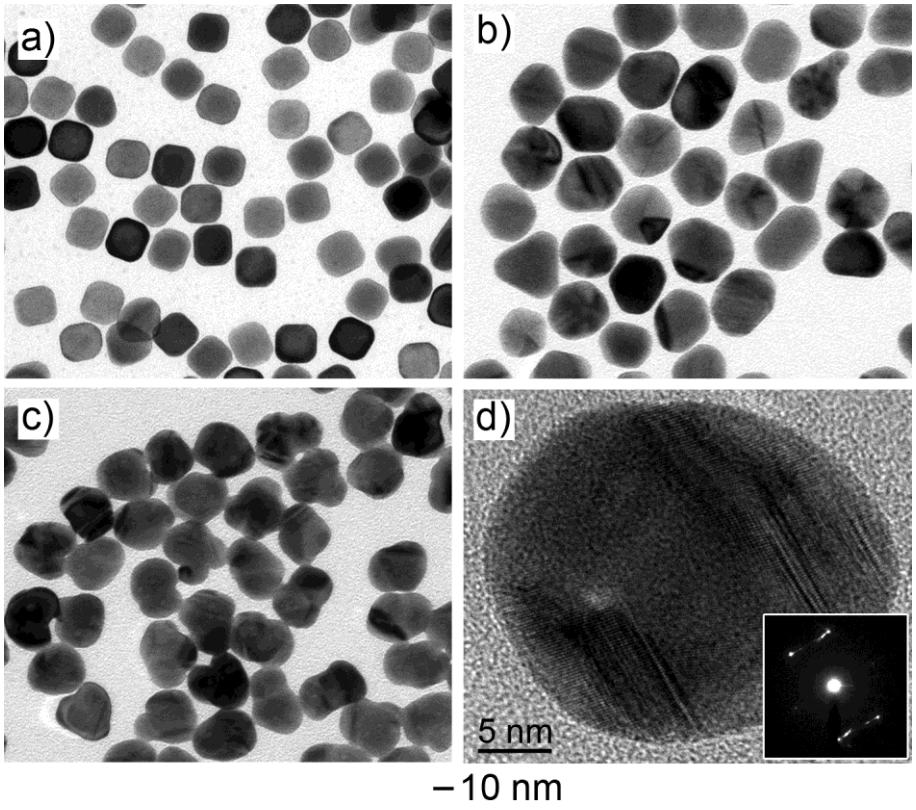

Figure 5.4. TEM images of Au nanocrystals obtained using the standard seed-mediated growth procedure, where the Au spherical seeds had been treated with (a) Na_2SO_4, (b) Na_2S, and (c) Na_2S_x, respectively. (d) High-resolution TEM image of a typical particle in (c). The inset shows the corresponding ED pattern.

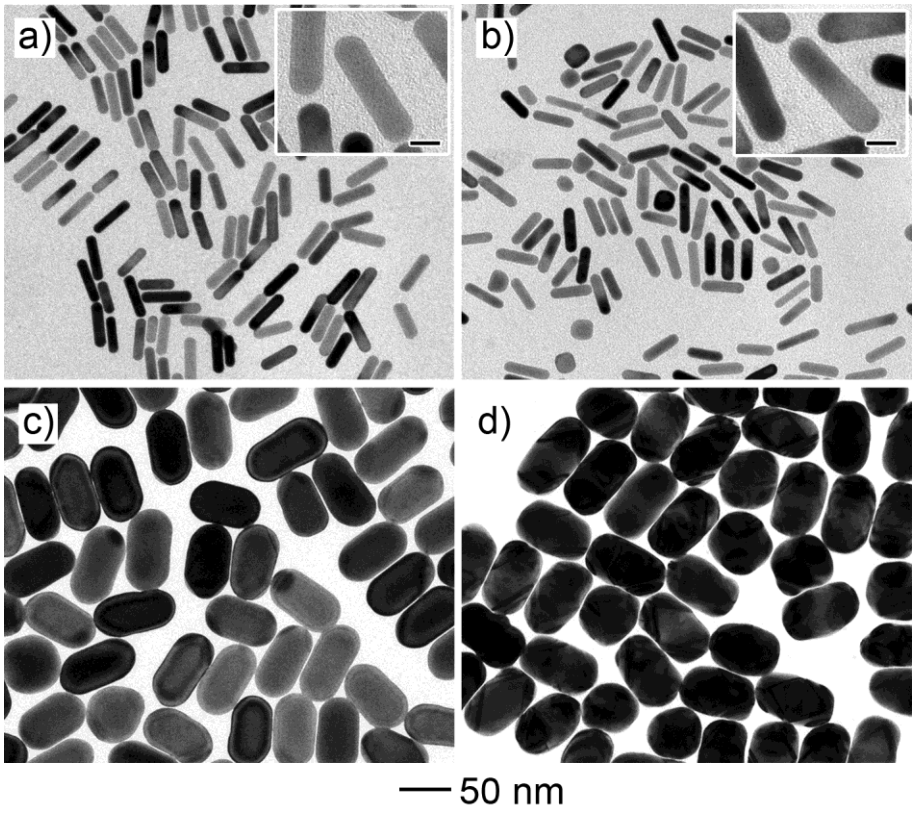

Figure 5.5. (a, b) TEM images of Au rod-like seeds (a) before and (b) after treatment with aqueous $Na_2S_2O_3$ solution. (c, d) TEM images of (c) single-crystal and (d) twinned nanorods that were obtained using the same procedure, expect that the rod-like seeds used for (b) had been treated with aqueous $Na_2S_2O_3$ solution. The scale bars in the insets of (a) and (b) are 10 nm.

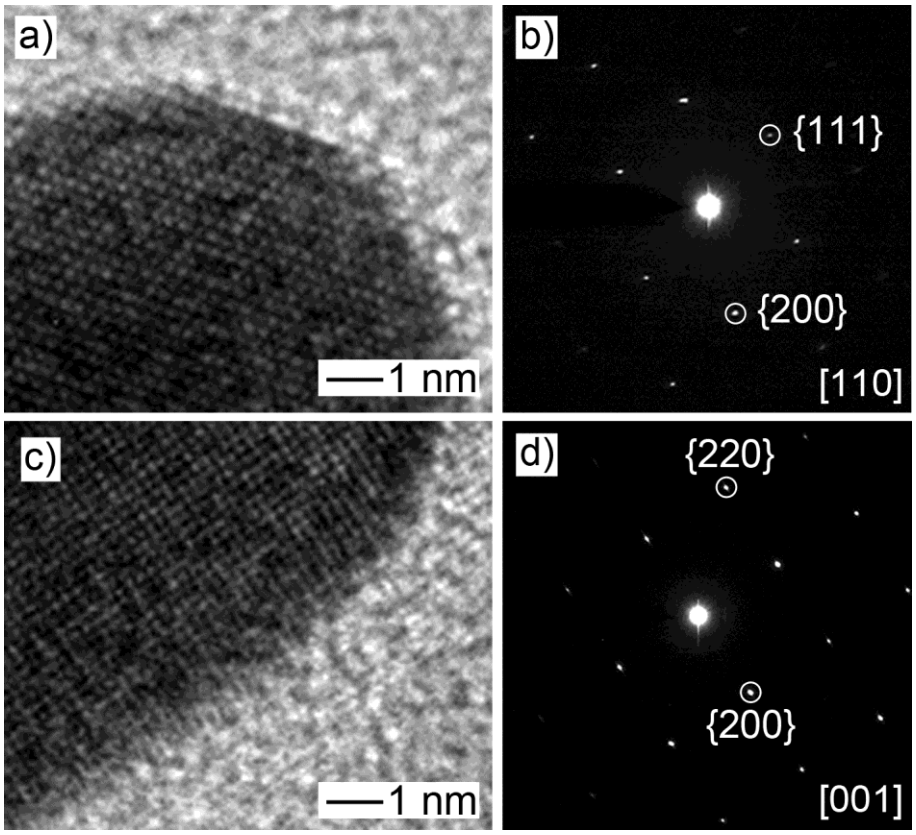

Figure 5.6. (a, c) High-resolution TEM images and (b, d) the corresponding ED patterns of a Au rod-like seed (a, b) before and (c, d) after treatment with $Na_2S_2O_3$.

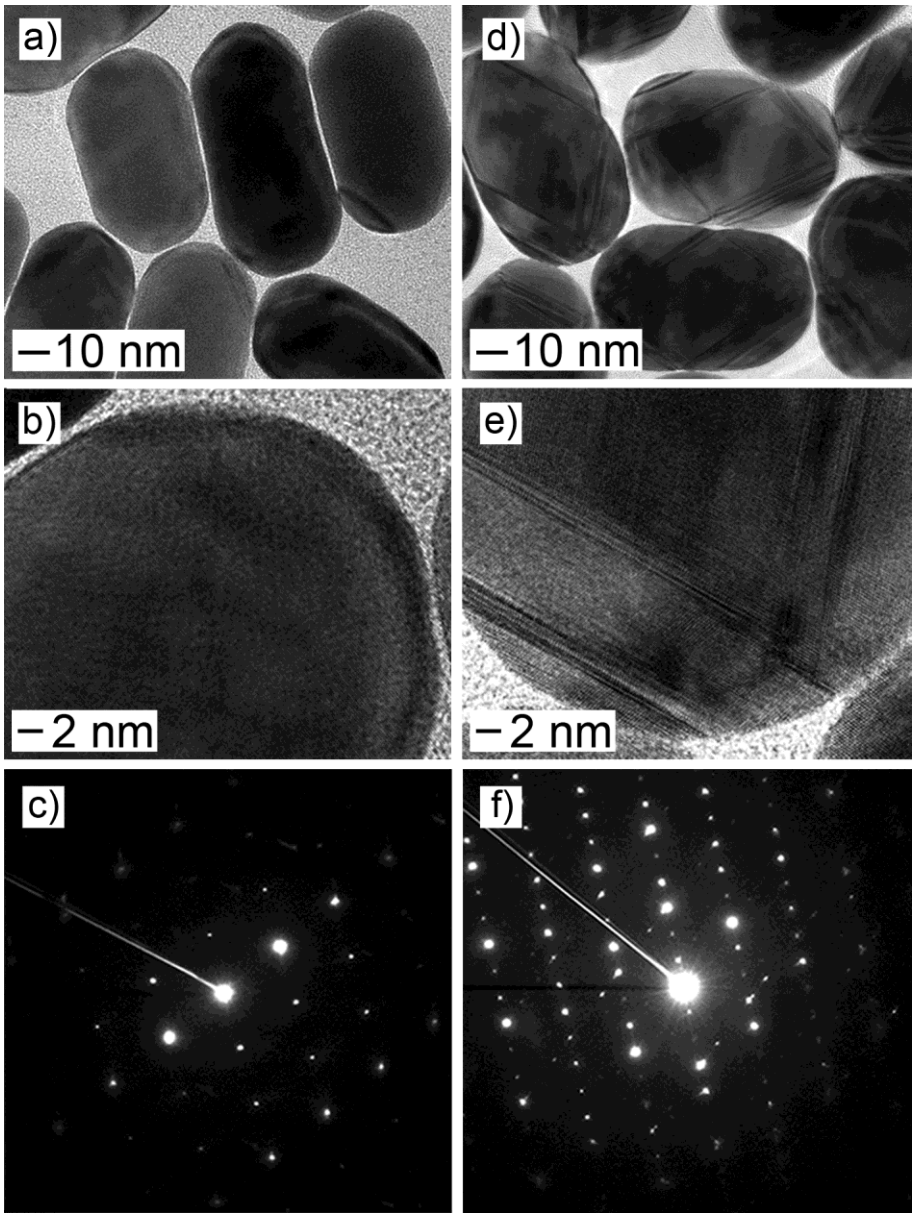

Figure 5.7. Detailed structural characterization of (a-c) single-crystal and (d-f) twinned Au nanorods shown in Figure 5.5, c and d, respectively: (a-d) high-resolution TEM images and (e, f) electron diffraction patterns.

5.5 References for Chapter 5

[1] M. -P. Pileni, *Acc. Chem. Res.* **2012**, *45*, 1965-1972.

[2] J. Moriarty, V. Vitek, V. Bulatov, S. Yip, *J. Comput. Aided Mater. Des.* **2002**, *9*, 99-132.

[3] L. D. Marks, *Rep. Prog. Phys.* **1994**, *57*, 603.

[4] Y. Xia, Y. Xiong, B. Lim, S. E. Skrabalak, *Angew. Chem. Int. Ed.* **2009**, *48*, 60-103.

[5] J. L. Elechiguerra, J. Reyes-Gasga, M. J. Yacaman, *J. Mater. Chem.* **2006**, *16*, 3906-3919.

[6] P. Yang, H. Portales, M.-P. Pileni, *J. Chem. Phys.* **2011**, *134*, 024507.

[7] G. Grimvall, *The Electron–Phonon Interaction in Metals*; North-Holland: New York, 1981.

[8] H. Portalès, N. Goubet, L. Saviot, P. Yang, S. Sirotkin, E. Duval, A. Mermet, M.-P. Pileni, *ACS Nano* **2010**, *4*, 3489-3497.

[9] S. C. Chang, L. W. H. Leung, M. J. Weaver, *J. Phys. Chem.* **1990**, *94*, 6013-6021.

[10] H. Portales, N. Goubet, L. Saviot, S. Adichtchev, D. B. Murray, A. Mermet, E. Duval, M.-P. Pileni, *Proc. Natl. Acad. Sci. USA* **2008**, *105*, 14784-14789.

[11] N. Goubet, C. Yan, D. Polli, H. Portalès, I. Arfaoui, G. Cerullo, M.-P. Pileni, *Nano Lett.* **2012**, *13*, 504-508.

[12] J. Zheng, Y. Ding, B. Tian, Z. L. Wang, X. Zhuang, *J. Am. Chem. Soc.* **2008**, *130*, 10472-10473.

[13] D. Polli, I. Lisiecki, H. Portalès, G. Cerullo, M.-P. Pileni, *ACS Nano* **2011**, *5*, 5785-5791.

[14] Q. F. Gu, G. Krauss, W. Steurer, F. Gramm, A. Cervellino, *Phys. Rev. Lett.* **2008**, *100*, 045502.

[15] W. Niu, G. Xu, *Nano Today* **2011**, *6*, 265-285.

[16] Y. Tang, M. Ouyang, *Nature Mater.* **2007**, *6*, 754-759.

[17] Q. Zhang, J. Xie, Y. Yu, J. Yang, J. Y. Lee, *Small* **2010**, *6*, 523-527.

[18] Y. Liu, Z. Zhu, G. Liu, Z. Xu, S. M. Kuznicki, H. Zhang, *J. Phys. Chem. C* **2011**, *115*, 14591-14597.

[19] X. Xia, Y. Xia, *Nano Lett.* **2012**, *12*, 6038-6042.

[20] Y. Zheng, J. Zeng, A. Ruditskiy, M. Liu, Y. Xia, *Chem. Mater.* **2013**, DOI: 10.1021/cm402023g.

[21] J. Li, Y. Zheng, J. Zeng, Y. Xia, *Chem. Eur. J.* **2012**, *18*, 8150-8156.

[22] Y. Ma, W. Li, E. C. Cho, Z. Li, T. Yu, J. Zeng, Z. Xie, Y. Xia, *ACS Nano* **2010**, *4*, 6725-6734.

[23] M. Eguchi, D. Mitsui, H.-L. Wu, R. Sato, T. Teranishi, *Langmuir* **2012**, *28*, 9021-9026.

[24] J. Zeng, Y. Zheng, M. Rycenga, J. Tao, Z.-Y. Li, Q. Zhang, Y. Zhu, Y. Xia, *J. Am. Chem. Soc.* **2010**, *132*, 8552-8553.

[25] C. Zhu, J. Zeng, P. Lu, J. Liu, Z. Gu, Y. Xia, *Chem. Eur. J.* **2013**, *19*, 5127-5133.

[26] F.-R. Fan, D.-Y. Liu, Y.-F. Wu, S. Duan, Z.-X. Xie, Z.-Y. Jiang, Z.-Q. Tian, *J. Am. Chem. Soc.* **2008**, *130*, 6949-6951.

[27] S. E. Habas, H. Lee, V. Radmilovic, G. A. Somorjai, P. Yang, *Nature Mater.* **2007**, *6*, 692-697.

[28] M. R. Langille, J. Zhang, M. L. Personick, S. Li, C. A. Mirkin, *Science* **2012**, *337*, 954-957.

[29] Y. Zheng, Y. Ma, J. Zeng, X. Zhong, M. Jin, Z.-Y. Li, Y. Xia, *Chem. Asian J.* **2013**, *8*, 792-799.

[30] Z. L. Wang, *J. Phys. Chem. B* **2000**, *104*, 1153-1175.

[31] B. Pelaz, V. Grazu, A. Ibarra, C. Magen, P. del Pino, J. M. de la Fuente, *Langmuir* **2012**, *28*, 8965-8970.

[32] V. K. LaMer, R. H. Dinegar, *J. Am. Chem. Soc.* **1950**, *72*, 4847-4854.

[33] B. Nikoobakht, M. A. El-Sayed, *Chem. Mater.* **2003**, *15*, 1957-1962.

[34] C. J. Johnson, E. Dujardin, S. A. Davis, C. J. Murphy, S. Mann, *J. Mater. Chem.* **2002**, *12*, 1765.

VITA

YIQUN ZHENG

ZHENG was born in Anhui, China. He received his B.S. degree in materials chemistry from the University of Science and Technology of China (USTC) in 2009. He has been working in the Xia group as a Ph.D. candidate since January 2010. His research interests include the synthesis of novel metal nanostructures for applications in plasmonics, catalysis, and fuel cell technology. When he is not working on his research, Mr. Zheng enjoys swimming, hiking, singing, and auto repair.